UCSF
UC San Francisco Electronic Theses and Dissertations

Title

Neuronal APOE4 Reduction Protects Against Alzheimer's Disease Pathology

Permalink

https://escholarship.org/uc/item/9197b1bv

ISBN

9798270227425

Author

Yip, Oscar

Publication Date

2025-12-17

Peer reviewed|Thesis/dissertation

eScholarship.org Powered by the California Digital Library
University of California

Neuronal APOE4 Reduction Protects Against Alzheimer's Disease Pathology

by

Oscar Yip

DISSERTATION

Submitted in partial satisfaction of the requirements for degree of

DOCTOR OF PHILOSOPHY

in

Biomedical Sciences

in the

GRADUATE DIVISION

of the

UNIVERSITY OF CALIFORNIA, SAN FRANCISCO

Approved:

Signed by:
Ryan Corces
38BEF237143F46A...

Ryan Corces

Chair

DocuSigned by:
Jorge Palop
Signed by:EC0437...

Jorge Palop

Yadong Huang
DCE6157D9AA1471...

Yadong Huang

Committee Members

Copyright 2025

by

Oscar Yip

This thesis is dedicated to my Gong Gong, Tat Tran, my parents, Vincent Diep & Lyn Tran, and my sister, Amanda Yip.

Acknowledgements

First, I want to thank my PhD advisor, Yadong Huang, for his incredible mentorship throughout this journey. Your guidance and support have shaped not just this work, but who I am as a scientist. To my thesis committee members, Ryan Corces, Jorge Palop, and Yadong Huang—thank you for your scientific guidance and for pushing me to think harder and deeper about my research. Your feedback has been invaluable. Next, I would like to thank the current graduate students, postdocs, and RAs in the lab: thanks for making our lab such an amazing place to work every day. A special thank you to Jessie Blumenfeld and Min Joo Kim, my fellow graduate students that embarked on this incredible and challenging PhD journey with me in this lab. Thank you for the endless support, the many great meals, and for making the lab feel like home through all the highs and lows of this PhD. I couldn't have done this without you two. Nicole, Maxine, and Antara, thank you for being amazing scientific mentors when I joined the lab! To the FG2C community at UCSF—thank you for giving me a space to decompress and connect with others who understand the stresses of graduate school. To my BMS cohort and my San Francisco chosen family—thank you for your support throughout my PhD! To my high school and college friends who've been cheering me on from near and far, your support has kept me going. And finally, a massive thank you to my family. To my sister, thank you for always having my back, no matter what. To my parents, thank you for every sacrifice you made to come to the U.S. and opening doors for my future – I wouldn't be here today without your love and encouragement. To my grandparents Ken and Karen Gerdes—thank you for encouraging me to pursue a PhD and for supporting me every step of the way. And to my grandparents Binh Huynh and Tat Tran, thank you for being the one of the reasons I started conducting research in the field of AD in the first place.

Contributions

Chapter I contains texts and figures adapted from a review article published with Nature Reviews Neuroscience, for which I served as first author with Jessica Blumenfeld. Jessica Blumenfeld, Min Joo Kim, Yadong Huang, and I all contributed to the research and writing involved in producing the paper.

Chapter II contains texts and figures that are currently under preparation for journal submission. Yadong Huang and I designed and coordinated the studies and wrote the manuscript. I performed the majority of studies and data analyses. Luokang Yao and Yaqiao Li performed the majority of the snRNA-seq analysis. Jessica Blumenfeld aided with stereotaxic mouse surgeries as well as mouse tissue collection and processing. Min Joo Kim, David Shostak, and Zoe Platow helped with immunohistochemical studies and data collection. Kaylie Suan, Yanxia Hao, and Alice An isolated cell nuclei and prepared samples for snRNA sequencing. Claire Ellis, Samuel De Leon, and Jeremy Nguyen managed all mouse lines. Claire Ellis helped with mouse tissue collection. Qin Xu provided valuable guidance on experimental designs. Theodora Pak provided editorial assistance. Yadong Huang supervised the project.

Neuronal APOE4 Reduction Protects Against Alzheimer's Disease Pathology

Oscar Yip

Abstract

Apolipoprotein E4 (APOE4) is the strongest genetic risk factor for late-onset Alzheimer's disease (AD). Within the central nervous system (CNS), APOE is produced by a variety of cell types, with differential roles in AD pathogenesis. Studies have shown that APOE4 produced by neurons plays a central role in promoting the development of major AD pathologies, including p-tau accumulation, neuroinflammation, and neurodegeneration, highlighting its role as an upstream initiating factor that affects other cell types and downstream AD-related pathologies. Here, we demonstrate that antisense oligonucleotides (ASOs) targeting APOE-I3, a neuron-specific splicing variant of APOE mRNA, effectively reduce APOE expression in neurons *in vitro* and *in vivo*. Treating PS19 tauopathy mice expressing APOE4 with this APOE-I3-targeting ASO reduces neuronal APOE4, rescues neurodegeneration, and diminishes neuroinflammation. Strikingly, the extent of neuronal APOE4 reduction predicts the efficacy of rescuing neurodegeneration. Single nucleus RNA-sequencing demonstrated that APOE-I3-targeting ASO treatment decreases disease associated neuronal and glial subtypes and increases a disease-protective microglial subtype. These findings suggest that preferential knockdown of neuronal APOE4 with an APOE-I3-targeting ASO protects against key hallmarks of AD pathology, elucidating a potential therapeutic approach for treating APOE4-driven AD.

Table of Contents

CHAPTER 1: Introduction 1

Cell type-specific roles of APOE4 in Alzheimer's disease 2

Astrocytic APOE4 in AD pathogenesis 6

Neuronal APOE4 in AD pathogenesis 13

Microglial APOE4 in AD pathogenesis 23

Oligodendrocytic APOE4 in AD pathogenesis 33

Vascular cell APOE4 in AD pathogenesis 35

Cell type-specific APOE4 cascade model of AD 40

Potential therapeutics targeting APOE4 43

Summary of Cell Type-Specific APOE Effects 45

CHAPTER 2: Neuronal APOE4 reduction with an APOE-I3-targeting ASO protects against neurodegeneration and neuroinflammation in an Alzheimer's disease mouse model 46

Introduction 47

Results 50

Discussion 88

Methods 93

References 113

List of Figures

Fig. 1.1 | CNS APOE expression and links to Alzheimer's disease. 5

Fig. 1.2 | Expression of APOE4 in astrocytes and its roles in AD pathogenesis 12

Fig. 1.3 | Expression of APOE4 in neurons and its roles in AD pathogenesis. 22

Fig. 1.4 | Expression of APOE4 in microglia and its roles in AD pathogenesis. 32

Fig. 1.5 | Expression of APOE4 in oligodendrocytes and vascular cells and its roles in AD pathogenesis. 39

Fig. 1.6 | Cell type-specific APOE4 cascade model of AD and related therapeutic strategies. 42

Fig. 2.1 | Identification of ASO candidates capable of reducing neuronal or global APOE expression. 54

Fig. 2.2 | ASO-E-4 and ASO-I3-75 effectively reduce APOE expression in the hippocampus of PS19/E4 mice in a cell-type-dependent manner. 57

Fig. 2.3 | ASO-I3-75, but not ASO-E-4, effectively reduces neurodegeneration in the hippocampus of PS19/E4 mice. 60

Fig. 2.4 | Trending Rescue of DG neuronal layer thickness in APOE ASO-treated PS19/E4 mice. 61

Fig. 2.5 | ASO-I3-75, but not ASO-E-4, diminishes p-tau contribution to neurodegeneration in the hippocampus of PS19/E4 mice. 63

Fig. 2.6 | Both ASO-E-4 and ASO-I3-75 reduces astrogliosis while only ASO-I3-75 alters the contribution of microgliosis to hippocampal degeneration in PS19/E4 mice. 67

Fig. 2.7 | ASO-E-4 and ASO-I3-75 diminishes disease-associated excitatory and inhibitory neurons (DAEN and DAIN) in the hippocampus of PS19/E4 mice. 73

Fig. 2.8 | snRNA-seq identification of cell clusters. 75

Fig. 2.9 | ASO-E-4 and ASO-I3-75 diminishes disease-associated excitatory neurons (DAEN) in the hippocampus of ASO-treated PS19/E4 mice. 76

Fig. 2.10 | Differentially expressed genes (DEGs) in disease-associated excitatory neurons (DAEN) in the hippocampus of ASO-treated PS19/E4 mice. 77

Fig. 2.11 | Characteristics of disease-associated inhibitory neurons (DAIN) in the hippocampus of ASO-treated PS19/E4 mice. 78

Fig. 2.12 | ASO-I3-75 is more effective than ASO-E-4 at reducing disease-associated astrocytes (DAA), reducing disease-associated microglia (DAM), and increasing disease-protective microglia (DPM) in the hippocampus of PS19/E4 mice. 84

Fig. 2.13 | Characteristics of disease-associated astrocytes (DAA), disease-associated microglia (DAM), and disease-protective microglia (DPM) in the hippocampus of ASO-treated PS19/E4 mice. 86

Fig. 2.14 | Differentially expressed genes (DEGs) in disease-associated astrocytes (DAA), disease-associated microglia (DAM), and disease-protective microglia (DPM) in the hippocampus of ASO-treated PS19/E4 mice. 87

CHAPTER 1: Introduction

Cell type-specific roles of APOE4 in Alzheimer's disease

Alzheimer's disease (AD) is a neurodegenerative disorder that is clinically characterized by a progressive decline in cognitive functions. Pathologically, AD is characterized by loss of synapses and neurons, extracellular deposition of amyloid-β (Aβ) peptides in the form of amyloid plaques, neuritic dystrophy, intraneuronal accumulation of hyperphosphorylated tau (p-tau) in the form of neurofibrillary tangles (NFTs), vascular alterations and inflammatory responses mediated by microglia and astrocytes.[1,2] AD starts with a long preclinical stage, lasting 20–30 years, during which amyloid plaques form without clinical symptoms.[3–5] This is followed by a prodromal stage, usually lasting 3–5 years, characterized by mild cognitive impairment (MCI). Finally, some but not all cases progress to dementia 3–5. Worldwide, the total number of people with preclinical AD, prodromal AD and AD dementia is estimated to be approximately 416 million (Fig. 1.1a).[6]

Despite over a century of AD research, we lack effective treatments or cures and those that have been proposed remain controversial. This is likely due to the complex etiology of AD pathogenesis, which involves interactions among diverse genetic, epigenetic and environmental factors. Causative genetic mutations have been identified for early-onset autosomal dominant AD (ADAD)[7,8]; however, ADAD accounts for fewer than 1% of all AD cases. For late-onset AD, which accounts for the vast majority of AD cases, researchers so far have identified only genetic loci that can alter disease risk, the strongest of which is the apolipoprotein E (*APOE*) locus.[9,10]

The human *APOE* gene is polymorphic, comprising three common alleles (*APOE ε4, ε3* and *ε2*) that translate into three APOE isoforms: APOE4, APOE3 and APOE2.[1,11] APOE's canonical function

is as a transporter of lipids between cells and organs. As a result of amino acid differences at residue 112 or 158,[12] the three APOE isoforms exhibit different binding properties with the APOE receptors through which they mediate this transport (Fig. 1.1b).[13] Carriers of the *APOE ε4* allele, the strongest genetic risk factor for late-onset AD,[10,14,15] account for approximately 24% of the healthy population[16] (Fig. 1.1b) but make up 55–75% of AD dementia cases (as well as approximately 57% of those with prodromal AD and approximately 55% of those with preclinical AD) (Fig 1.1a).[14,17]

Along with its unique structural and functional properties,[12,13,18] the presence of APOE4 has been linked to more severe AD pathologies.[1,2,19–21] Having a copy of the *APOE ε4* allele increases the formation of amyloid plaques[1,2,19,20] and NFTs in humans and animal models.[1,2,22–24] APOE4 is also associated with increased gliosis and elevated levels of proinflammatory cytokines.[23–26] This APOE4-enhanced gliosis is, in turn, associated with other pathological phenotypes such as lipid accumulation in glial cells,[27–29] neurodegeneration[23,24,28,30] and hippocampal atrophy.[23,24,28,30] Moreover, humans with AD, especially those carrying the *APOE ε4* allele, and AD mouse models carrying the same allele exhibit oligodendrocyte dysfunction and myelination defects[24,31–33] as well as blood-brain barrier (BBB) impairments.[34–36] Given this complicated picture, it is critical to dissect the detrimental effects of APOE4 at a cell type-specific level and to identify the underlying molecular mechanisms that drive AD pathogenesis in the most relevant cell populations. Although numerous studies and recent reviews have examined the pathobiological effects of APOE4 in general,[20,25,37,38] a comprehensive review of APOE4's roles in AD pathogenesis at a cell type-specific level is lacking: this is therefore the focus of this chapter. Several cell types in the

mammalian CNS can produce APOE, including astrocytes, neurons, microglia, oligodendrocytes and vascular cells, although the production levels vary by cell type and condition (Fig. 1.1c).[1,20,39] Studies leveraging new research tools and experimental models have revealed that the effects of APOE4 on AD pathologies depend on its cellular sources and expression levels. Here, we review the roles of APOE4 derived from various CNS cell types, summarize the potential mechanisms underlying the cell type-specific effects of APOE4, present a novel cell type-specific APOE4 cascade model of AD, and provide perspectives on future APOE4 research and related therapeutic developments.

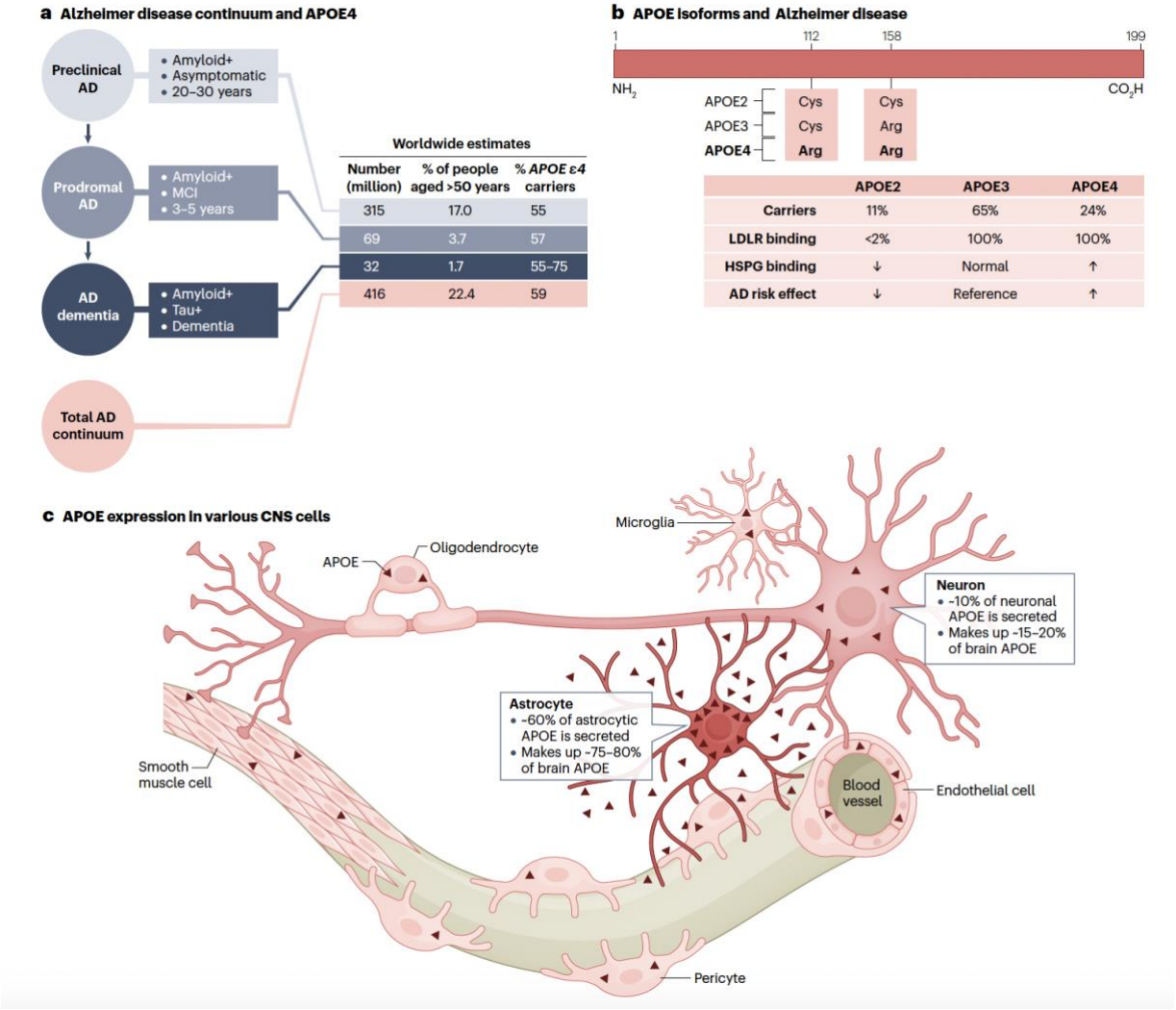


Fig. 1.1 | CNS APOE expression and links to Alzheimer's disease.

a, An overview of the Alzheimer's disease (AD) continuum,[3–5] worldwide estimates of numbers of individuals with preclinical AD, prodromal AD and AD dementia,[6] and their relationship with the E4 isoform of apolipoprotein E (APOE4).[6] **b**, There are three common APOE isoforms: APOE2, APOE3 and APOE4.[1,11] They exhibit sequence differences at amino acid residues 112 and 158,[12] differential receptor binding properties[13] and varying impacts on AD risk.[6,10,14–17] Downward-pointing arrows indicate reduced heparan sulfate proteoglycan (HSPG) binding or AD risk; upward-pointing arrows indicate increased HSPG binding or AD risk. **c**, Multiple cell types in the CNS can produce APOE at different levels (indicated by the depth of red shading) under normal conditions.[1,20,39] These include astrocytes, neurons, microglia, oligodendrocytes and vascular cells (endothelial cells, pericytes and smooth muscle cells). In studies in which astrocytic APOE was selectively removed in mice, there was a loss of 75–80% of brain APOE levels,[42–44] whereas removing neuronal APOE led to a 15–20% reduction of brain APOE levels.[24,42] (figure caption continued on next page).

(figure caption continued from the previous page). Thus, astrocytic and neuronal APOE seem to account for approximately 75–80%[42–44] and 15–20%[24,42] of total APOE in the brain, respectively. After production, approximately 60% of astrocytic APOE is secreted into the extracellular space,[47,48] whereas most APOE produced in neurons remain intracellular.[48] The proportions of total and secreted APOE in the brain that are contributed by microglia, oligodendrocytes and vascular cells have yet to be determined. LDLR, low-density lipoprotein receptor; MCI, mild cognitive impairment.

Astrocytic APOE4 in AD pathogenesis

Expression and regulation of astrocytic APOE

Astrocytes produce most of the APOE in the CNS (Fig. 1.2a),[39–41] contributing approximately 75–80% of the total APOE in the mouse brain (Fig. 1.1c).[42–44] Although the regulation of astrocytic APOE production remains to be fully elucidated, the transcription factor C/EBPβ is known to bind the *APOE* promoter and regulate APOE expression in astrocytes.[45] Mitochondrial function may also modulate APOE levels, as treatment of human astrocytes with an inhibitor of mitochondrial respiration increased APOE mRNA and protein levels.[46] After production, approximately 60% of astrocytic APOE is secreted into the extracellular space.[47,48] This process may be regulated by 25-hydroxycholesterol (25-HC), an oxysterol secreted by microglia, as treatment of primary mouse astrocytes expressing human *APOE* with 25-HC led to a 2-fold increase in secreted APOE.[49] Since astrocytes are the major source of brain APOE, the roles that intracellular and extracellular astrocytic APOE may play in health and AD have been a major focus in APOE research (Fig. 1.2a–c).

Astrocytic APOE4 in inflammation, metabolism and BBB function

Under normal conditions, astrocytic APOE helps astrocytes maintain homeostatic lipid metabolism, controls synaptic pruning, regulates clearance of extracellular Ab aggregates and cell debris, and helps to preserve BBB integrity (Fig. 1.2a).[50–58] However, APOE can also promote astrocytic inflammatory responses in an isoform-dependent manner (Fig. 1.2b,c).[43,50,51,59] In primary mouse astrocytes and astrocytes derived from human induced pluripotent stem cells (hiPSCs), expression of APOE4 increased the secretion of inflammatory cytokines, including interleukin-1β (IL-1b), IL-6, and inducible NO synthase (NOS2), as compared to expression of APOE3 or APOE2.[50,51,59] In a tauopathy model in which mice express mutant human tau (PS19 mice), additional expression of APOE4 (PS19-APOE4 mice) enhanced the reactive astrocytosis elicited by tau pathology, while its selective removal from astrocytes induced a more physiological state,[43] suggesting a role of astrocytic APOE4 in tauopathy-induced reactive astrocytosis.

APOE isoforms also differentially affect astrocytic lipid metabolism and accumulation (Fig. 1.2b,c). APOE4 expression increased cholesterol synthesis and accumulation in astrocytes of human *APOE4* knock-in (*APOE4*-KI) mice and astrocytes generated from hiPSCs derived from inviduals carrying the APOE ε4 allele (APOE4 hiPSCs).[31,53–55,60] Sterol regulatory element-binding protein 2, a key activator of cholesterol synthesis, was elevated in APOE4 hiPSC-derived astrocytes, suggesting a potential pathway through which astrocytic APOE4 may promote cholesterol production.[60] Primary astrocytes from *APOE4*-KI mice exhibited changes in lipid pathway proteins, including reduced levels of peroxisome proliferator-activated receptor-γ (PPARγ, a transcription factor involved in maintaining lipid homeostasis) and altered levels of receptors and transporters

involved in lipid uptake and efflux.[55] Compared with APOE3 hiPSC-derived astrocytes, APOE4 hiPSC-derived astrocytes exhibited increased localization of cholesterol to lysosomes.[51] Furthermore, a recent preprint has reported that immortalized astrocytes from *APOE4*-KI mice developed larger lipid droplets and greatly impaired lipid turnover compared to their *APOE3*-KI counterparts.[61] In addition, selectively removing astrocytic APOE in mice markedly decreased the number of lipid-accumulating reactive astrocytes.[62] Beyond affecting lipid composition intracellularly, astrocytic APOE4 also reduces the lipidation of secreted lipoprotein particles, compared to APOE3.[56]

The differential effects of the APOE isoforms also extend to astrocytic glucose metabolism. Primary astrocytes from *APOE4*-KI mice demonstrated reduced mitochondrial membrane potential and respiration compared to those from APOE3-expressing controls.[63] Similarly, immortalized astrocytes from *APOE*-KI mice, primary *APOE*-KI mouse astrocytes, and hiPSC-derived astrocytes displayed changes in glucose utilization, with APOE4-expressing astrocytes showing elevated levels of glycolytic activity relative to their APOE3 counterparts.[64–66] Interestingly, treatment with cholesterol-depleting agents restored mitochondrial respiration and activity in APOE4 hiPSC-derived astrocytes, suggesting that APOE4-induced cholesterol accumulation may contribute to glucose metabolism shifts in astrocytes.[66]

Astrocytic APOE4 also affects many other cell types, especially under stressed and AD-like conditions (Fig. 1.2c). For instance, selectively removing APOE4 from astrocytes prevented disease-associated gene signatures in neurons, oligodendrocytes and microglia in PS19-APOE4

mice: fewer oligodendrocytes expressed AD-associated immune pathway genes and microglia showed less phagocytosis of synapses and disease-associated microglial (DAM) transcriptional signatures.[43] These results suggest that astrocytic APOE4 enhances glial reactivity.[43] In addition, astrocytic APOE4 seems to affect lipid metabolism in neurons. For example, primary neurons from wildtype (WT) mice showed elevated levels of cholesterol biosynthesis when treated with APOE derived from primary astrocytes of *APOE4*-KI mice, as compared to those treated with APOE from *APOE3*-KI mouse astrocytes.[67] In a similar vein, in an organoid model containing hiPSC-derived neurons and astrocytes of various APOE genotype pairings, the presence of APOE4-producing human astrocytes elevated cholesterol levels and promoted lipid accumulation in human neurons.[68] Additionally, astrocytic APOE4 may also affect synaptic plasticity by impairing neuronal APOE receptor recycling via the endosomal pathway.[69]

Astrocytic APOE4 also influences BBB integrity and function (Fig. 1.2c). In an in vitro BBB model consisting of primary astrocytes derived from *APOE*-KI or *ApoE* knockout (*ApoE*-KO) mice together with WT primary brain endothelial cells and pericytes, astrocytic APOE4 impaired endothelial cell tight junctions by reducing the levels of threonine-phosphorylated occluding.[57] This effect was recapitulated in an in vivo model, in which selective removal of astrocytic APOE4 prevented the impairments of the BBB, endothelial tight junctions and astrocytic end-foot coverage of blood vessels observed in *APOE4*-KI mice.[70] In a mouse *ApoE*-KO model, selective astrocytic expression of APOE4, but not APOE3, led to BBB leakiness.[58] Taken together, these findings suggest that astrocytic APOE4 affects multiple CNS cell types that might contribute to AD pathogenesis.

Astrocytic APOE4 and hallmark AD pathologies

In mouse and cell culture models, astrocytic expression of APOE4 promotes amyloid plaque pathology and impairs astrocytic Aβ uptake, as compared to APOE3 (Fig. 1.2c).[51,54,71–73] Furthermore, selective removal of astrocytic APOE4 reduced plaque loads in a model of amyloidosis in which mice co-express APOE4, mutant amyloid precursor protein (APP) and mutant presenilin 1 (PSEN1, a protein involved in Aβ production) (APP/PS1-21 mice).[74] In another amyloidosis model (5xFAD mice) that co-expresses APOE4, selective ablation of astrocytic APOE4 reduced gliosis and BBB disruption and shifted Aβ deposition from the brain parenchyma to the vasculature.[44]

The connection between astrocytic APOE4 and tau pathology is less straightforward. Selective expression of APOE4 in astrocytes on an *ApoE*-KO background caused little or no accumulation of endogenous mouse p-tau.[75,76] However, selective removal of astrocytic APOE4 in PS19-APOE4 mice moderately lowered p-tau levels.[43] Glypican-4 (GPC4), a protein that is secreted by astrocytes and has been shown to preferentially bind APOE4 (relative to APOE2),[77] may provide a link between astrocytic APOE4 and this effect. Notably, GPC4 treatment increased p-tau accumulation in primary neurons from PS19 mice.[77] Similarly, inducing greater GPC4 expression in astrocytes of young PS19 mice increased hippocampal p-tau levels.[77] Thus, the suggestion that astrocytic APOE4 might augment tau pathology warrants further studies.

APOE4 in disease-associated astrocytic subtypes

Single-nucleus RNA-sequencing (snRNA-seq) studies examining different types of cells in AD have identified a distinct group of disease-associated astrocytes (DAAs) (Fig. 1.2c).[78,79] These DAAs generally have elevated APOE expression, suggesting an involvement of astrocytic APOE in their formation.[78] DAAs also exhibit increased expression of the genes encoding cathepsin and serine protease inhibitor A3N, which are thought to be involved in AD pathogenesis,[80,81] as well as genes involved in lipid and cholesterol pathways, the complement system, endocytosis and inflammatory responses.[78] APOE4 hiPSC-derived astrocytes also showed upregulation of lipid metabolism-related genes and downregulation of lipid transport-related genes.[54] Notably, selective ablation of neuronal APOE4 in PS19-APOE4 mice reduced the abundance of one DAA subtype, referred to as neuronal APOE4-promoted DAA (nE4-DAA), which showed increased expression of APOE and cathepsin genes.[24] Intriguingly, the reduction of nE4-DAAs corresponded with ameliorated AD pathologies.[24] Thus, the emergence of DAA subtypes may also be brought about indirectly by the effects of neuronal APOE4 expression (see below).

Taken together, these studies demonstrate that astrocytic APOE4 can enhance diverse aspects of AD pathogenesis directly or indirectly, through exacerbation of amyloid and tau pathology and the promotion of glial reactivity, adoption of a DAA phenotype, proinflammatory cytokine production and release, altered metabolism and BBB disruption (Fig. 1.2b,c).

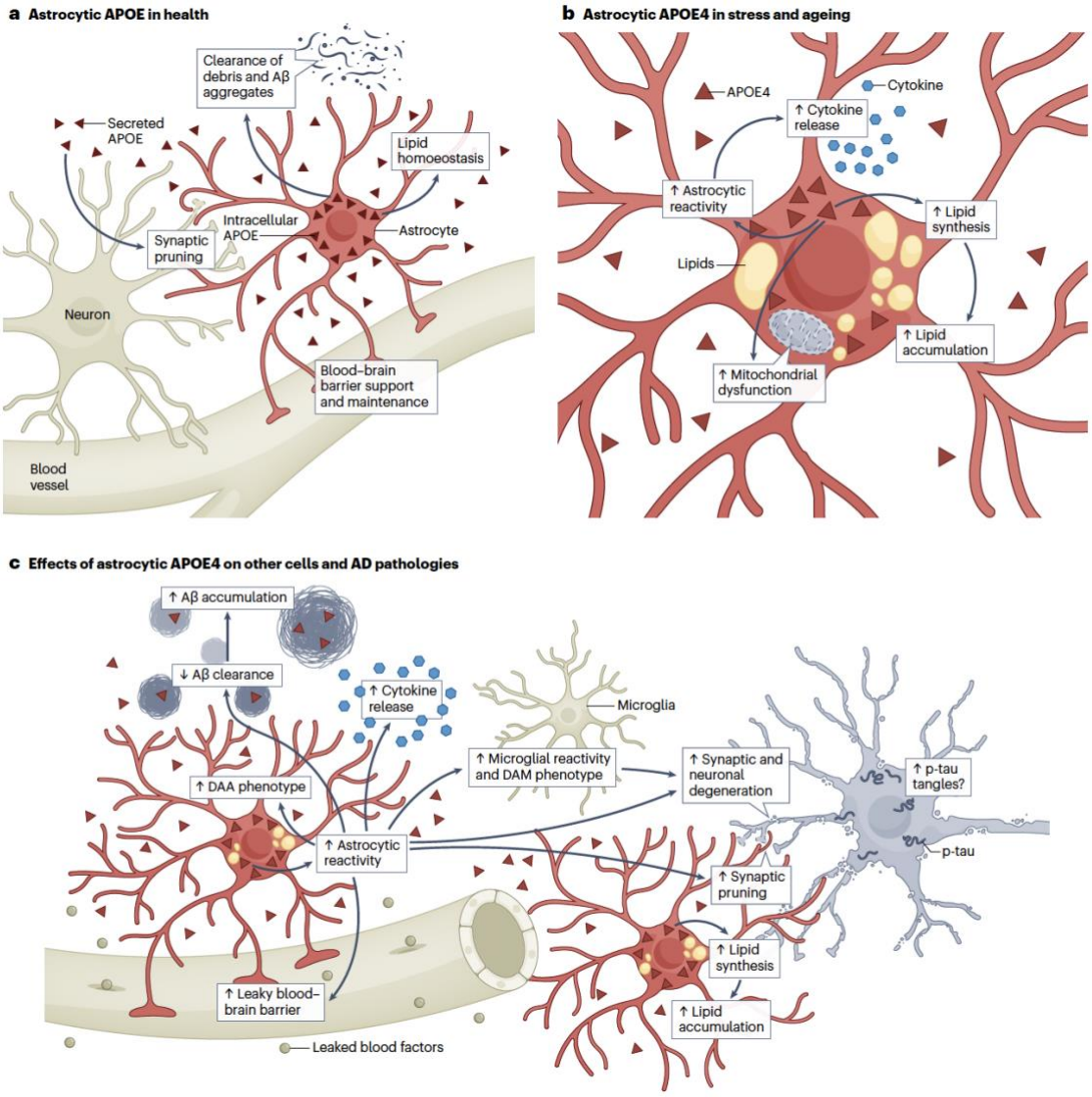


Fig. 1.2 | Expression of APOE4 in astrocytes and its roles in AD pathogenesis

a, Healthy astrocytes produce and secrete most of the apolipoprotein E (APOE) found in the brain.[39–41] This APOE participates in many astrocyte functions, including synaptic pruning, lipid homoeostasis, clearance of amyloid-β (Aβ) aggregates and cell debris, and blood–brain barrier (BBB) support and maintenance.[50–58] **b,** During stress and ageing, astrocytic APOE4 contributes to astrocytic reactivity,[43,50,51,59] elevated pro-inflammatory cytokine release,[50,51,59] augmented mitochondrial dysfunction,[63–66] and increased lipid synthesis[31,53–55,60] and intracellular lipid accumulation.[31,51,53–55,60] **c,** Astrocytic APOE4 also affects other CNS cells and can promote AD pathologies. For example, it drives an increase in microglial reactivity and adoption of a disease-associated microglia (DAM) phenotype.[43] *(figure caption continued on next page)*

(figure caption continued from the previous page). In addition, it contributes to AD pathogenesis by increasing astrocytic reactivity,[43,50,51,59] the transition to a disease-associated astrocyte (DAA) phenotype,[78] cytokine release,[50,51,59] synaptic pruning[43,52] and lipid accumulation.[31,51,53–55,60] In turn, these changes may lead to BBB leakiness,[57,58,70] Aβ accumulation,[51,54,71,74] tau accumulation[43,77] and (in conjunction with neuronal APOE4) synaptic and neuronal degeneration.[43] The potential relationships among the effects of astrocytic APOE4 on other cells and AD pathologies are depicted using arrows. Note that non-astrocytic sources of APOE4 have been omitted from this figure for clarity.

Neuronal APOE4 in AD pathogenesis

Expression and regulation of neuronal APOE

Under physiological conditions, mammalian neurons express low levels of APOE (Fig. 1.3a), contributing approximately 15–20% of total brain APOE in mice (Fig. 1.1c).[24,42] However, they upregulate APOE expression in response to stress and aging (Fig. 1.3b).[39,82–89] snRNA-seq studies of WT mice, human *APOE*-KI mice and human brains from young subjects or from older individuals with AD have shown that APOE is expressed in both inhibitory and excitatory neurons, albeit at lower levels than in astrocytes.[24,90] Interestingly, unlike astrocytes, which secrete most of the APOE that they produce, neurons secrete only about 10% of the APOE that they generate,[48] likely setting the stage for its intracellular accumulation.

The cellular and molecular mechanisms that control neuronal APOE expression are not fully understood. One study identified a neuron-specific splicing variant of *APOE* mRNA with an intron-3 retention (*APOE-I3*) that may help regulate neuronal APOE expression (Fig. 1.3a).[91] The authors suggested that *APOE* transcripts are continuously produced in neurons under normal conditions, and the subsequently generated *APOE-I3* pre-mRNA is retained in the nucleus without being translated. However, in response to neuronal stress or injury, it is quickly processed into mature

APOE mRNA for protein translation (Fig. 1.3b).[91] Consistent with this model, neuronal APOE expression is increased in response to CNS injury, potentially enabling time-sensitive neuronal protection and repair.[92,93] Indeed, neuronal APOE may be important for neurogenesis[94] and neuronal remodeling (Fig. 1.3a).[1,95] RNA-seq analysis has shown that the abundance of *APOE-I3* transcripts in the brains of individuals with AD is related to the severity of tau and amyloid pathologies.[96] Interestingly, the level of *APOE-I3* transcripts increased with the number of *APOE ε4* alleles that an individual possessed,[96] possibly reflecting increasing levels of neuronal stress and injury. A recent study identified a stress-inducible transcriptional mechanism involving R-loops and RNA abasic sites that regulates an enhancer RNA that activates *APOE* transcription in non-neuronal cells.[97] An interesting question is whether this enhancer RNA also regulates *APOE* expression in stressed neurons and, if so, whether it affects the production or splicing of *APOE-I3* pre-mRNA.

Like astrocytic APOE expression, neuronal APOE expression is also regulated by C/EBPβ (Fig. 1.3b).[45,98] Notably, C/EBPβ promotes the expression of APOE4 more than APOE3.[45,98] Interestingly, neuronal APOE has also been found to stimulate C/EBPβ activation, resulting in a feed-forward loop in which downstream AD pathology can be further exacerbated.[98] In addition, astrocytes may secrete factor(s) that regulate neuronal APOE expression through an extracellular signal-regulated kinases (ERK)-dependent pathway,[48] possibly by promoting the splicing of *APOE-I3* into mature *APOE* mRNA (Fig. 1.3b).[91] Clearly, further studies are needed to fully elucidate the mechanisms that regulate neuronal APOE expression.

Neuronal APOE4 causes cellular and network dysfunction

Neuronal APOE4 can have detrimental effects on synaptic and neuronal network functions (Fig. 1.3b,c) that occur early in life. Neuron-specific APOE4 expression in mice with a mouse *ApoE*-KO background resulted in synaptic loss as well as learning and memory deficits at 6–9 months of age.[99–101] This APOE4-induced synaptic loss may be related to an increase in phosphorylation of vasodilator-stimulated phosphoprotein (VASP) S235 that disrupts its interactions with numerous actin cytoskeletal and microtubular proteins.[102] A recent preprint reported that ex vivo hippocampal neurons taken from 7–9-month-old *APOE4*-KI mice, compared to *APOE3*-KI controls, displayed hyperexcitability that was prevented by removal of neuronal, but not astrocytic, APOE4.[103] This neuronal hyperexcitability persisted as the mice aged, probably due to an age- and APOE4-dependent loss of inhibitory tone.[103,104] Recordings of local field potentials in 6–8-month-old *APOE4*-KI mice revealed reductions in hippocampal sharp wave ripple (SWR) activity and in the power of associated slow gamma oscillations, which are critical for memory consolidation.[105,106] Strikingly, the presence of a SWR-associated slow gamma oscillation deficit at a younger age predicted the development of learning and memory impairments 10 months later in these mice.[105,106] Moreover, selective removal of neuronal, but not astrocytic, APOE4 — especially from GABAergic interneurons — prevented these abnormalities,[42,103,105] highlighting the pathogenic importance of neuronal APOE4. In fact, the extent of APOE4-induced GABAergic interneuron loss (especially somatostatin (SST)-expressing interneuron loss) correlated with the severity of learning and memory deficits in aged *APOE4*-KI mice.[42,107,108] Interestingly, in *APOE*-KI mice, APOE expression in SST interneurons was ~40% higher than it was in dentate gyrus granule

cells and CA1 neurons, suggesting that higher APOE expression (especially APOE4) renders SST interneurons selectively vulnerable to degeneration and loss in AD.[90]

Although the mechanisms by which neuronal APOE4 impairs the functions and survival of neurons remain to be fully defined, several studies suggest that impairments of specific subcellular compartments may be involved. Neuronal APOE4 impairs the function and integrity of mitochondria (Fig. 1.3b,c),[95,109–111] which could result in energy failure. Primary neurons from transgenic mice with neuron-specific expression of APOE4 had reduced levels of mitochondrial respiratory complexes, as compared to those expressing APOE3.[112] Proteomic analysis of mouse neuroblastoma cell lines expressing human APOE4 versus APOE3 yielded compatible results.[113] Notably, no significant differences in the levels of neuronal mitochondrial complexes were detected in transgenic mice expressing APOE4 versus APOE3 specifically in astrocytes, making it unlikely that these changes result from the indirect effects of astrocytic APOE4.[112] In a similar vein, neuronal (but not astrocytic) expression of APOE4 sensitized mice to excitotoxin-induced neurodegeneration.[114] In humans with early-stage AD[115] and in cultured neuronal cells,[116] APOE4 is also associated with neuronal endo-lysosomal defects (Fig. 1.3c), which could contribute to its detrimental effect on receptor recycling and synaptic plasticity.[69]

Neuronal APOE4 and hallmark AD pathologies

Neuronal APOE4 also affects major AD pathologies, including amyloid and tau pathologies, gliosis, neurodegeneration and myelin deficits (Fig. 1.3c). APOE4 hiPSC-derived neurons produced more Aβ, had higher levels of APOE fragments and p-tau and more degeneration of GABAergic neurons

than APOE3 controls.[85] These pathologies were rescued by gene-editing of APOE4 to APOE3.[85] In another study, APOE4 hiPSC-derived neurons were more susceptible to cytotoxicity than APOE3 controls and had higher p-tau levels.[117] Although the mechanisms that link neuronal APOE4 and p-tau remain to be fully defined, several interesting leads have emerged. For example, heparan sulfate proteoglycans (HSPGs) are cell-surface receptors that interact more strongly with APOE4 than APOE3[13,118] and are involved in the inter-neuronal spread of tau.[119–121] Treatment of APOE4 neurons with an HSPG inhibitor reduced their p-tau levels.[117] Moreover, APOE4 hiPSC-derived neurons carrying the APOE-R136S mutation, which strongly protects against ADAD,[122,123] had lower p-tau levels and reduced tau uptake via HSPG than isogenic APOE4 neurons without this mutation.[28] Taken together, these results identify HSPGs as a critical mediator of copathogenic interactions between APOE4 and tau.

The effects of neuronal APOE4 on AD pathologies are also evident in vivo. In transgenic mice, expressing APOE4 in neurons increased neuronal p-tau levels, whereas expressing APOE4 in astrocytes did not,[75,76] indicating that neuronal APOE4 is more directly linked than astrocytic APOE4 to neuronal p-tau accumulation. In PS19-APOE4 mice, selective removal of APOE4 from neurons markedly reduced tau pathology,[24] whereas selective removal of astrocytic APOE4 in a similar model lowered p-tau levels only moderately[43] (an effect that might have resulted secondarily from a reduction in astrocytosis and microgliosis).[124] Moreover, neuronal, but not astrocytic APOE4 promoted excitotoxic neuronal death.[114] A recent study further suggests that neuronal APOE4 activates C/EBPβ, which regulates the expression of *APP*, *MAPT* (the gene encoding tau) and beta-secretase 1 (*BACE1*, encoding an enzyme involved in APP processing),

promoting Aβ deposition, tau aggregation, and neurodegeneration.[98] A recent preprint has reported that, in experiments in which APOE4 hiPSC-derived neurons were transplanted into the hippocampi of *APOE4*-KI mice in conjunction with microglial depletion, both human neuronal APOE4 and microglia were important for the formation of dense-core Aβ plaques and tau aggregates.[125]

Although the mechanisms linking neuronal APOE4 to the pathological hallmarks of AD are likely multifarious, diverse lines of evidence suggest several mechanisms that have a prominent role and may make interesting targets for therapeutic interventions. One of these mechanisms involves the intraneuronal proteolytic cleavage of APOE, to which APOE4 is much more susceptible than APOE3, and which results in the generation of C-terminally truncated, neurotoxic APOE fragments.[22] Such APOE4 fragments can elicit the formation of intraneuronal p-tau accumulation and neurodegeneration in neuronal cultures and transgenic mice[22,126] and reduce Ab clearance in mutant APP transgenic mice.[127] Transgenic mice expressing full-length APOE4 in neurons showed an age-dependent accumulation of APOE4 fragments in the hippocampus, whereas transgenic mice expressing APOE4 in astrocytes did not.[75] Furthermore, APOE4 hiPSC-derived neurons[85] and AD brains from APOE4 carriers[126,128] had higher levels of APOE fragments than those from non-carriers. Taken together, these findings indicate that APOE4 proteolysis in neurons promotes the intraneuronal accumulation of p-tau as well as other AD-related neuronal deficits (Fig. 1.3b,c).

Another mechanism linking APOE4 to such deficits is the interaction between neuronal APOE and major histocompatibility complex class 1 (MHC1) molecules (Fig. 1.3b,c). Neuronal expression of APOE and MHC1 molecules have been shown to be tightly and positively correlated, and reducing neuronal MHC1 molecule levels resulted in reduced intraneuronal accumulation and mislocalization of p-tau in mouse primary neurons overexpressing APOE4.[90] It was proposed that the APOE4-induced increase in neuronal MHC1 molecule expression serves as an 'eat me' signal to recruit microglia (and potentially T cells) to engage with the 'tagged' neurons, causing synaptic and neuronal loss.[90] In line with this model, selective removal of APOE4 from neurons in PS19-APOE4 mice markedly reduced not only tau pathology, but also gliosis, neurodegeneration and myelin deficits in the hippocampus.[24] More specifically, PS19-APOE4 mice exhibited significantly higher levels of pathological tau accumulation, astrocytosis, microgliosis, hippocampal neuronal loss and myelin deficits compared to PS19-APOE4 mice in which neuronal APOE4 was selectively removed, suggesting that neuronal APOE4 is an upstream initiator and potent driver of these AD-related pathologies and that its removal is sufficient to attenuate these phenotypes.[24]

In addition to MHC1 molecules, another proinflammatory molecule that may promote pathogenic neuronal–glial interactions is high mobility group box 1 (HMGB1). Compared to APOE3, neuronal expression of APOE4, together with tau pathology, increased the nucleo-cytoplamic translocation and cellular release of HMGB1. This triggered gliosis, likely by binding to toll-like receptors (TLRs) on glial cells (Fig. 1.3c).[129] Clinical studies of individuals with MCI have revealed an increase in HMGB1 levels in their cerebrospinal fluid (CSF)[130] and an interactive association of APOE4 and plasma HMGB1 levels with widespread cortical thinning.[131] Notably,

pharmacological inhibition of HMGB1 release from neurons ameliorated neuroinflammation, neurodegeneration and myelin deficits in PS19-APOE4 mice.[129] Interestingly, HMGB1 can upregulate MHC1 molecule expression in response to cellular stress.[132,133] Thus, in response to neuronal APOE4 expression, HMGB1 and MHC1 molecules may act in concert to trigger glia-mediated synaptic and neuronal degeneration (Fig. 1.3c).

APOE4 in Disease-associated neuronal subtypes

snRNA-seq studies have identified neuronal states that are enriched in disease, known as disease-associated neuron (DAN) phenotypes. A comparative snRNA-seq analysis identified two excitatory neuronal clusters with abnormally high expression of genes encoding major heat shock proteins, calmodulin, and ubiquitin B in the hippocampus of PS19-APOE4 mice that were not seen in PS19-APOE4 mice with neuronal APOE4 removal (these were referred to as neuronal APOE4-promoted DAN or nE4-DAN).[24] nE4-DAN had high levels of APOE4 expression, as compared to other excitatory neuron subpopulations, and were associated with high levels of tau pathology and hippocampal atrophy (Fig. 1.3c).[24]

Relative levels of APOE expression may also provide insight into the vulnerability of different subtypes of neurons in AD. In *APOE4*-KI mice, snRNA-seq revealed higher levels of APOE4 expression in inhibitory than excitatory neurons,[90] paralleling the earlier onset of the detrimental effects of APOE4 on inhibitory neurons.[42,107,108] In a similar vein, snRNA-seq analyses of human cortices from individuals with AD revealed that disease progression was related to the proportion of neuronal cells, especially inhibitory interneurons, expressing high levels of APOE.[90,134]

Specifically, the proportion of APOE-expression-high neurons, especially inhibitory neurons, was relatively low in individuals with no cognitive impairment, was highest in individuals with MCI, and was relatively low in individuals with AD. This pattern suggests that neuronal (especially inhibitory neuronal) APOE expression is upregulated early in the clinical progression of AD and declines thereafter as neurodegeneration advances,[90] which is in line with the observation that vulnerable inhibitory neuron subtypes were selectively depleted in the brains of individuals with AD.[135]

In summary, in response to stress, aging or disease, some (but not all) neurons increase their APOE expression (Fig. 1.3b). In APOE4 carriers (to a greater extent than in APOE3 carriers), this process results in the intraneuronal generation of neurotoxic APOE fragments, neuronal dysfunction, the emergence of nE4-DAN and the overproduction or increased release of proinflammatory molecules, triggering glial responses that further promote synaptic and neuronal degeneration (Fig. 1.3b,c). Specific subpopulations of inhibitory neurons produce more APOE and may also be more vulnerable to detrimental APOE4 effects than other types of neurons. Their dysfunction and loss lead to excitation-inhibition imbalance and network hyperexcitability, which is associated with faster cognitive decline in AD.[136,137] Thus, neuronal APOE4 is likely to be a critical upstream pathogenic initiator and driver that directly or indirectly affects many AD-related cell types, genes and pathways (Fig. 1.3c).

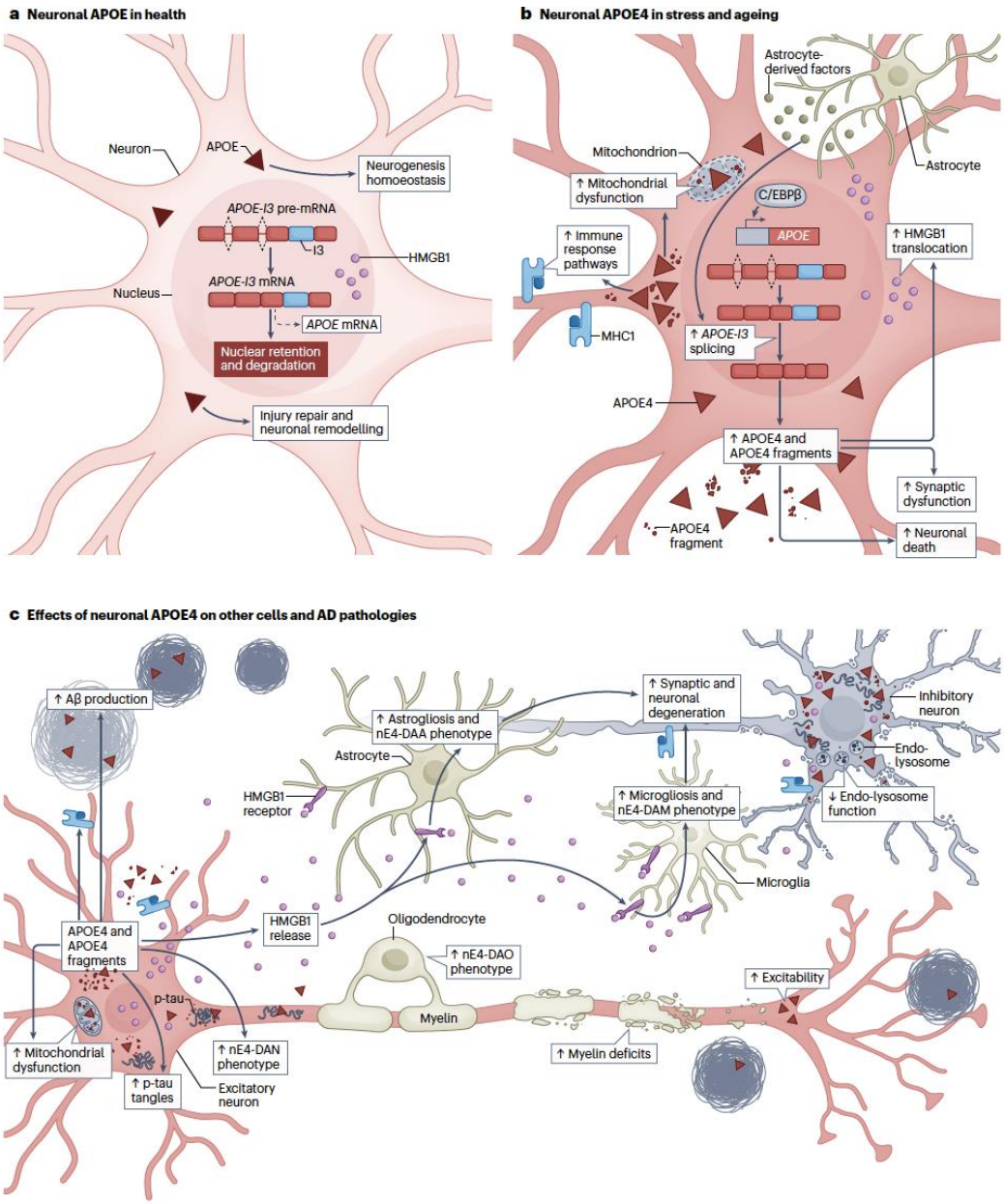


Fig. 1.3 | Expression of APOE4 in neurons and its roles in AD pathogenesis.

a, Healthy neurons express low levels of apolipoprotein E (APOE)[39,82–89]: the APOE mRNA they produce has an intron 3 retention (APOE-I3 mRNA), which ensures that it is largely retained in the nucleus, in which it is degraded rather than being processed into mature APOE mRNA.[91] Neurons also retain high mobility group box 1 (HMGB1), a pro-inflammatory molecule, within the nucleus.[129] Neuronal APOE is involved in the maintenance of neurogenesis,[94] injury repair,[92,93] and neuronal remodelling.[1,95] **b,** Under conditions of stress and ageing, neurons increase APOE expression by active splicing of APOE-I3 into mature APOE mRNA.[91] *(figure caption continued on next page)*

(figure caption continued from the previous page). The transcription factor C/EBPβ[45,98] and astrocyte-derived factor(s)[48] also upregulate APOE expression in neurons. Increased neuronal APOE4 production leads to increased APOE4 fragmentation,[22,75,85,126,128] expression of immune response pathway genes (such as major histocompatibility complex class 1 (MHC1) genes),[90] nucleo-cytoplasmic translocation of HMGB1,[129] mitochondrial dysfunction,[95,109–113] synaptic dysfunction,[99,101] and neuronal death.[24,85,90,98,114] **c,** Neuronal APOE4 affects other CNS cells. For example, it increases astrogliosis and the adoption of a neuronal APOE4-promoted disease-associated astrocyte (nE4-DAA) phenotype[24], microgliosis and the adoption of a neuronal APOE4-promoted disease-associated microglial (nE4-DAM) phenotype,[24] the adoption of neuronal APOE4-promoted disease-associated oligodendrocyte (nE4-DAO) phenotype and myelin deficits.[24] Neuronal APOE4 also increases intraneuronal tau tangles,[24,75,76,85,98] endo-lysosomal dysfunction,[115,116] neuronal hyperexcitability,[103–106] amyloid-β (Aβ) production and accumulation,[85,98] the adoption of a neuronal APOE4-promoted disease-associated neuronal (nE4-DAN) phenotype,[24] HMGB1 release (resulting in binding with its receptors on glial cells and consequently inducing gliosis),[129] neuronal MHC1-mediated microglia engagement,[90] and synaptic and neuronal degeneration.[24,85,90,98,114] The potential relationship among these neuronal APOE4 effects on other cells and AD pathologies is depicted using arrows. Note that non-neuronal sources of APOE4 have been omitted for clarity. APOE4, E4 isoform of apolipoprotein E.

Microglial APOE4 in AD pathogenesis

Expression and regulation of microglial APOE

Like neurons, microglia can express APOE in a stress and injury-dependent manner (Fig. 1.4a,b).[39,47,138–140] While APOE expression is low in microglia under normal conditions (Fig. 1.4a), microglia in both aging and diseased brains have been shown to greatly upregulate their APOE expression (Fig. 1.4b).[39,138–142] For instance, microglial APOE expression was increased in aged human *APOE*-KI mice,[141] PS19 mice,[33] and 5xFAD mice.[139] Notably, microglia surrounding Aβ plaques displayed the greatest increase in APOE expression.[124,140,143]

The low-density lipoprotein receptor (LDLR) pathway may directly or indirectly contribute to the regulation of APOE expression in microglia, as LDLR overexpression in microglia in mice suppressed microglial activation and expression of APOE.[33] APOE produced by other CNS cells

may also affect microglia, as selective removal of neuronal APOE4 in PS19-APOE4 mice decreased the sizes of populations of microglia exhibiting high levels of APOE expression.[24] This suggests that neuronal APOE4, or the pathological alterations that it causes, augment microglial APOE expression. Since microglia have been implicated in a variety of APOE4-related AD pathologies,[23,144] it is crucial to understand the effects of microglia-derived APOE4.

Microglial APOE4 in metabolism and lipid accumulation

APOE genotype influences microglial metabolism and lipid accumulation (Fig. 1.4b). Homeostatic microglia have been shown to rely on oxidative phosphorylation for energy production, while activated microglia with high APOE expression shift toward the glycolytic pathway and increase their expression of hypoxia inducible factor 1-alpha (HIF1a), a gene highly upregulated during glycolysis.[141,145] These findings are in line with observations indicating that aged *APOE4*-KI mice had increased aerobic glycolysis and higher HIF1a expression.[141]

Emerging evidence highlights the role of APOE in microglial lipid metabolism and accumulation (Fig. 1.4b). APOE is a major lipid transporter between neurons and glial cells.[11,19] APOE-containing lipid particles produced by APOE4-KI mouse microglia were smaller than those produced by astrocytes, implying cellular source-dependent differences in the lipidation state of APOE.[146] Furthermore, lipid droplet accumulation was a major phenotype observed in aged and diseased microglia (Fig. 1.4b,c).[27,29,147,148] Similarly, APOE4 hiPSC-derived microglia (hiMGL) accumulated more lipid droplets than APOE3 microglia.[27,149] Additionally, when human APOE was selectively expressed in microglia in an amyloidosis model in which mice expressing APP harboring the

Swedish FAD mutation are crossed with mice in which PSEN1 exon 9 is deleted *(APPswe/PS1ΔE9 mice)* on a mouse *ApoE*-KO background, APOE4 microglia showed increased lipid accumulation compared to APOE3 microglia.[149] APOE4 microglia also demonstrated excessive buildup of lipid droplets in *APOE*-KI mice fed with cuprizone, which induces demyelination, compared to APOE3 and APOE2 microglia, indicating an impairment in lipid metabolism in APOE4 microglia in response to demyelination.[150]

Notably, in hiMGL, human post mortem brains, and *APOE*-KI mouse brains, APOE4 increased de novo cholesterol synthesis in microglia and impaired cholesterol trafficking, possibly through lysosomal sequestration.[60] Several other studies also showed that microglial APOE4 expression caused lysosomal dysfunction through aberrant lysosomal trafficking[151] and impaired endosomal-lysosomal activities.[86,151,152] Additionally, during de novo fat synthesis, APOE4 hiMGL exhibited lipogenesis that promoted proinflammatory signals and reduced the uptake of extracellular fatty acids and lipoproteins, thereby disrupting neuronal network activity.[147]

Microglial APOE4, functional deficits and AD pathologies

Microglial APOE appears to be a key regulator of microglial function and reactivity, which consequently affect global brain health and disease progression (Fig. 1.4b,c). Ingenuity pathway analysis (IPA), a pathway analysis application used for high throughput omics data analysis, on isolated microglia from APP-PS1 mice revealed that APOE affected the relative proportions of homeostatic microglia versus microglia associated with neurodegeneration.[143] In *APOE*-KI mice, APOE4 microglia displayed increased activation and exacerbated pro-inflammatory

responses[86,152] and, in postmortem human brains, APOE4 carriers had increased numbers of microglia compared to non-carriers.[153,154] In hiMGL, APOE4 promoted a more reactive morphology and enhanced inflammatory gene signatures compared to APOE3.[54] Lastly, when stimulated with lipopolysaccharide (LPS), microglia from *APOE4*-KI mice exhibited higher levels of proinflammatory signals compared to microglia from *APOE3*-KI mice.[155]

APOE genotype also influences vital microglial functions such as phagocytosis and chemotaxis (Fig. 1.4a,b).[53,156] For instance, in murine N9 microglia expressing human APOE isoforms, those expressing APOE4 showed impaired phagocytosis of $A\beta_{42}$ (an aggregation prone form of Aβ peptides) and dysfunctional motility.[156] Moreover, in *APPswe/PS1ΔE9* mice that received bone marrow transplants from human *APOE4*-KI mice (APOE4-*KI*-BMT*),* microglia exhibited reduced association with Aβ deposits and dystrophic changes and amyloid plaques were larger and more abundant than in *APPswe/PS1ΔE9 mice that received* APOE3-*KI-BMT.*[157] Meanwhile, selectively removing microglial APOE4 in APP/PS1 mice led to significant reduction in plaque loads compared to APOE4-APP/PS1 mice,[158] suggesting a 'gain-of-toxic' effect of APOE4 on microglia-mediated Ab clearance. Similarly, when APOE was selectively expressed in microglia in *APPswe/PS1ΔE9* mice on a mouse *ApoE*-KO background, the presence of APOE3 microglia sufficiently protected against the development of amyloid pathology, whereas APOE4 microglia did not.[149] This defective response of APOE4 microglia to Aβ pathology seemed to be mediated by the APOE4–ITGB8–TGFβ pathway, which acted as a negative regulator.[158] A similar defective response of APOE4 microglia to Aβ was also observed in a chimeric model in which hiPSC-derived neurons were transplanted into *APOE*-KI mouse hippocampus: here, APOE4 microglia tended to colocalize less with Aβ

deposits than APOE3 microglia.[159] Mechanistically, IL-33 has been shown to mediate microglial migration towards APOE-associated Ab plaques by inducing microglial VCAM1, and when this VCAM1–APOE interaction was disrupted, Ab clearance was reduced in APP/PS1 mice.[160]

In contrast to these effects, APOE4-expressing microglia actually exhibited increased phagocytosis of apoptotic cells in culture (N9 murine microglia overexpressing APOE4)[156] and increased synaptic engulfment in PS19-APOE4 mice (Fig. 1.4c).[161] Some studies even suggest that microglia may actively participate in tau spreading and seeding.[162–164] According to these studies, reactive microglia may phagocytose tau or tau-containing synapses and/or neurons. Due to APOE4-dependent lysosomal defects and resulting inefficiencies in processing the internalized tau,[86,151,152] pathological tau aggregates then begin to accumulate within the microglia and are released via exosome transfer to spread and seed tau pathology (Fig. 1.4c).[162–164] Consistent with this model, a human brain imaging study found greater levels of microglial activation and tau accumulation in medial temporal structures of APOE4 carriers than in non-carriers, possibly contributing to their increased neurodegeneration and clinical impairment.[165] Likewise, a recent preprint has reported that, in a chimeric AD model in which APOE4 hiPSC-derived neurons were transplanted into *APOE4*-KI mouse hippocampus, microglial depletion reduced human neuronal APOE4-driven tau pathology.[125] Interestingly, selectively removing microglial APOE4 in PS19-APOE4 mice restored microglia to a neuroprotective phenotype[158] and microglial depletion in these mice reduced tau pathology and neurodegeneration, possibly by reducing cerebral infiltration by T cells responding to MHC2 molecule-expressing microglia (Fig. 1.4c).[166]

APOE4 in disease-associated microglial subtypes

Microglia are an extremely heterogeneous cell type whose roles and functions in the CNS confer unique spatial-temporal gene signatures. The transcriptional profile of microglia is markedly altered in AD and in the presence of APOE4, with an increased proportion of microglia showing disease-associated rather than homeostatic profiles.[140,152,167] Disease-associated subtypes or states of microglia include disease-associated microglia (DAM),[140,152] lipid-droplet-accumulating microglia (LDAM),[29] interferon responsive microglia (IRM),[168] and antigen-presenting microglia (MHC2-M).[161,168] Among these, DAM and LDAM have been studied most extensively in the context of APOE4 (Fig. 1.4c).

DAM are characterized by increased expression of genes associated with proinflammatory immune responses, phagocytosis and lipid metabolism, and decreased expression of genes associated with surveillant microglia.[140,152] Interestingly, even in the absence of overt AD pathology, the combination of APOE4 and aging was sufficient to elicit changes in microglia of *APOE4*-KI mice that strongly resembled the DAM phenotype.[141] In AD-related mouse models with amyloid or tau pathology, DAM localized around Aβ plaques and NFT-bearing neurons.[169] Remarkably, selectively ablating endogenous microglial APOE using *Cx3cr1-Cre*:*ApoE* mice prevented the emergence of microglia with a neurodegenerative phenotype (MGnD, another type of DAM), compared to WT mice.[143] The same study showed that global *ApoE*-KO conferred no additional protection, suggesting that microglial APOE is particularly crucial in initiating the appearance of MGnD.[143] However, selectively removing microglial APOE4 in APP/PS1/APOE4 or PS19-APOE4 mice increased MGnD[158] and, conversely, selectively expressing APOE4 in microglia

in *APPswe/PS1ΔE9* mice on a mouse *ApoE*-KO background decreased activated response microglia (ARM, another type of DAM), which highly expressed MHC genes.[149] Together, these findings suggest that mouse APOE and human APOE4 might affect MGnD and ARM differently, which warrants further in-depth study. It should be noted that the proportion of DAM was not reduced in PS19-APOE4 versus PS19-APOE3 mice in other studies.[24,28,43,129]

As may be expected, DAM (or MGnD) have increased APOE expression, which precedes the decrease in homeostatic markers (such as P2Y purinoceptor 12 (P2RY12) and C–X–C motif chemokine ligand 3 (CXCL3)) and increase in disease-associated signatures (including lipoprotein lipase (LPL), cystatin-F (CST7), and secreted phosphoprotein-1 (SPP1),[140,143] suggesting that APOE influences microglial gene expression. Human *APOE4* carriers and human *APOE*-KI mice crossed with APP/PS1 mice or stimulated with LPS demonstrate that APOE4 primes microglia for conversion into the phagocytic and proinflammatory state of DAM or promotes the proliferation of such cells.[167] In PS19-APOE4 mice with or without neuronal APOE4 removal, neuronal APOE4-promoted DAM (nE4-DAM) subtypes were identified and found to positively associate with tau pathology and hippocampal degeneration.[24] Furthermore, introduction of the APOE-R136S mutation, which protects against ADAD,[122,123] markedly reduced the number of DAM as well as tau pathology and neurodegeneration in PS19-APOE4 mice.[28] Interestingly, removing APOE4 selectively from astrocytes[43] or neurons[24] in PS19-APOE4 mice also decreased DAM and nE4-DAM, respectively, suggesting that both astrocytic and neuronal APOE4 promote the emergence of DAM subtypes.

LDAM are another emerging subtype of diseased microglia, defined by an increased expression of genes, such as *ACSL1*, that are involved in pathways related to lipid handling, transport and metabolism.[29] LDAM also exhibit an accumulation of lipid droplets in the cell soma, which may indicate increased endogenous lipid production, excessive uptake of extracellular lipids from degenerating neurons, or an inability to degrade lipids.[29] Notably, APOE4 hiMGL show more lipid droplet accumulation than APOE3 microglia.[27,147,149] Recent research has raised the possibility that dysfunctional lipid metabolism and lipid droplet formation in APOE4 microglia impair microglial surveillance of neuronal network activity.[147] Furthermore, a recent preprint has reported that this can promote neuronal p-tau accumulation and neurotoxicity.[27] Interestingly, introduction of the protective APOE-R136S mutation markedly reduced lipid droplet accumulation in microglia of PS19-APOE4 mice.[28]

Beyond DAM and LDAM, other disease-associated microglial subtypes continue to be identified. For example, in a chimeric AD model in which APOE4 hiPSC-derived neurons were transplanted into *APOE4*-KI mouse hippocampus, there was an enrichment in microglial subpopulations highly expressing MHC2 genes (MHC2-M) that contributed to neuronal APOE4-promoted Aβ and tau pathologies.[125] Comparing to the data from *APPswe/PS1ΔE9* mice selectively expressing APOE4 in microglia on a mouse *ApoE*-KO background,[149] the data from the chimeric AD model suggest that APOE4 microglia might respond differently to human neuron-produced versus mouse neuron-produced AD pathologies, which warrants further in-depth study. MHC2-M have been found to be enriched in human AD patient brains, close to amyloid plaques and tau tangles.[170,171]

MHC2-M were also enriched in the hippocampus of PS19-APOE4 mice, which was important for recruiting infiltrating T cells.[166]

Altogether, these findings have begun to highlight the heterogeneity of microglia and their differential contributions to AD pathogenesis, especially in the context of APOE4 (Fig. 1.4c). Clearly, microglial APOE4 promotes the emergence of DAM subtypes. Notably, APOE4 in DAM and LDAM may increase the phagocytosis of neuronal synapses containing pathological tau, leading to increased synaptic loss and neurodegeneration. APOE4-associated endo-lysosomal defects in microglia may impede the degradation of pathological tau and promote the accumulation of tau in microglia, a process that may contribute to tau spreading and seeding (Fig. 1.4c). APOE4 also seems to enhance MHC2-M-dependent T-cell infiltration, which may further exacerbate tau pathology and neurodegeneration.

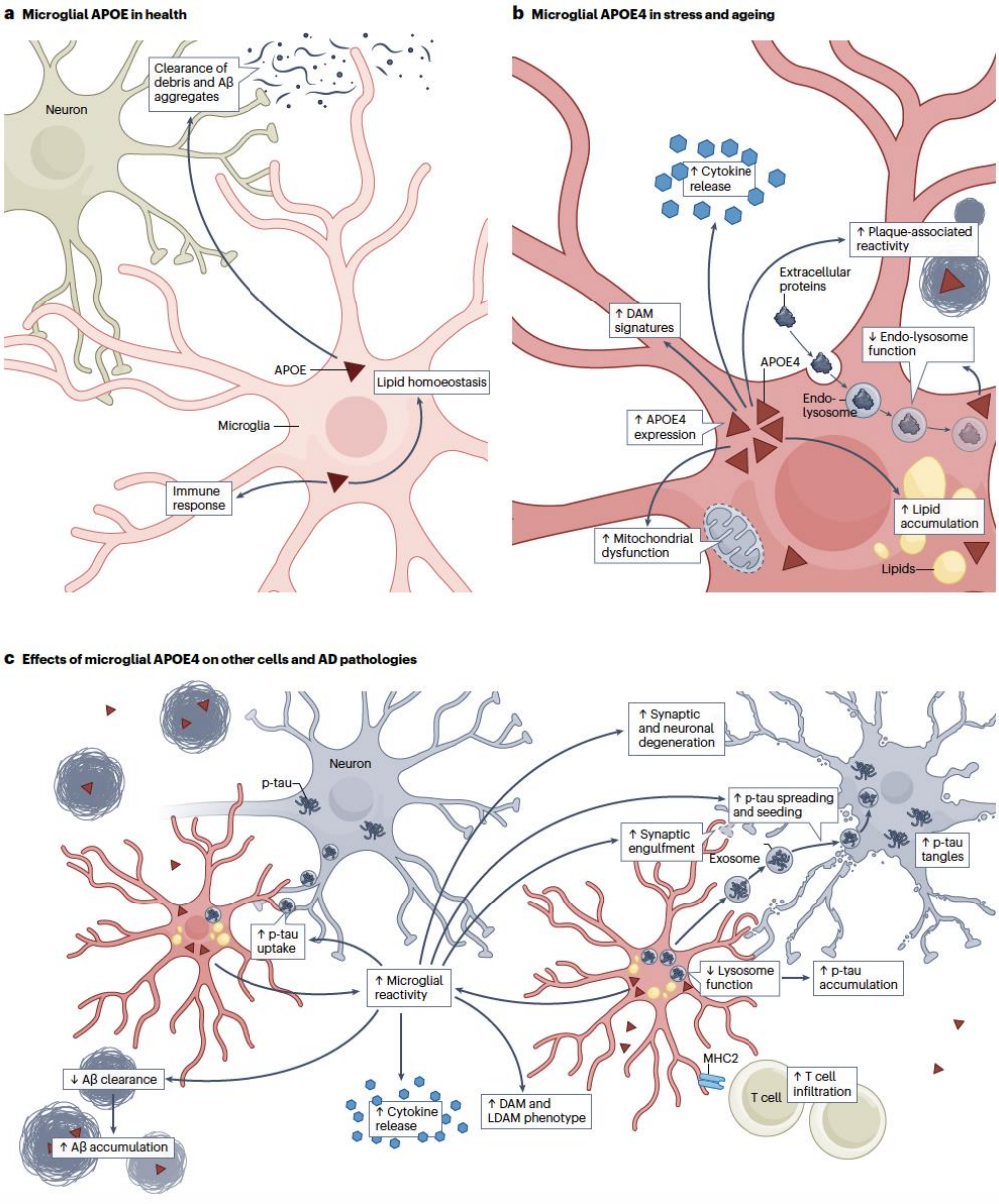


Fig. 1.4 | Expression of APOE4 in microglia and its roles in AD pathogenesis.

a, Healthy microglia express low levels of apolipoprotein E (APOE).[39] This APOE is involved in immune responses, in lipid homoeostasis and in clearing amyloid-β (Aβ) aggregates and cell debris.[23,53,143] **b,** During stress and ageing, microglia increase their APOE expression.[138–141] Microglial APOE4 leads to an increase in amyloid plaque-associated reactivity,[54] lipid accumulation,[27,148] lysosomal defects,[151,152] mitochondrial dysfunction,[141] disease-associated microglial (DAM) signatures,[140,167] and pro-inflammatory cytokine release.[167] *(figure caption continued on next page)*

(figure caption continued from the previous page). **c,** Microglial APOE4 affects other cells, including neurons and T cells,[166] and contributes to AD pathogenesis by reducing Aβ clearance[157] and lysosome function[151] and by increasing synaptic engulfment,[161] p-tau uptake and accumulation,[86,151,152] DAM signatures,[140,152] lipid droplet-accumulating microglia (LDAM)[29,147] and cytokine release.[167] Together, these APOE4-induced microglial dysfunctions facilitate tau spreading and seeding[162–164] and, ultimately, synaptic and neuronal degeneration (in conjunction with neuronal APOE4).[140,152] The potential relationships among these microglial APOE4 effects on other cells and AD pathologies are depicted using arrows. Note that non-microglial sources of APOE have been omitted for clarity. APOE4, E4 isoform of apolipoprotein E; MHC2, major histocompatibilitycomplex class 2.

Oligodendrocytic APOE4 in AD pathogenesis

Expression and regulation of oligodendrocytic APOE

Like the other glial cells of the CNS, oligodendrocytes can express APOE (Fig. 1.5a).[24,31,90] In PS19-APOE4 mice, a subgroup of oligodendrocytes exhibited increased expression of APOE compared to PS19-APOE3 mice.[24] This suggests that increased APOE expression is part of their injury response, and that this is augmented in PS19-APOE4 mice because they have more tauopathy and neurodegeneration than PS19-APOE3 mice (Fig. 1.5b). Consistent with this interpretation, rat primary oligodendrocytes increased their expression and secretion of APOE when they were treated with conditioned medium from mechanically injured neurons.[172] Notably, oligodendrocytic APOE expression is also affected by neuronal APOE, as selective ablation of APOE4 from neurons reduced oligodendrocytic APOE expression in PS19-APOE4 mice.[24]

Oligodendrocytic APOE4 in lipid metabolism and myelination

APOE isoforms differentially affect oligodendrocytic lipid metabolism and myelination (Fig. 1.5a,b). Notably, oligodendrocytes of the prefrontal cortex of human APOE4 carriers exhibited elevation of cholesterol biosynthesis-associated gene expression compared to oligodendrocytes

of non-carriers.[31] Interestingly, this APOE4 effect was gene dose-dependent.[31] Similarly, APOE4 hiPSC-derived oligodendrocytes displayed increased cholesterol synthesis and intracellular cholesterol storage compared to APOE3 oligodendrocytes.[31] The APOE4 oligodendrocytes also had reduced cholesterol localization in the plasma membrane, increased cholesteryl esters and lipid droplets, and elevated endoplasmic reticulum (ER) stress.[31] When co-cultured with hiPSC-derived neurons, APOE4 oligodendrocytes displayed less myelin basic protein (MBP) and axonal colocalization than their APOE3 counterparts (Fig. 1.5b).[31] Furthermore, aged *APOE4*-KI mice showed fewer cells in the oligodendrocyte lineage and an abnormal accumulation of oligodendrocyte precursors, suggesting that APOE4 disrupts oligodendrocyte differentiation and maturation.[173] Indeed, neural stem/progenitor cell differentiation into oligodendrocytes is affected by interactions between APOE and LDLR-related protein-1.[174] Together, these findings raise the possibility that alterations in the differentiation and cholesterol metabolism of oligodendrocytes may causally contribute to the link between APOE4 and AD (Fig. 1.5b), although this hypothesis requires further testing.

APOE4 in disease-associated oligodendrocyte subtypes

snRNA-seq analyses have identified subpopulations of oligodendrocytes that are enriched in brains of patients with neurodegenerative diseases and related mouse models, termed disease-associated oligodendrocytes (DAO) (Fig. 1.5b).[175] In a variety of pathological conditions, including animal models of multiple sclerosis, amyloidosis, tauopathy and aging brains, DAO show increased expression of immune-related genes,[175] suggesting neuroinflammation as a common driver of DAO formation.[175]

Selective neuronal ablation of APOE in PS19-APOE4 mice identified a specific subtype of DAO (neuronal APOE4-promoted DAO or nE4-DAO).[24] nE4-DAO had increased expression of genes encoding APOE, heat shock protein, calmodulin, or ubiquitin B, and reduced expression of genes encoding MBP or myelin-associated oligodendrocyte basic protein, as compared to other oligodendrocyte subpopulations.[24] The number of nE4-DAO was negatively related to hippocampal volume and MBP coverage area and positively related to the extent of tau pathology.[24] Removal of neuronal APOE4 diminished the number of nE4-DAO, demonstrating their dependence on neuronal APOE4 effects. Interestingly, the protective APOE-R136S mutation markedly reduced the number of DAO in PS19-APOE4 mice.[28]

Taken together, these findings suggest that oligodendrocytes respond to APOE4 effects from other types of brain cells, especially neurons (Fig. 1.3c), but are also directly impacted by the APOE isoforms that they express (Fig. 1.5b). The detrimental effects of APOE4, either directly or indirectly, on oligodendrocytes can lead to myelin impairments in AD.

Vascular cell APOE4 in AD pathogenesis

Expression and regulation of APOE in vascular cells

Multiple vascular cell types, including endothelial cells, pericytes, and smooth muscle cells, express APOE (Fig. 1.5c).[39,176–182] Several transcription factors, including C/EBPβ and NFAT, may regulate APOE expression in these cells.[178] Pericytes seem to secrete large amounts of APOE that they produce[39,178,181] and are located in a position in which they can affect the neurovascular junction. Interestingly, both cultured APOE4 hiPSC-derived pericytes and pericytes in the

hippocampus of human APOE4 carriers expressed higher levels of APOE than APOE3 pericytes.[178] Though APOE from vascular cells has been studied much less than APOE produced by other CNS cell types, it is possible that it may also affect brain health and disease in an isoform-dependent manner (Fig. 1.5c,d).

Vascular cell APOE4 in stress and AD

APOE4 produced by vascular cells has detrimental effects on endothelial cell function, pericyte mobility, Aβ-driven cytotoxicity and BBB integrity (Fig. 1.5d).[176–178,183] Human endothelial cells co-cultured with pericytes from *APOE4*-KI mice exhibited reduced extracellular matrix protein production, impaired formation of normal tube-like structures and decreased barrier formation compared to those cultured with APOE3 pericytes.[183] In cultures of primary human brain vascular pericytes in which endogenous APOE3 was 90% knocked down via small interfering RNA treatment, addition of exogenous APOE3 led to typical levels of pericyte migration, whereas cells treated with APOE4 had aberrantly high pericyte mobility.[176] Conceivably, this effect could contribute to BBB dysfunction in AD, as the BBB becomes increasingly vulnerable when pericytes migrate away towards sites of pathology.[176] By increasing pericyte mobility, APOE4 may promote leakiness of this important barrier. In addition, APOE4 increases and activates the BBB-degrading pro-inflammatory cyclophilin A (CYPA)–matrix metalloproteinase 9 (MMP9) pathway in pericytes, leading to breakdown of the BBB via degradation of BBB tight junction proteins.[36,184] Increased activity of this pathway in the CSF of human APOE4 carriers was associated with high baseline levels of soluble platelet-derived growth factor receptor beta (PDGFRB), a marker of pericyte injury linked to BBB breakdown, and this was predictive of future cognitive decline.[35]

APOE isoforms may also differentially affect the susceptibility of pericytes to Aβ (**Fig. 1.5d**). When treated with exogenous Aβ, primary human APOE4-expressing brain pericytes showed higher levels of cell death than their APOE3 counterparts.[177] Similarly, in a 3-dimensional in vitro BBB model that included hiPSC-derived pericyte-like cells, amyloid deposition was highly elevated only in cultures containing APOE4 pericytes.[178] Inhibition of NFAT–calcineurin signaling in pericytes decreased their APOE4 expression and reduced amyloid accumulation in this model.[178] These findings suggest a role for pericyte-derived APOE4 in cerebral amyloid angiopathy (CAA) and pinpoint calcineurin–NFAT signaling as a potential therapeutic target. APOE4 hiPSC-derived endothelial cells exhibited increased binding of platelets and higher secretion of cytokines and Aβ compared to endothelial cells expressing APOE3,[180] indicating that APOE4 may exert detrimental effects also on this cell type (Fig. 1.5d).

Beyond these in vitro models, human APOE4 and APOE3 have been expressed in *ApoE*-KO mice under the control of the smooth muscle cell-specific promoter SM22alpha in vivo.[185] In this model, smooth muscle cell-produced APOE4 reduced cerebral blood flow, decreased synaptic plasticity, and increased astrocyte reactivity.[185] These mice also exhibited increased anxiety-like behavior and impaired spatial learning.[185]

APOE4 in disease-associated vascular cell subtypes

In a transcriptomic study, pericytes demonstrated a number of differentially expressed genes in APOE4 versus APOE3 mice at young and old ages.[34] These included genes critical to cell adhesion, BBB function, inflammatory response, DNA damage and apoptosis.[34] Transcriptomic and protein

analyses of hiPSC-derived pericyte-like cells revealed that, relative to APOE3, APOE4 was associated with increased expression of genes related to protein targeting to the membrane and endoplasmic reticulum and decreased expression of genes related to mitosis and cell cycle progression.[178] In post-mortem brain tissues from individuals with AD, pericytes showed altered expression of genes related to blood flow and vasoconstriction,[182] while pericytes from APOE4 carriers also had downregulation of genes involved in cell migration regulation, transport across the BBB, and cell junction maintenance.[186] In contrast to non-carriers, endothelial cells of APOE4 carriers had increased expression of interferon genes,[182] and decreased expression of genes related to transport across the BBB and cell junction organization.[186] In conjunction with the findings from cell culture and animal models, these single-cell data suggest that vascular cell APOE4 could contribute to AD pathogenesis through multiple mechanisms (Fig. 1.5d).

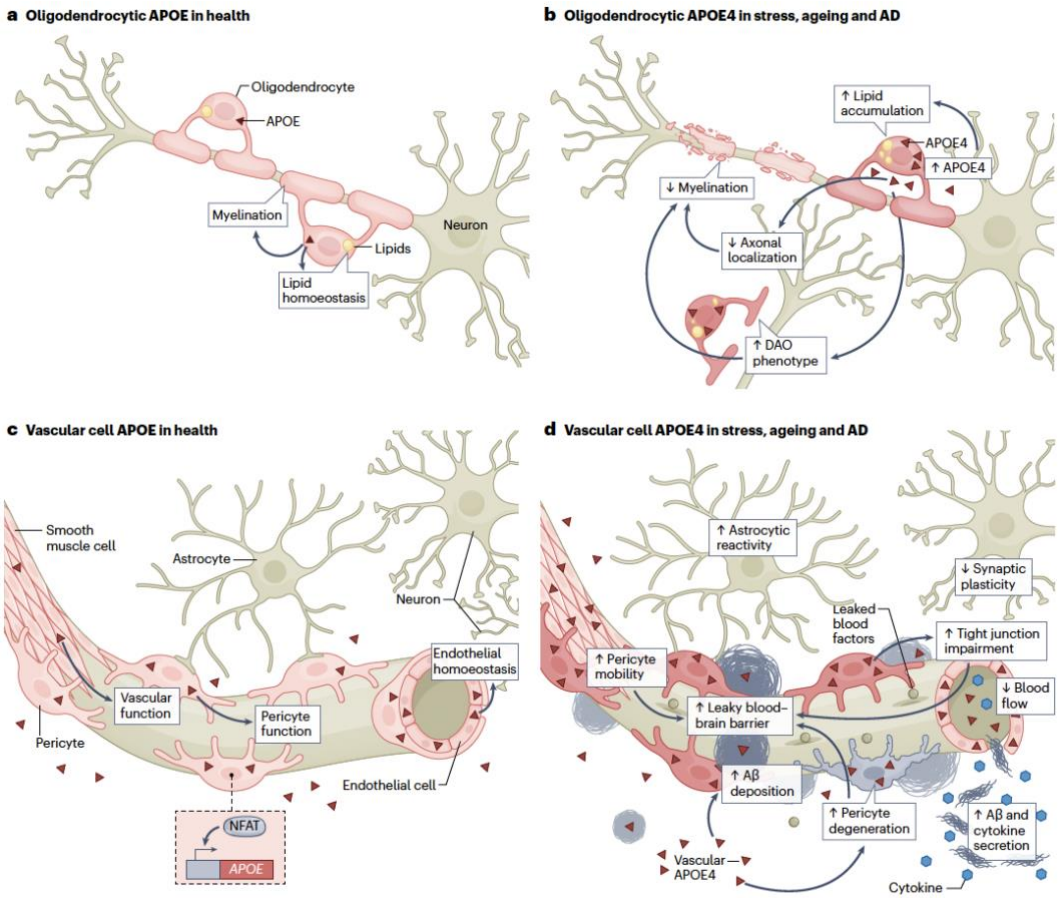


Fig. 1.5 | Expression of APOE4 in oligodendrocytes and vascular cells and its roles in AD pathogenesis.

a, Healthy oligodendrocytes express low levels of apolipoprotein E (APOE).[24,31,90] Oligodendrocytic APOE is involved in lipid homoeostasis and myelination of neurons.[31] **b,** Under conditions of stress, ageing and AD, oligodendrocytes increase their APOE4 expression.[24,172] Oligodendrocytic APOE4 increases intracellular lipid accumulation and disease-associated oligodendrocyte (DAO) phenotypes[24,31] and decreases oligodendrocytic axonal localization and myelination of neuronal axons.[31] The potential relationship among oligodendrocytic APOE4 effects on AD pathologies is depicted using arrows. **c,** Healthy cells of the brain vasculature, including smooth muscle cells, pericytes and endothelial cells, produce and secrete APOE.[39,176–182] The transcription factor NFAT regulates APOE expression in pericytes.[178] Vascular cell-produced APOE is involved in maintaining vascular function, pericyte function and endothelial homoeostasis.[176–178,183] **d,** Under conditions of stress, ageing and AD, vascular cell APOE4 leads to tight junction impairments,[36,183] astrocyte reactivity,[185] increased pericyte migration and degeneration,[176,177] decreased synaptic plasticity,[185] reduced blood flow,[185] elevated secretion of amyloid-β (Aβ) and cytokines,[180] increased Aβ deposition in the form of cerebral amyloid angiopathy,[178] and blood–brain barrier leakage.[35,36,176] *(figure caption continued on next page)*

(figure caption continued from the previous page) The potential relationship among vascular APOE4 effects on other cells and AD pathologies is depicted using arrows. Note that non-oligodendrocytic and non-vascular sources

Cell type-specific APOE4 cascade model of AD

Based on the literature reviewed above, it is evident that, in AD pathogenesis, the APOE4 produced in each of several CNS cell types (astrocytes, neurons, microglia, oligodendrocytes and vascular cells) exerts distinct roles, probably in a spatiotemporally specific and interactive manner.

Thus, we propose a cell type-specific APOE4 cascade model (Fig. 1.6) to help explain how the different cellular sources of APOE4 may act in a stepwise and interactive manner to drive AD pathogenesis. During the first stage (neuronal initiation), stress and aging trigger increased APOE4 expression in neurons, leading to neuronal dysfunction and the appearance of nE4-DAN. The dysfunctional neurons may start to overproduce and release proinflammatory molecules, such as MHC1 molecules and HMGB1. Simultaneously, dysfunctional neurons may also increase their Aβ production and secretion and accumulate pathological p-tau intracellularly. During the second stage (glial response), astrocytes and microglia become activated in response to proinflammatory molecules released by dysfunctional neurons and to the elevated levels of pathological Aβ and p-tau assemblies. As this stage evolves, disease-associated glia (such as DAA, DAM, LDAM, IRM and MHC2-M) in which APOE expression and secretion are increased start to appear, disrupting the BBB and further promoting the formation and spread of Aβ and tau pathologies. The combination of these processes, in concert with elevated APOE4 expression in neurons, oligodendrocytes and vascular cells, ultimately triggers the third stage (degeneration), which is characterized by the loss of synapses, neurons, and myelin. These cellular impairments and degeneration further augment

the expression of APOE4 in neurons and other cell types, promoting vicious cycles and ultimately leading to the fourth stage (AD dementia).

Additional studies are needed to further test this model and to address the following questions: How is APOE4 expression regulated in neurons, astrocytes, microglia, oligodendrocytes and vascular cells? What protease is responsible for neuron-specific APOE4 cleavage? How does APOE4 in dysfunctional neurons promote the neuronal production and release of proinflammatory molecules? How exactly do the distinct cellular sources of APOE4 affect amyloid and tau pathologies? What are the mechanisms underlying the formation of disease-associated glial subtypes? To what extent is the emergence of these glial subtypes pathogenic or adaptive? Do they cause neurodegeneration, BBB impairments, and oligodendrocyte and/or myelin deficits? Answering these questions will help further elucidate the cell type-specific roles of APOE4 in AD pathogenesis and foster the development of novel therapeutics for this challenging condition.

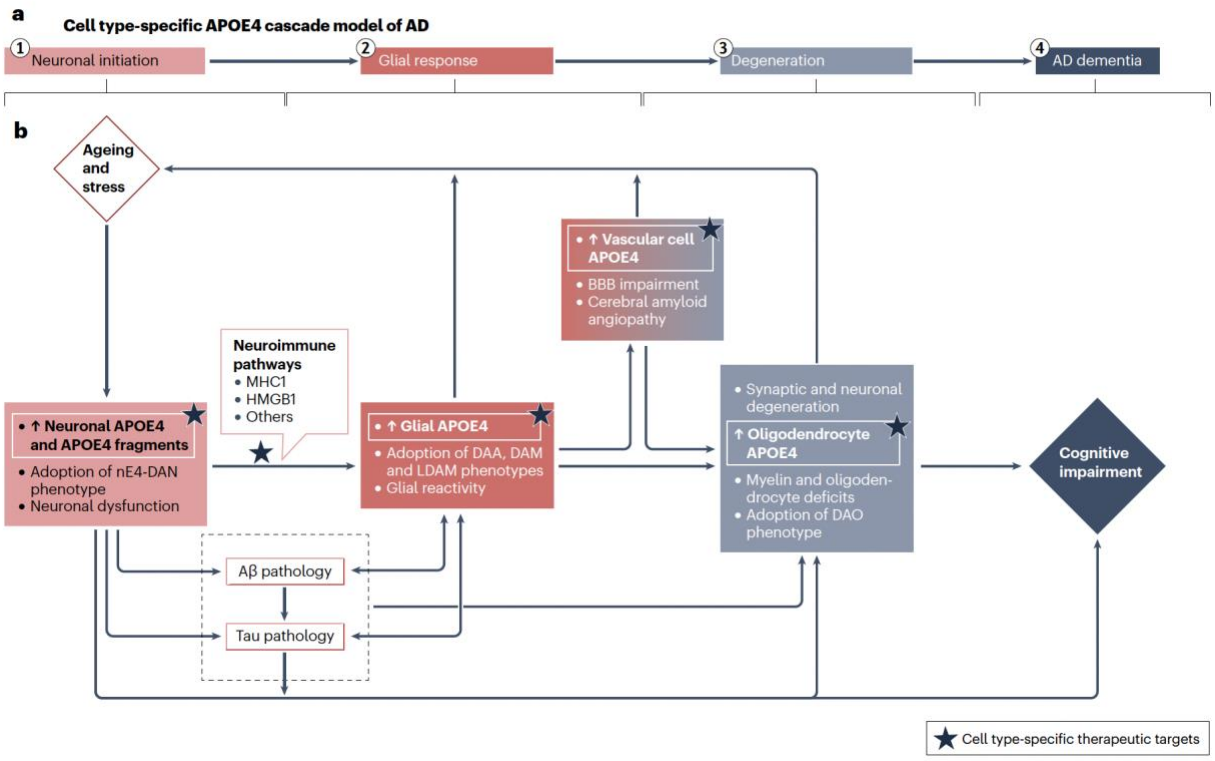


Fig. 1.6 | Cell type-specific APOE4 cascade model of AD and related therapeutic strategies. **a,** Overview of the four stages of the cascade model. **b,** During the first stage (neuronal initiation), stress and ageing trigger increased neuronal expression of the E4 isoform of apolipoprotein E (APOE4), leading to neuronal dysfunction and the appearance of neuronal APOE4-promoted disease-associated neurons (nE4-DAN). The dysfunctional neurons may startmto overproduce and release pro-inflammatory molecules (such as major histocompatibility complex class 1 (MHC1) molecules and high mobility group box 1 (HMGB1)) and increase their amyloid-β (Aβ) production and secretion and intracellular accumulation of pathological p-tau. During the second stage (glial response), astrocytes and microglia become activated in response to pro-inflammatory molecules released by dysfunctional neurons and to the elevated levels of pathological Aβ and p-tau assemblies. As this stage evolves, disease-associated glia (such as disease-associated astrocytes (DAA), disease-associated microglia (DAM), lipid droplet-accumulating microglia (LDAM), interferon-responsive microglia (IRM) and antigen-presenting microglia (MHC2-M)) with increased APOE expression and secretion start to appear, disrupting the blood–brain barrier (BBB) and further promoting the formation and spread of Aβ and tau pathologies. The combination of these processes, in concert with elevated APOE4 expression in neurons, oligodendrocytes and vascular cells, ultimately triggers the third stage (degeneration), which is characterized by the loss of synapses, neurons and myelin. *(figure caption continued on next page)*

(figure caption continued from the previous page). These cellular impairments and degeneration further augment the expression of APOE4 in neurons and other cell types, promoting vicious cycles and, ultimately, leading to the fourth stage (AD dementia). On the basis of the proposed cascade model, cell type-specific APOE4-guided AD therapeutic targets are highlighted, as indicated by stars.

Potential therapeutics targeting APOE4

Although there has been progress on AD therapeutic development with the recent US Food and Drug Administration (FDA) approval of Lecanemab and Aducanumab (anti-Aβ monoclonal antibodies), APOE4 carriers have unfortunately been found to be at high risk for developing serious side effects, such as amyloid-related imaging abnormalities (ARIA), to these therapies.[187,188] In addition, *APOE* genotype seems to also differentially modulate the amyloid lowering efficacy and microglial response to anti-Aβ immunotherapy in an AD mouse model.[189] Given the high proportion of APOE4 carriers in the AD population, there is an urgent need to devise therapeutic strategies that take into account the APOE4 carrier status, such as therapies directly targeting the detrimental effects of APOE4 expression.

A key question in developing APOE4-targeting therapies has been and continues to be whether APOE4 differs from the other APOE isoforms primarily through loss-of-function mechanisms or through gain-of-function mechanisms in AD-relevant contexts. In hiPSC-derived neuronal cultures, APOE-deficient neurons resembled those expressing APOE3, whereas APOE4-expressing neurons showed a range of AD-relevant pathological phenotypes, suggesting an adverse gain-of-function at least for APOE4 produced by neurons.[85] In vivo studies also support a gain-of-function mechanism for APOE4 produced by neurons or other cell types. Genetically reducing APOE4 by 50% markedly lowered amyloid pathology in mutant human APP transgenic mice with

hemizygous APOE4 expression.[189,190] Furthermore, ablation of APOE4 specifically in neurons or astrocytes protected against tau pathology, gliosis, and degeneration in PS19-APOE4 mice.[24,43] Human case studies also support the conclusion of predominant gain-of-function effects of APOE4. For example, a recent preprint has reported that an APOE3/4 heterozygote with the *APOE4* allele-specific loss-of-function mutation did not develop AD at old age[192] and an older study reported a similar effect in one person with complete APOE deficiency.[191,192] Likewise, genetic studies revealed that APOE4 carriers with European ancestry have higher APOE4 expression levels in various types of CNS cells than those with African ancestry and, interestingly, the former have a relatively higher AD risk than the latter.[193,194] Together, these findings highlight the potential therapeutic benefit of reducing APOE4 levels. Indeed, anti-APOE immunotherapies and antisense oligonucleotides (ASO) targeting APOE are in development. In amyloidosis mouse models, such therapies efficiently inhibited the formation of amyloid plaques when initiated before the onset of pathology.[196,197] Treatment with an APOE-ASO also reduced tau pathology, neuroinflammation, and neurodegeneration in a tauopathy mouse model.[198]

Based on the cascade model we proposed above (Fig. 1.6), one could also envision directing therapeutic interventions at APOE4 in specific cell types, which may yield more precise outcomes and help avoid unexpected side effects from broader APOE reductions. Potential AD-relevant targets include neuronal APOE4 and its proteolytic cleavage as well as the APOE4-dependent neuronal production and release of proinflammatory molecules, astrocytic and microglial APOE4, and oligodendrocytic or vascular cell APOE4. The rapidly evolving development of viral vectors and gene editing approaches[199,200] may also enable the isoform-specific deletion or conversion of

APOE4 in neurons or other CNS cell types. To monitor the effects of APOE4-targeting therapies and for the stratification of AD patient populations in general, it will also be important to develop better APOE-related biomarkers. Potential examples include the detection and quantification of neuron-derived APOE4 fragments and of APOE4-induced molecules released from specific CNS cell types, such as MHC1 molecules and HMGB1, in the CSF and plasma.

Summary of Cell Type-Specific APOE Effects

Recent scientific advances have revealed the importance of cell type-specific roles of APOE4 in AD pathogenesis. APOE4 produced in various CNS cell types, such as neurons, astrocytes, microglia, oligodendrocytes, and vascular cells, exert differential effects on amyloid and tau pathology, altered lipid metabolism, glial reactivity, neurodegeneration, myelin deficits, and blood-brain barrier dysfunction, likely in a spatiotemporal and interactive manner. The cell type-specific APOE4 cascade model that we outline above poses neuronal APOE4 as a critical upstream initiator and driver of AD pathogenesis, instigating glial response and subsequent degeneration. This model also indicates that targeting specific cellular sources of APOE4 may provide new therapeutic strategies for the prevention or treatment of AD.

CHAPTER 2: Neuronal APOE4 reduction with an APOE-I3-targeting ASO protects against neurodegeneration and neuroinflammation in an Alzheimer's disease mouse model

Introduction

Alzheimer's disease (AD) is a neurodegenerative disorder with pathological changes in the brain that lead to progressive cognitive decline. Despite over a century of AD research, it still lacks effective treatments or cures – likely due to the complex causes of AD pathogenesis, which involves interactions among diverse genetic, epigenetic, and environmental factors. During the past decades, researchers have identified many genetic loci that can alter AD risk with the apolipoprotein E (APOE) locus emerging as the strongest risk factor for late-onset AD.[1]

APOE plays important roles in the brain, such as redistributing lipids among CNS cells for normal lipid homeostasis, repairing injured neurons, maintaining synaptodendritic connections, and scavenging toxins.[2] Within the brain, APOE is expressed primarily by astrocytes, but upon stress, injury, and aging, other cell types, such as neurons and microglia, upregulate their APOE expression.[3] In humans, the *APOE* gene has three common alleles, ε2, ε3 and ε4, and the *APOE* ε4 allele is considered the strongest genetic risk factor, leading to increased AD risk and decreased age of disease onset.[1,4,5] Although numerous studies have demonstrated that APOE4 is linked to more severe AD pathologies,[3,6,7] its roles in AD pathogenesis at a cell type-specific level has been understudied. With more recent studies incorporating single cell omics, it is becoming increasingly clear that the effects of APOE4 on AD pathologies depend on its cellular sources and expression levels.[3]

Previous studies have demonstrated the detrimental effects of APOE4 produced by neurons, including phosphorylated tau (p-tau) accumulation, inhibitory neuron loss, and learning and

memory deficits.[8–10] Recently, it has been shown that selective genetic removal of APOE4 from neurons in a tauopathy mouse model resulted in a significant reduction in p-tau pathology, neuroinflammation, and neurodegeneration.[11] Furthermore, it has been reported that neuronal APOE regulates cellular stress and immune response pathways under both health and disease conditions, with the level of neuronal APOE expression tracking with disease progression in patients with MCI and AD.[12] Based on these findings, identifying a strategy to reduce neuronal APOE4 could offer a promising therapeutic approach for APOE4-driven AD.

Antisense oligonucleotides (ASOs) offer an encouraging therapeutic strategy that has the potential to treat neurodegenerative diseases,[13,14] like AD. One key mechanism of ASO action involves sequence-specific binding to target mRNA transcripts, which subsequently recruits the endogenous enzyme RNase H. This recruitment triggers enzymatic cleavage and degradation of the mRNA-ASO duplex, resulting in reduced mRNA stability and ultimately decreased protein translation from the target mRNA.[13,15] For many neurodegenerative diseases that have been linked to the aggregation of toxic proteins, reducing levels of these accumulated proteins can be a powerful therapeutic approach. In fact, ASO drugs are currently in development for the treatment of amyotrophic lateral sclerosis, Huntington's disease, and AD.[16] When continuously infused intraventricularly, ASOs have been shown to distribute widely throughout the CNS of rodents and primates, including the regions affected in major neurodegenerative diseases.[17] Recent studies treating mice with ASOs via intracerebroventricular (ICV) injection or infusion have found that they can efficiently reduce APOE at both the mRNA and protein levels in the

hippocampus and the cortex.[18,19] However, these ASO studies targeted all APOE produced in the brain, and targeting APOE in a cell type-specific manner has not been explored.

Our lab has previously identified a splicing variant of *APOE* mRNA with intron-3 retention, termed *APOE-I3*, which is specific to neurons.[20] This *APOE-I3* transcript was detected in human neuronal cell lines and mouse primary neurons, but was not in human astrocytic cell lines and mouse primary astrocytes.[20] Additionally, RNA-sequencing analysis has shown that the abundance of *APOE-I3* transcripts in the brains of individuals with AD correlates with the severity of tau and amyloid pathologies, and the level of *APOE-I3* transcripts increases with *APOE* ε4 allele number.[21] Thus, targeting this neuron-specific APOE4 transcript may be a promising avenue for reducing neuronal APOE4 and its related AD pathologies.

In this study, we designed an ASO targeting intron-3 of the *APOE-I3* transcript and investigated its effects on cell type-specific APOE4 levels and AD pathologies in a human APOE4-expressing tauopathy mouse model. The outcomes of this study provide new insights into how preferential knockdown of neuronal APOE4, using an APOE-I3-targeting ASO, affects the pathogenesis of AD and highlights its promising potential as a therapeutic strategy for treating APOE4-driven AD.

Results

Identification of ASO candidates capable of reducing neuronal or global APOE expression

To identify ASOs that target APOE and reduce their expression levels via an RNase-H-mediated knockdown, we designed 20-mer oligonucleotides targeting the APOE gene. To preferentially target the neuron-specific splicing variant of *APOE* mRNA with intron-3 retention (APOE-I3 mRNA), we designed five ASOs against the intron-3 sequence of the human *APOE* gene (ASO-I3) (Fig. 2.1a). Five ASOs targeting exon regions of the APOE gene were also designed to target the *APOE* gene (ASO-E) in any cell type as controls (two targeting exon 3 and three targeting exon 4) (Fig. 2.1a). To test the efficacy of the designed ASOs, we transfected mouse neuroblastoma Neuro-2a cells stably expressing APOE from a 17-Kb human APOE3 genomic DNA (N2a-E3)[22] with the ASO candidates.

To determine the dose-responsive effect of ASOs, we transfected N2a-E3 cells with a representative ASO-I3 and an ASO-E for 24 hours at 0, 1, 3, 10, and 30 nM and measured APOE expression levels via quantitative PCR (qPCR). We found that at 10 nM, ASO-E and ASO-I3 reduced APOE mRNA by ~69% and ~25%, respectively (Fig. 2.1b). At 30 nM, ASO-E and ASO-I3 reduced APOE mRNA by ~73% and ~34%, respectively (Fig. 2.1b). We then decided to treat N2a-E3 cells with the full panel of 10 ASOs for 24 hours at 10 and 30 nM to identify lead ASOs. Two ASO-I3 and two ASO-E (one targeting exon 3 of APOE and one targeting exon 4 of APOE) showed the greatest reduction of APOE mRNA levels (Fig. 2.1c). The ASO-E-174, targeting exon 3, reduced APOE mRNA by ~71% and ~78% at 10 and 30 nM treatment, respectively (Fig. 2.1c). The ASO-E-4, targeting exon 4, reduced APOE mRNA by ~69% and ~74% at 10 and 30 nM treatment, respectively (Fig.

2.1c). The ASO-I3-75 reduced APOE mRNA by ~25% and ~35% at 10 and 30 nM treatment, respectively (Fig. 2.1c). The ASO-I3-415 reduced APOE mRNA by ~18% and ~36% at 10 and 30 nM treatment, respectively (Fig. 2.1c).

These four ASOs (ASO-E-174, ASO-E-4, ASO-I3-75, and ASO-I3-415) were then selected for further validation and optimization. N2a-E3 were separately treated with the four ASOs for a longer period of 48 hours and the APOE expression levels were measured via qPCR. For 10 and 30 nM treatments, respectively, ASO-E-174 significantly reduced APOE mRNA by ~78% and ~67%, ASO-E-4 significantly reduced APOE mRNA by ~74% and ~64%, ASO-I3-75 significantly reduced APOE mRNA by ~59% and ~71%, and ASO-I3-415 significantly reduced APOE mRNA by ~45% and ~44% (Fig. 2.1d).

Based on their efficacy and region of target in the APOE gene, we selected ASO-E-4 (targeting global APOE expression) and ASO-I3-75 (targeting neuronal APOE expression) for further validation of their effects on APOE protein production. N2a-E3 cells were treated with ASO-E-4 and ASO-I3-75 for 48 hours at 30 nM, and APOE protein levels were determined by western blot analysis relative to cells treated with 30 nM of a non-targeting control ASO (ASO-NTC). Importantly, ASO-E-4 treatment significantly reduced APOE protein levels by ~58%, and ASO-I3-75 treatment significantly reduced APOE protein levels by ~38% (Fig. 2.1e,f). Together, these data demonstrate that both ASO-E-4 and ASO-I3-75 can effectively reduce both APOE mRNA and protein levels in N2a-E3 cells.

ASO-E-4 and ASO-I3-75 effectively reduce APOE expression in mouse primary neurons

To further examine the efficacy of ASO-E-4 and ASO-I3-75 in neurons, we treated primary mouse neurons derived from mice expressing human APOE4 from a transgenic DNA construct containing intron-3 and under the control of neuron-specific enolase (NSE) promoter (NSE-E4) on a mouse APOE-KO background.[23,24] The primary neuron cultures were treated with 10 μM of ASO-E-4 or ASO-I3-75 on Day 3 for 1 week. Cells were collected on Day 10, and APOE mRNA levels were measured by qPCR. ASO-E-4 significantly reduced APOE mRNA by ~87% (Fig. 2.1g), and ASO-I3-75 significantly reduced it by ~64% (Fig. 2.1g). These data confirm that both ASO-E-4 and ASO-I3-75 can significantly reduce APOE expression in mouse primary neurons compared to treatment with ASO-NTC.

ASO-E-4, but not ASO-I3-75, effectively reduces APOE expression in human and mouse astrocytic cells

To test whether the ASO-I3-75 preferentially targets neuronal APOE, we next determined its effect on APOE expression in astrocytes as compared to the ASO-E-4. First, we treated the human astrocytoma cell line, SW-1088, with 3 μM of either ASO for 48 hours and measured APOE mRNA by qPCR. ASO-E-4 significantly reduced APOE mRNA by ~41% compared to control SW-1088 cells (Fig. 2.1h). In sharp contrast, ASO-I3-75 did not significantly reduce APOE mRNA, as compared to control SW-1088 cells (Fig. 2.1h). This suggests that ASO-I3-75 does not effectively alter APOE expression in human astrocytic cells that lack a large, stable pool of APOE-I3 transcripts,[20] whereas ASO-E-4 does effectively reduce APOE expression in human astrocytic cells. These data

confirm that ASO-I3-75 effectively reduces APOE expression in neurons without affecting APOE expression in other cell types such as astrocytes.

To further validate the differential efficacy of ASO-I3-75 versus ASO-E-4 in astrocytic cells, we treated primary mouse astrocytes derived from PS19/E4 mice previously generated in our lab.[11,25,26] The cultured astrocytes received either 20 or 40 µM of ASO-E-4, ASO-I3-75, or ASO-NTC on Day 14 for 1 week before qPCR measurement of APOE mRNA levels. ASO-E-4 significantly reduced APOE mRNA by ~51% and ~49% at the 20 and 40 µM treatments, respectively, while ASO-I3-75 only reduced APOE mRNA by ~22% and ~14% at the same doses (Fig. 2.1i). Taken together, these data demonstrate that in primary mouse astrocytes, ASO-E-4 effectively reduces APOE expression (~50%), while ASO-I3-75 does not effectively do so (~15–20%), thus highlighting ASO-I3-75 as a neuron-preferential APOE ASO.

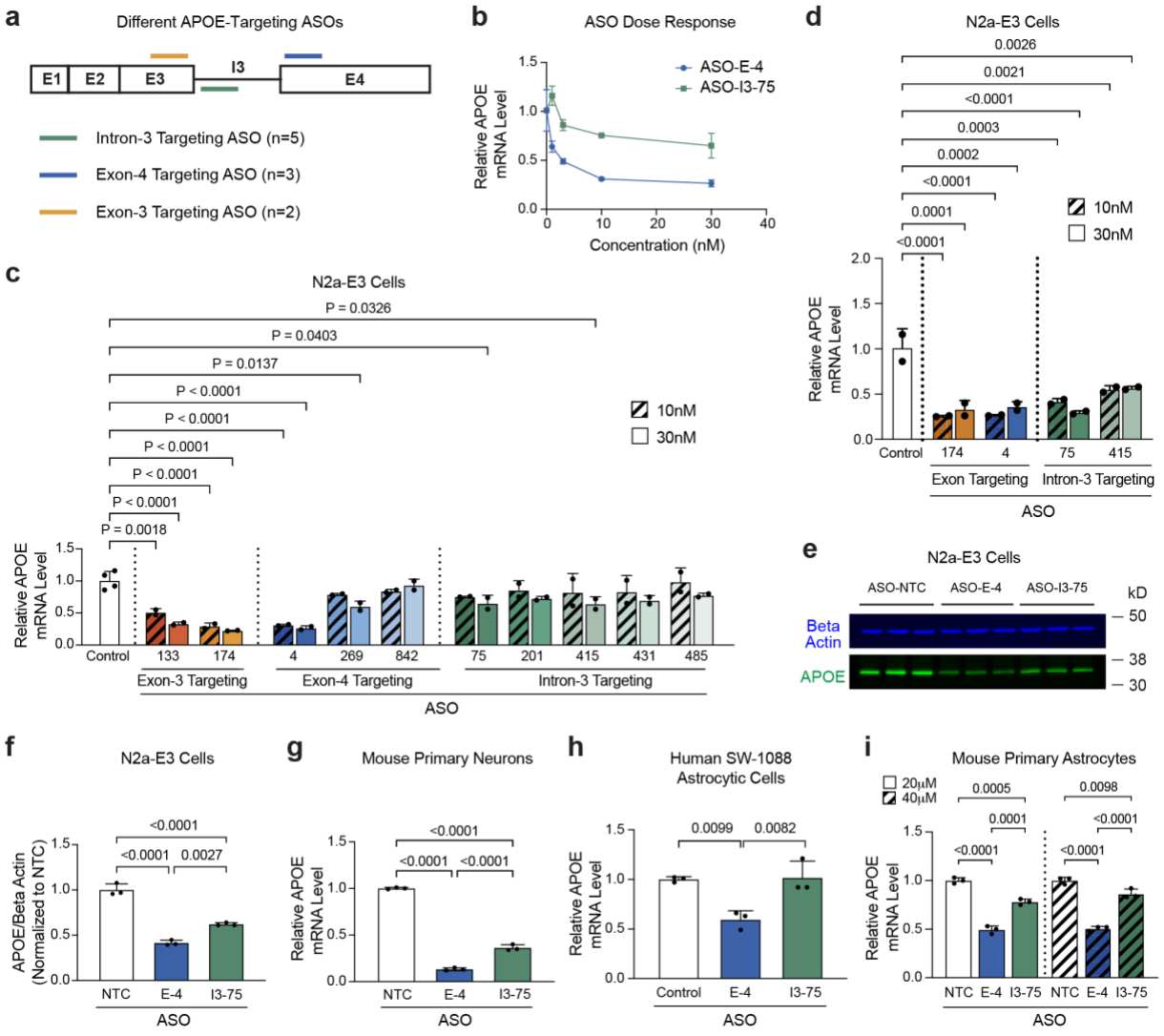


Fig. 2.1 | Identification of ASO candidates capable of reducing neuronal or global APOE expression.

a, Schematic of APOE-I3 transcript and where differentially designed ASOs target in the intron-3, exon-3, or exon-4 of the APOE-I3 transcript. **b,** qPCR quantification of APOE mRNA levels of neuroblastoma Neuro2a-E3 (N2a-E3) cells treated with an ASO-E-4 or ASO-I3-75 for 24 hours at 0, 1, 3, 10, or 30 nM. **c**, qPCR quantification of APOE mRNA levels of N2a-E3 cells treated with the full panel of 10 ASOs for 24 hours at 10 and 30 nM, respectively. **d**, qPCR quantification of APOE mRNA levels of N2a-E3 cells treated with the four selected ASOs: ASO-E-174, ASO-E-4, ASO-I3-75, and ASO-I3-415 for 48 hours at 10 and 30 nM, respectively. **e**,**f,** Representative western blot images (**e**) and quantification of APOE levels (**f**) in N2a-E3 cells treated with the two selected ASOs: ASO-E-4 and ASO-I3-75, as well as ASO-NTC (a non-targeting control ASO). In **f**, APOE levels were normalized to N2a-E3 cells treated with ASO-NTC. Beta actin was used as loading control.
(figure caption continued on next page)

(figure caption continued from the previous page) **g**, qPCR quantification of APOE mRNA levels of primary neurons derived from mice expressing human APOE4 from a transgenic APOE4 DNA construct containing intron-3 under the control of a neuron-specific enolase (NSE) promoter (NSE-E4) on a mouse APOE-KO background treated with 10 μM of ASO-NTC, ASO-E-4, or ASO-I3-75 for 1 week. **h**, qPCR quantification of APOE mRNA levels of human SW-1088 astrocytoma cells treated with 3 μM of ASO-NTC, ASO-E-4, or ASO-I3-75 for 48 hours. **i**, qPCR quantification of APOE mRNA levels of primary astrocytes from PS19/E4 mice treated with 20 or 40 μM of ASO-NTC, ASO-E-4, or ASO-I3-75 for 1 week. Throughout, data are expressed as mean ± s.d.. Differences between groups were determined by ordinary one-way ANOVA followed by Dunnett's multiple comparison test (**c,d**) or ordinary one-way ANOVA followed by Tukey's multiple comparison test (**f-i**).

ASO-E-4 and ASO-I3-75 effectively reduce APOE expression in the hippocampus of PS19/E4 mice in a cell-type-dependent manner

To determine the efficacy of ASO-E-4 and ASO-I3-75 in reducing APOE expression in an AD mouse model, we next treated PS19/E4 tauopathy mice previously generated in our lab[11,25,26] with the ASOs. To best characterize the therapeutic potential of APOE reduction, we began ASO treatment at 8.5 months of age, when mice have already begun developing some AD pathologies. Treatment was conducted via an osmotic pump ICV infusion, allowing for slow delivery of 850 ug of ASO-E-4, ASO-I3-75, or ASO-NTC for 4 weeks (Fig. 2.2a). Following treatment, APOE protein levels were quantified via immunostaining for APOE and determining APOE percent coverage area in the dentate gyrus (DG) and CA1 hippocampal subregions. PS19/E4 mice treated with either ASO-E-4 or ASO-I3-75 had a significant reduction in overall APOE protein levels, as compared to PS19/E4 mice treated with ASO-NTC (Fig. 2.2b,c). Thus, treatment of PS19/E4 mice with ASO-E-4 or ASO-I3-75 via osmotic pump infusion into the ventricle for 4 weeks effectively reduces APOE protein levels in the hippocampus.

To gain a better understanding of cell type-specific APOE reduction from the two ASOs, we measured the APOE percent coverage area in neurons, labeled with NeuN, and astrocytes, labeled with GFAP. PS19/E4 mice treated with either ASO-E-4 or ASO-I3-75 showed a significant reduction in neuronal APOE levels compared to PS19/E4 mice treated with ASO-NTC (Fig. 2.2d,f). Meanwhile, for astrocytic APOE levels, PS19/E4 mice treated with ASO-E-4 exhibited a significant reduction relative to mice treated with ASO-NTC, while PS19/E4 mice treated with ASO-I3-75 showed a trending but not significant reduction of APOE (Fig. 2.2e,g). Thus, ASO-E-4 and ASO-I3-75 can effectively reduce APOE expression in the hippocampus of PS19/E4 mice in a cell-type-dependent manner.

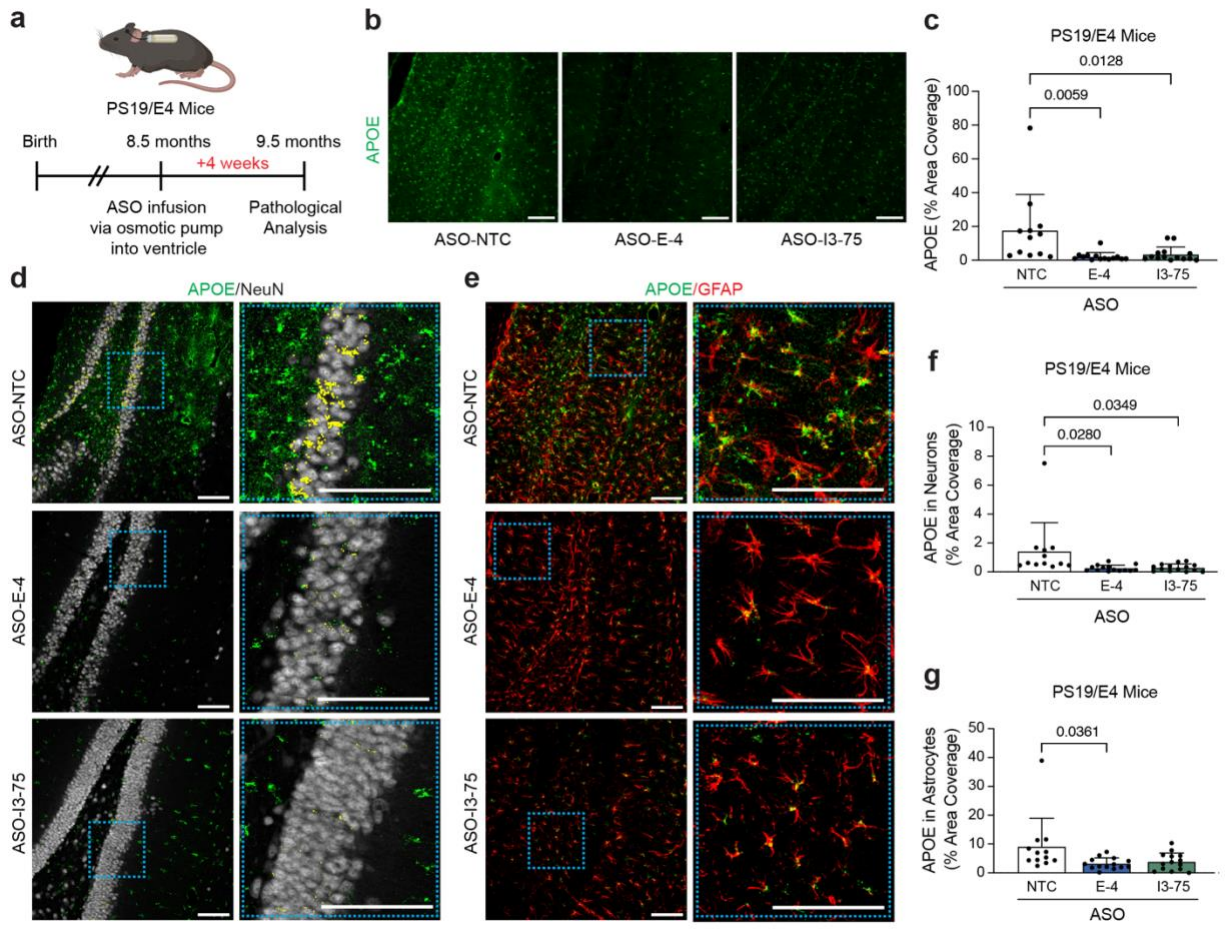


Fig. 2.2 | ASO-E-4 and ASO-I3-75 effectively reduce APOE expression in the hippocampus of PS19/E4 mice in a cell-type-dependent manner.

a, Schematic timeline of ASO treatment via osmotic pump infusion into ventricle and pathological analysis of PS19/E4 mice. **b**, Representative images showing immunostaining of APOE in the hippocampus of PS19/E4 mice treated with ASO-NTC, ASO-E-4, or ASO-I3-75 for four weeks. Scale bars are 100μm. **c**, Quantification of APOE percent area coverage in the dentate gyrus (DG) and CA1 of PS19/E4 mice treated with ASO-NTC, ASO-E-4, or ASO-I3-75. For all mice, data is averaged from 4 fields of view from 2 brain sections (2 fields of view from the DG and 2 fields of view from the CA1). ASO-NTC, n=12 mice; ASO-E-4, n=14 mice; ASO-I3-75, n=14 mice. **d**, Representative images showing immunostaining of APOE (green) and NeuN (white) in the DG of PS19/E4 mice treated with ASO-NTC, ASO-E-4, or ASO-I3-75. Each representative image includes a magnified image of a region in the DG to the right, with areas positive for both APOE and NeuN pseudo-colored in yellow for clear visualization. Scale bars are 100μm. **e**, Representative images showing immunostaining of APOE (green) and GFAP (red) in the DG of PS19/E4 mice treated with ASO-NTC, ASO-E-4, or ASO-I3-75. Each representative image includes a magnified image of a region in the DG to the right, with areas positive for both APOE and GFAP in yellow. Scale bars are 100μm.

(figure caption continued on next page)

(figure caption continued from the previous page) **f,** Quantification of APOE percent area coverage in neurons of PS19/E4 mice treated with ASO-NTC, ASO-E-4, or ASO-I3-75. **g**, Quantification of APOE percent area coverage in astrocytes of PS19-E4 mice treated with ASO-NTC, ASO-E-4, or ASO-I3-75. Throughout, data are expressed as mean ± s.d.. Differences between groups were determined by ordinary one-way ANOVA followed by Tukey's multiple comparison test.

ASO-I3-75, but not ASO-E-4, effectively reduces neurodegeneration in the hippocampus of PS19/E4 mice

Next, we evaluated the effects of the two ASOs on neurodegeneration, as determined by hippocampal volume, in the same PS19/E4 mice after 4 weeks of ASO treatment (at 9.5 months of age). Hippocampal volume was significantly higher in PS19/E4 mice treated with ASO-I3-75 compared to those treated with ASO-NTC (Fig. 2.3a,b), showing reduced hippocampal atrophy. Interestingly, PS19/E4 mice treated with ASO-E-4 exhibited a trending, but not significant, increase in hippocampal volume relative to those treated with ASO-NTC (Fig. 2.3a,b). These findings suggest that preferentially reducing neuronal APOE4 by targeting the neuron-specific splicing variant APOE-I3, as ASO-I3-75 did, is more efficient and beneficial for rescuing neurodegeneration, as compared to targeting global APOE4 in the brain, as ASO-E-4 did.

To gain a better understanding of how APOE4 levels in different cell types contribute to neurodegeneration, we assessed the relationship between hippocampal volume and APOE4 levels in neurons and astrocytes. Strikingly, there were no significant correlations between astrocytic APOE4 levels and hippocampal volumes in mice treated with either ASO-NTC, ASO-E-4, or ASO-I3-75 (Fig. 2.3c-e), suggesting that astrocytic APOE4 is not a driver of APOE4-promoted hippocampal degeneration in PS19/E4 mice. In sharp contrast, there was a strong negative correlation between neuronal APOE4 levels and hippocampal volumes in PS19/E4 mice treated

with ASO-I3-75 (Fig. 2.3h), although such a correlation was not present in the mice treated with either ASO-NTC or ASO-E-4 (Fig. 2.3f,g). Thus, neuron-preferential reduction of APOE4 likely drives the protection of hippocampal degeneration.

In line with these observations, there was also a strong negative correlation between neuronal APOE4 levels and DG NeuN+ granular layer thickness, another measurement of neurodegeneration,[11,25] in PS19/E4 mice treated with ASO-I3-75 (Fig. 2.3i), but not in those treated with ASO-E-4 (Fig. 2.3j). Importantly, there was no significant correlation between astrocytic APOE4 levels and DG $NeuN^+$ granular layer thickness in PS19/E4 mice treated with either ASO-I3-75 (Fig. 2.3k) or ASO-E-4 (Fig. 2.4a). There was a trending, but not statistically significant, increase in the average DG $NeuN^+$ granular layer thickness in PS19/E4 mice treated with either ASO-I3-75 or ASO-E-4 versus those treated with ASO-NTC (Fig. 2.4b). Notably, for mice treated with ASO-NTC, ASO-E-4, or ASO-I3-75, DG NeuN+ granular layer thickness had a significant positive correlation with hippocampal volume, suggesting that neuronal loss in the DG contributes to the observed hippocampal volume reduction (Extended Data Fig 1c-e). Together, these findings suggest that preferentially reducing neuronal APOE4 with ASO-I3-75 treatment leads to efficient rescue of neurodegeneration, including hippocampal atrophy and DG neuronal layer shrinkage.

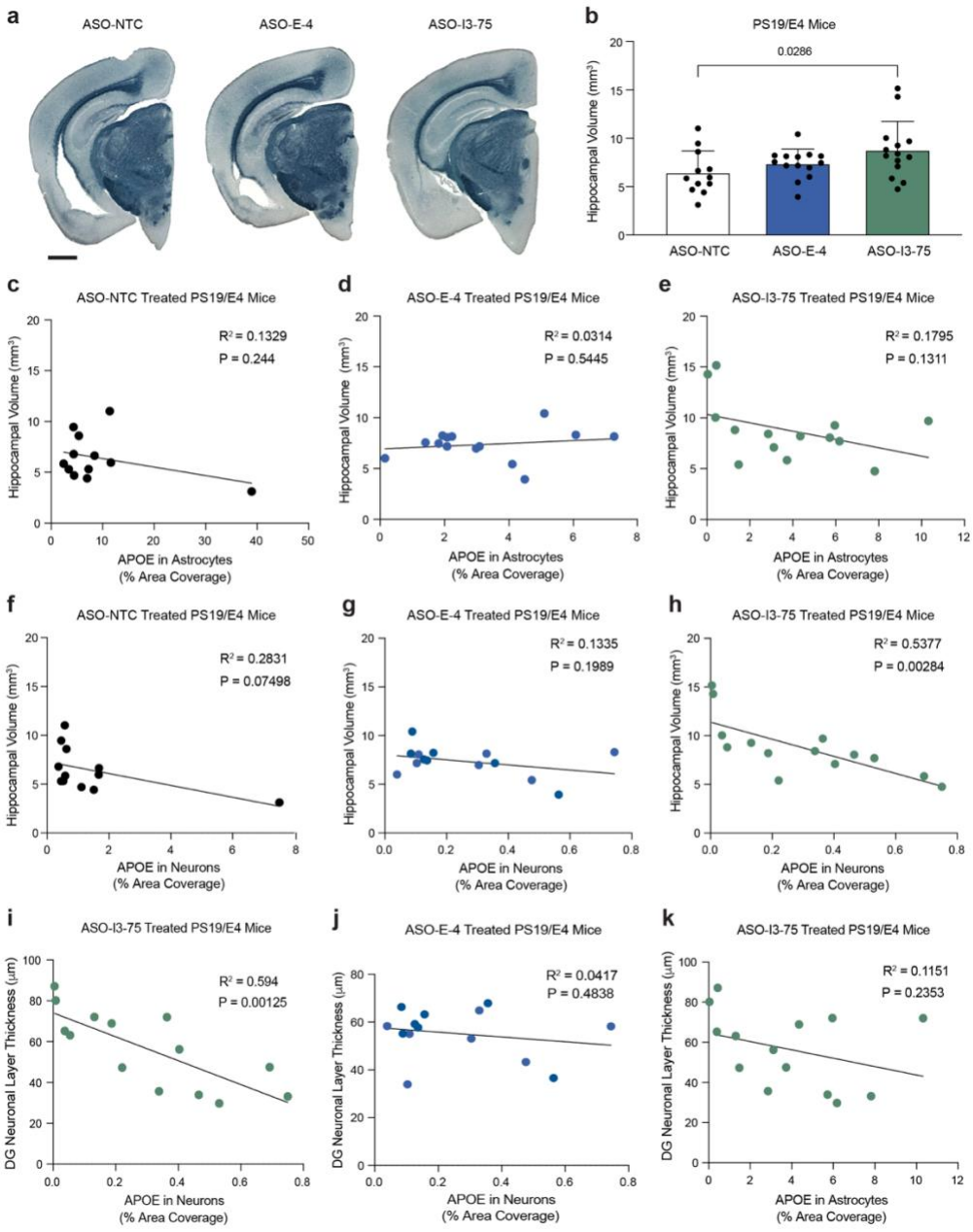


Fig. 2.3 | ASO-I3-75, but not ASO-E-4, effectively reduces neurodegeneration in the hippocampus of PS19/E4 mice.

a, Representative images of the ventral hippocampus of 9.5-month-old PS19/E4 mice treated with ASO-NTC, ASO-E-4, or ASO-I3-75 for 4 weeks after staining with Sudan Black to enhance hippocampal visualization. ASO-NTC, n=12 mice; ASO-E-4, n=14 mice; ASO-I3-75, n=14 mice. Scale bar is 1mm. **b**, Quantification of hippocampal volume in 9.5-month-old PS19/E4 mice treated with ASO-NTC, ASO-E-4, or ASO-I3-75 for 4 weeks. *(figure caption continued on next page)*

(figure caption continued from the previous page) Data are expressed as mean ± s.d., and differences between groups were determined by ordinary one-way ANOVA followed by Dunnett's multiple comparison test**. c-e**, Correlations between hippocampal volume (mm^3) and APOE level in astrocytes (% area coverage) in PS19/E4 mice treated with ASO-NTC (**c,** n=12), ASO-E-4 (**d**, n=14), or ASO-I3-75 (**e**, n=14). **f-h**, Correlations between hippocampal volume (mm^3) and APOE level in neurons (% area coverage) in PS19/E4 mice treated with ASO-NTC (**f**), ASO-E-4 (**g**), or ASO-I3-75 (**h**). **i**, Correlations between DG neuronal layer thickness (μm) and APOE level in neurons (% area coverage) in PS19/E4 mice treated with ASO-I3-75 (n=14). **j**, Correlations between DG neuronal layer thickness (μm) and APOE level in neurons (% area coverage) in PS19/E4 mice treated with ASO-E-4 (n=14). **k**, Correlations between DG neuronal layer thickness (μm) and APOE level in astrocytes (% area coverage) in PS19/E4 mice treated with ASO-I3-75 (n=14). For all correlations, Pearson's correlation analysis (two-sided) was performed.

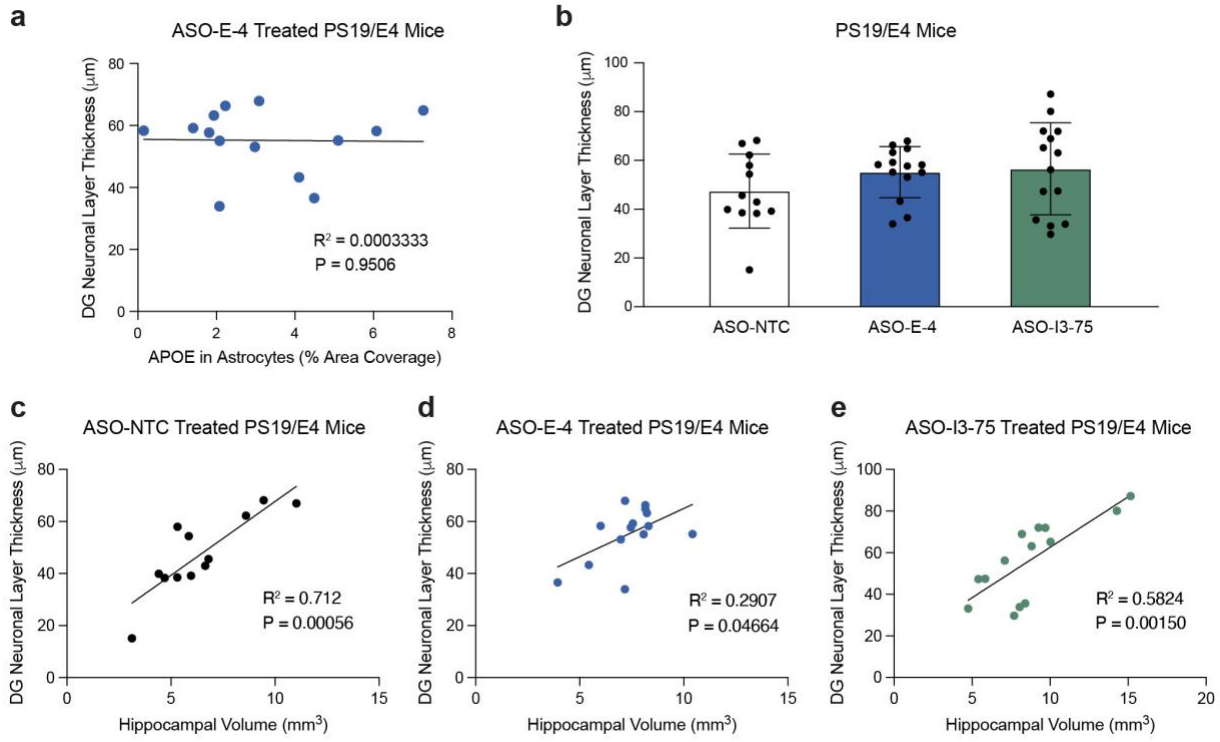


Fig. 2.4 | Trending Rescue of DG neuronal layer thickness in APOE ASO-treated PS19/E4 mice. **a,** Correlation between DG neuronal layer thickness (μm) and APOE in astrocytes (% area coverage) in PS19/E4 mice treated with ASO-E-4 (n = 14). **b**, Quantification of DG neuronal layer thickness (μm) in 9.5-month-old PS19/E4 mice treated with ASO-NTC, ASO-E-4, or ASO-I3-75 for 4 weeks. *(figure caption continued on next page)*

(figure caption continued from the previous page) Data are expressed as mean ± s.d. and differences between groups were determined by ordinary one-way ANOVA followed by Tukey's multiple comparison test. **c-e**, Correlations between DG neuronal layer thickness (μm) and hippocampal volume (mm^3) in PS19/E4 mice treated with ASO-NTC (**c**, n=12), PS19/E4 mice treated with ASO-E-4 (**d**, n=14), and PS19/E4 mice treated with ASO-I3-75 (**e**, n=14). For all correlations, Pearson's correlation analysis (two-sided) was performed.

ASO-I3-75, but not ASO-E-4, diminishes p-tau contribution to neurodegeneration in the hippocampus of PS19/E4 mice

To determine whether treatment with the different APOE-targeting ASOs protects against p-tau accumulation in PS19/E4, we immunostained brain sections with a p-tau-specific AT8 monoclonal antibody.[11,25,27] There were no significant differences in $AT8^+$ percent area coverage in the hippocampus between mice treated with ASO-E4, ASO-I3-75, or ASO-NTC (Fig. 2.5a-d). Correlation analysis revealed that p-tau ($AT8^+$) percent coverage areas negatively correlated with hippocampal volumes in PS19/E4 mice treated with ASO-NTC (Fig. 2.5e), suggesting the contribution of p-tau to neurodegeneration. Strikingly, although such a negative correlation was still present in PS19/E4 mice treated with ASO-E-4 (Fig. 2.5f), it was no longer present in the mice treated with the neuronal-APOE-targeting ASO-I3-75 (Fig. 2.5g). Similarly, there was a negative correlation between p-tau ($AT8^+$) coverage area and DG $NeuN^+$ layer thickness in PS19/E4 mice treated with ASO-NTC or ASO-E-4, which was also no longer present in the PS19/E4 mice treated with ASO-I3-75 (Fig. 2.5h-j). Taken together, all these data indicate that neuron-preferential reduction of APOE4 diminishes p-tau contribution to neurodegeneration in the hippocampus of PS19/E4 mice, and this protective effect does not apply to global APOE4 reduction.

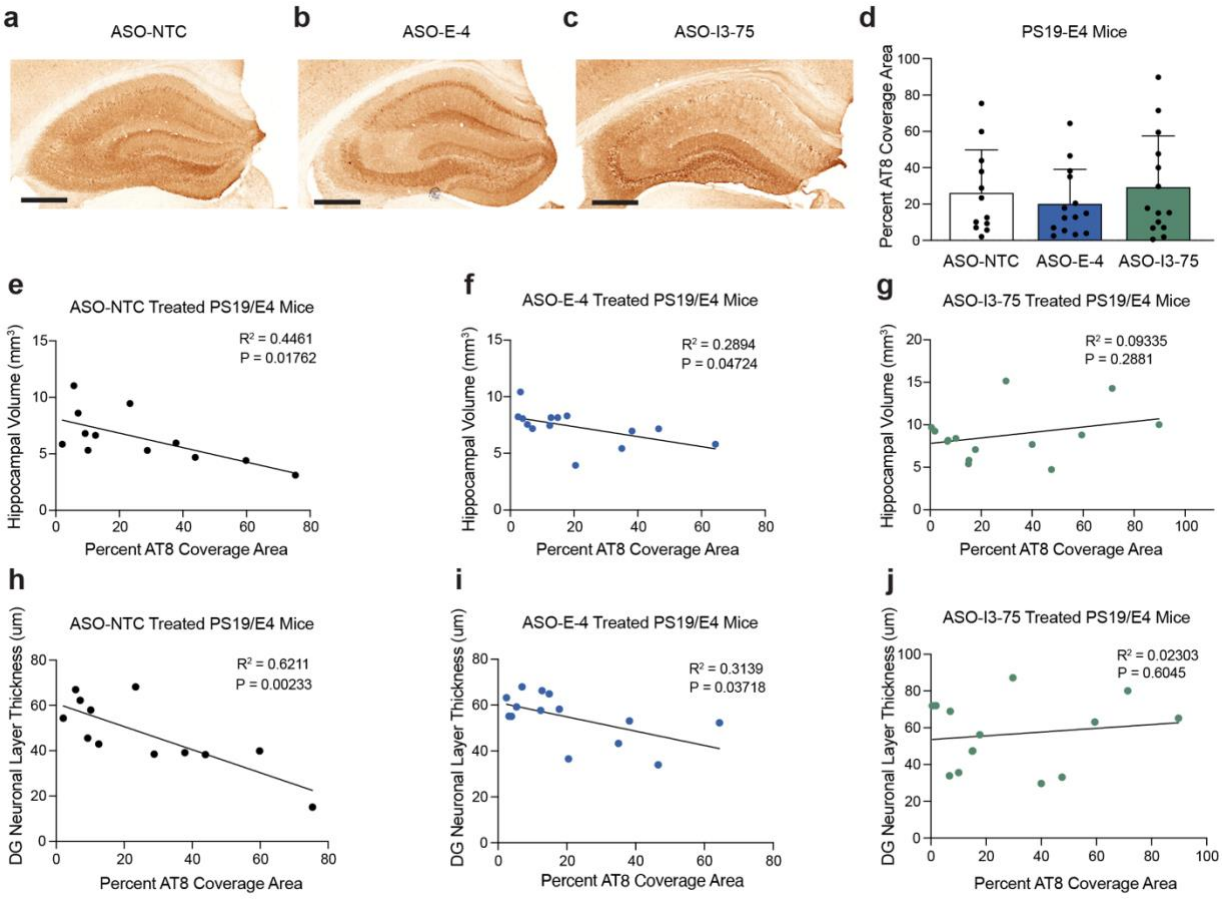


Fig. 2.5 | ASO-I3-75, but not ASO-E-4, diminishes p-tau contribution to neurodegeneration in the hippocampus of PS19/E4 mice.

a-c, Representative images of p-tau immunostaining with the monoclonal antibody AT8 in the hippocampus of 9.5-month-old PS19/E4 mice treated with ASO-NTC (**a**), ASO-E-4 (**b**), or ASO-I3-75 (**c**) for 4 weeks (scale bar, 500μm). **d**, Quantifications of percent p-tau coverage area in the hippocampus of 9.5-month-old PS19/E4 mice treated with ASO-NTC, ASO-E-4, or ASO-I3-75 for 4 weeks. Data are expressed as mean ± s.d., and differences between groups were determined by ordinary one-way analysis of variance (ANOVA) with Tukey's post hoc multiple comparisons test. **e-g**, Correlations between hippocampal volume (mm^3) and percent AT8 coverage area in PS19/E4 mice treated with ASO-NTC (**e**, n=12), PS19/E4 mice treated with ASO-E-4 (**f,** n=14), and PS19/E4 mice treated with ASO-I3-75 (**g**, n=14). **h-j** Correlations between DG neuronal layer thickness (μm) and percent AT8 coverage area in PS19/E4 mice treated with ASO-NTC (**h**, n=12), PS19/E4 mice treated with ASO-E-4 (**i**, n=14), and PS19/E4 mice treated with ASO-I3-75 (**j**, n=14). For all correlations, Pearson's correlation analysis (two-sided) was performed.

ASO-E-4 and ASO-I3-75 reduces astrogliosis in the hippocampus of PS19/E4 mice

We then tested whether treatment with the different APOE-targeting ASOs protects against APOE4-driven gliosis in the same cohort of PS19/E4 mice. To assess for astrogliosis, we stained with a GFAP-specific antibody (Fig. 2.6a) and calculated for $GFAP^+$ percent coverage area in the hippocampus.[11,25] PS19/E4 mice treated with either ASO-E-4 or ASO-I3-75 exhibited a significantly lower percent coverage area of $GFAP^+$ astrocytes in the DG and CA1 of the hippocampus relative to mice treated with ASO-NTC (Fig. 2.6a,b), indicating that both global and neuron-preferential reduction of APOE4 decreases astrogliosis. There was a significant negative correlation between $GFAP^+$ percent coverage area and hippocampal volume across all treatment groups (Fig. 2.6i), suggesting that in PS19/E4 mice, astrogliosis is a good indicator (or potentially a contributing factor) to hippocampal degeneration.

We also assessed the percent coverage area of activated astrocytes by staining for S100β (Fig. 2.6c). PS19/E4 mice treated with either ASO-E-4 or ASO-I3-75 exhibited a trending, but not significant reduction of percent coverage area of $S100\beta^+$ astrocytes relative to mice treated with ASO-NTC (Fig. 2.6c,d). However, when correlating $S100\beta^+$ percent coverage area with hippocampal volume, there was a significant negative correlation in PS19/E4 mice treated with either ASO-NTC or ASO-E-4 (Fig. 2.6j). Interestingly, there was no longer a significant negative correlation in PS19/E4 mice treated with ASO-I3-75 (Fig. 2.6j). Collectively, these data suggest that preferentially reducing neuronal APOE4 eliminates the contribution of activated astrocytes to hippocampal degeneration.

ASO-I3-75, but not ASO-E-4, alters the contribution of microgliosis to hippocampal degeneration in PS19/E4 mice

Next, to assess the effects of different APOE-targeting ASOs on microgliosis in the same cohort of PS19/E4 mice, we immunostained for IBA1 and analyzed the $IBA1^+$ percent coverage area in the hippocampus (Fig. 2.6e). PS19/E4 mice treated with either ASO-E-4 or ASO-I3-75 did not exhibit a significant (although trending) reduction of the percent coverage area of $IBA1^+$ microglia, as compared to the mice treated with ASO-NTC (Fig. 2.6e,f). When correlating $IBA1^+$ percent coverage area to hippocampal volume, similar to the case with S100β, there was a significant negative correlation in PS19/E4 mice treated with either ASO-NTC or ASO-E-4, but not in mice treated with ASO-I3-75 (Fig. 2.6k). These data suggest that microgliosis is a good indicator or contributing factor to hippocampal degeneration, as seen in PS19/E4 mice treated with ASO-NTC or ASO-E4-4; however, neuron-preferential reduction of APOE4 eliminates such a relationship.

We also assessed the percent coverage of activated microglia by staining for CD68 in the same cohort of mice (Fig. 2.6g). PS19/E4 mice treated with either ASO-E-4 or ASO-I3-75 did not exhibit a significant change in the percent coverage area of $CD68^+$ microglia compared to the mice treated with ASO-NTC (Fig. 2.6g,h). When correlating $CD68^+$ percent coverage area to hippocampal volume, there was a trending negative correlation in PS19/E4 mice treated with ASO-NTC and a significant negative correlation in PS19/E4 mice treated with ASO-E-4 (Fig. 2.6l). However, there was no longer a significant negative correlation in PS19/E4 mice treated with ASO-I3-75. Again, these data suggest that increased activated microglia is a good indicator or contributing factor to hippocampal degeneration, as seen in PS19/E4 mice treated with ASO-NTC

or ASO-E4-4; however, neuron-preferential reduction of APOE4 eliminates such a relationship. In other words, in mice treated with ASO-I3-75, activated microglia are no longer a good indicator of hippocampal degeneration, perhaps due to shifts in disease-associated and disease-protective subpopulations of microglia in response to decreased neuronal APOE expression. Taken together, the contributions of microglia or activated microglia to hippocampal degeneration depend on neuronal expression of APOE4.

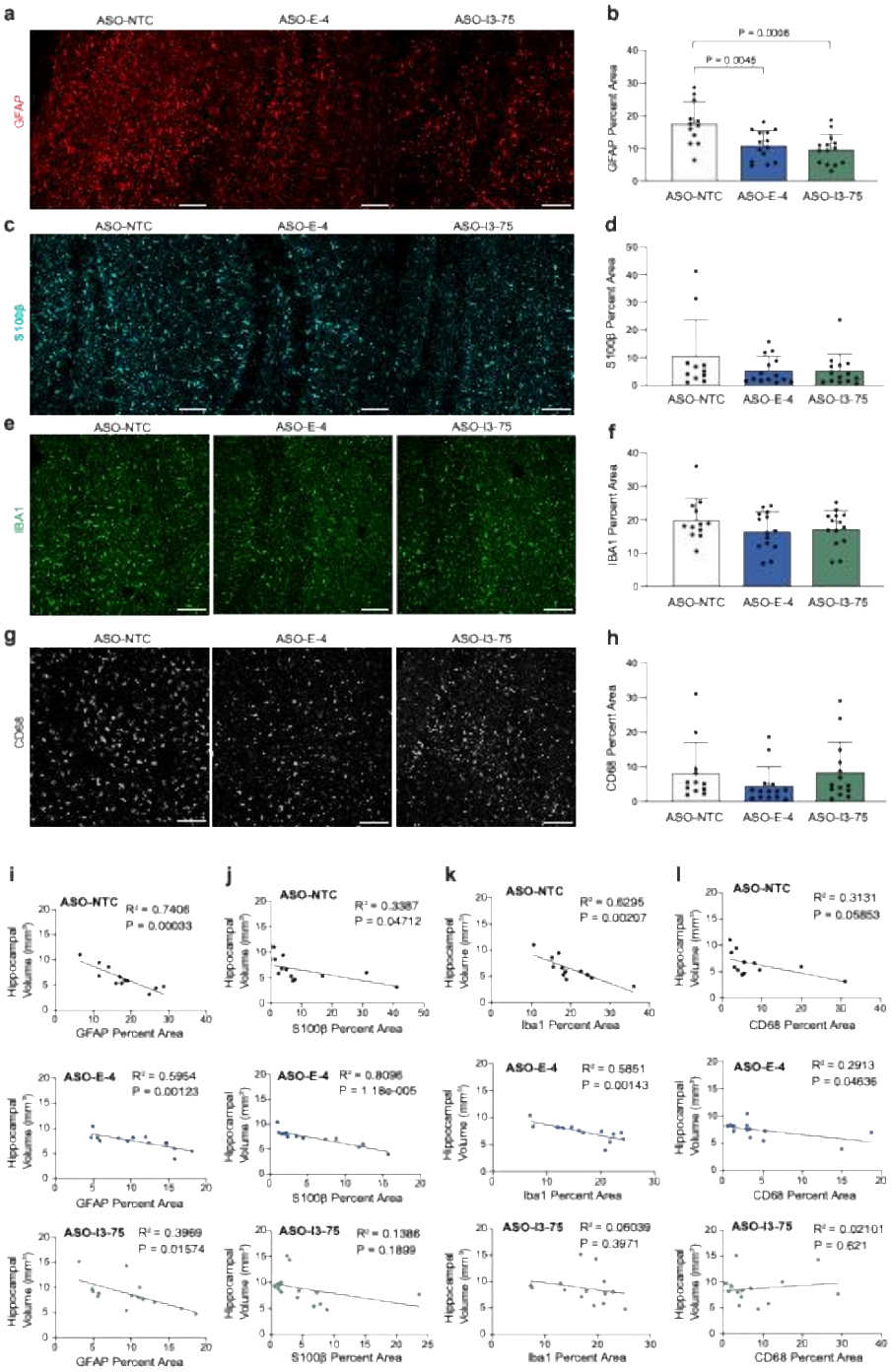


Fig. 2.6 | Both ASO-E-4 and ASO-I3-75 reduces astrogliosis while only ASO-I3-75 alters the contribution of microgliosis to hippocampal degeneration in PS19/E4 mice.

a, Representative images of astrocyte immunostaining with anti-GFAP in the dentate gyrus (DG) of 9.5-month-old PS19/E4 mice treated with ASO-NTC, ASO-E-4, or ASO-I3-75 for 4 weeks. *(figure caption continued on next page)*

(figure caption continued from the previous page) **b**, Quantification of percent GFAP coverage area in the DG and CA1 of 9.5-month-old PS19/E4 mice treated with ASO-NTC, ASO-E-4, or ASO-I3-75. **c,** Representative images of activated astrocyte immunostaining with anti-S100β in the DG of 9.5-month-old PS19/E4 mice treated with different ASOs. **d**, Quantification of percent S100β coverage area in the DG and CA1 of 9.5-month-old PS19/E4 mice treated with different ASOs. **e**, Representative images of microglia immunostaining with anti-Iba1 in the DG of 9.5-month-old PS19/E4 mice treated with different ASOs. **f**, Quantification of the percent Iba1 coverage area in the DG and CA1 of 9.5-month-old PS19/E4 mice treated with different ASOs. **g**, Representative images of activated microglia immunostaining with anti-CD68 in the DG of 9.5-month-old PS19/E4 mice treated with different ASOs. **h**, Quantification of the percent CD68 coverage area in the DG and CA1 of 9.5-month-old PS19/E4 mice treated with different ASOs. For all images, scale bars are 100μm. For all image quantifications, data is averaged from 4 fields of view from 2 brain sections (2 fields of view from the DG and 2 fields of view from the CA1). ASO-NTC, n=12 mice; ASOE-4, n=14 mice; ASO-I3-75, n=14 mice. **i**, Correlations between hippocampal volume (mm^3) and percent GFAP coverage area in PS19/E4 mice treated with ASO-NTC, ASO-E-4, or ASO-I3-75. **j**, Correlations between hippocampal volume (mm^3) and percent S100β coverage area in PS19/E4 mice treated with ASO-NTC, ASO-E-4, or ASO-I3-75. **k**, Correlations between hippocampal volume (mm^3) and percent IBA1 coverage area in PS19/E4 mice treated with ASO-NTC, ASO-E-4, or ASO-I3-75. **l**, Correlations between hippocampal volume (mm^3) and percent CD68 coverage area in PS19/E4 mice treated with ASO-NTC, ASO-E-4, or ASO-I3-75. For all quantifications of percent area coverage, data are expressed as mean ± s.d., and differences between groups were determined by ordinary one-way ANOVA followed by Tukey's multiple comparison test. For all correlations, Pearson's correlation analysis (two-sided) was performed.

ASO-E-4 and ASO-I3-75 diminishes disease-associated excitatory neurons in the hippocampus of PS19/E4 mice

To gain an in-depth understanding of the cell type-specific effects of the two APOE-targeting ASOs at a transcriptomic level, we performed single nucleus RNA-sequencing (snRNA-seq) on isolated hippocampi from the same cohort of PS19/E4 mice after 4 weeks of ASO treatment (at 9.5 months of age). The snRNA-seq dataset contained 161,796 nuclei covering 26,885 genes after normalization and filtering for quality control. Clustering by the Louvain algorithm and visualization by Uniform Manifold Approximation and Projection (UMAP) revealed 38 distinct cell clusters (Fig. 2.7a). Based on their expression of marker genes (Supplementary Table 1), these clusters were assigned to 13 excitatory neuron (Ex) clusters (2-4, 7, 9, 16, 22, 27, 28, 30, 31, 34,

and 37), 4 inhibitory neuron (In) clusters (8, 11, 15, and 26), 7 subiculum clusters (10, 14, 17, 18, 20, 25, and 33), 3 oligodendrocyte clusters (1, 5, and 24), 1 astrocyte cluster (13), 2 microglia clusters (6 and 21), 3 OPC clusters (12, 29, and 38) and 4 unknown clusters (23, 32, 35, and 36) (Fig. 2.7a and Fig. 2.8a,b).

To understand how pathology relates to transcriptomic results, we used log odds ratio (LOR) estimates from a generalized linear mixed-effects model (GLMM) to assess associations with histopathology (GLMM_histopathology). This analysis revealed various excitatory neuron clusters that exhibited significant correlations with disease pathology (Fig. 2.7c, Fig. 2.9c, Supplementary Table 1). Cell clusters 22, 27, and 31 exhibited significant negative associations with hippocampal volume and positive associations with certain gliosis measurements (Fig. 2.7c, Fig. 2.9c, Supplementary Table 1). For instance, cluster 22 and 27 were positively correlated with the coverage area of GFAP and APOE4 in neurons (Fig. 2.7c, Fig. 2.9c), while cluster 31 was positively correlated with coverage area of GFAP, S100β, and CD68 (Fig. 2.7c, Fig. 2.9c). These associations suggest that these excitatory neuron clusters are disease-associated excitatory neuron (DAEN) subtypes.

To further examine cell type-specific alterations in PS19/E4 mice treated with the different APOE-targeting ASOs, we also used LOR estimates from a GLMM to assess association with animal models (GLMM_AM). Such analysis revealed cell clusters in which there was a significant change in the likelihood that the cluster contained more or fewer cells from PS19/E4 mice treated with ASO-E-4 or ASO-I3-75 than from the mice treated with ASO-NTC. Excitatory neuron clusters 22,

27, and 31 had significantly lower odds of having cells from PS19/E4 mice treated with ASO-E-4 or ASO-I3-75 than from the mice treated with ASO-NTC (Fig. 2.7b, Fig. 2.9a,b), suggesting diminished DAEN in mice with either global or neuron-preferential reduction of APOE4.

Based on differentially expressed gene (DEG) analyses, cells in neuron clusters 22, 27, and 31 had significantly upregulated expression of the following genes relative to the other excitatory neuron clusters: *Pde4b, St18, Prr5l, Sox2ot, Neat1, Plcl1, Erbin, Plxdc2, Cdk19*, and *Rtn4* (Fig. 2.9d, Fig. 2.10a-c, Supplementary Table 1). Interestingly, *Pde4b* has been implicated in AD in previous studies where inhibition offered protective effects.[28] Notably, DAEN clusters 22, 27, and 31 from PS19/E4 mice treated with either ASO-E-4 or ASO-I3-75 had remarkably similar top upregulated and top downregulated genes when compared to mice treated with ASO-NTC (Fig. 2.7d,e, Fig. 2.10d-g). This suggests that ASO-E-4 and ASO-I3-75 induce similar transcriptomic changes in these clusters of DAEN, supporting the conclusion that the DEGs induced by global APOE4 reduction in DAEN of PS19/E4 are primarily driven by neuronal APOE4 reduction.

ASO-E-4 and ASO-I3-75 diminishes disease-associated inhibitory neurons in the hippocampus of PS19/E4 mice

To gain deeper insights into the effects of the two APOE-targeting ASOs on transcriptomics in inhibitory neurons, we did further subclustering analyses of inhibitory neurons in the snRNA-seq dataset. Subclustering of inhibitory neurons (clusters 8, 11, 15, and 26 in Fig. 2.7a) identified 23 inhibitory neuron subpopulations (Fig. 2.7f, Supplementary Table 2). LOR estimates from a GLMM_histopathology revealed that the proportion of cells in inhibitory neuron subclusters 15

and 22 exhibited a significant negative association with hippocampal volume and a significant positive association with neuronal APOE coverage area in the hippocampus (Fig. 2.7i, Fig. 2.11a, Supplementary Table 2). Additionally, cluster 22 exhibited a significant positive association with markers of gliosis, such as GFAP and CD68 coverage area (Fig. 2.7i, Fig. 2.11a). Together, these data suggest that inhibitory neuron subclusters 15 and 22 represent disease-associated inhibitory neuron (DAIN) subtypes.

LOR estimates from a GLMM_AM revealed that inhibitory neuron subclusters 15 and 22 had significantly lower odds of having cells from PS19/E4 mice treated with ASO-E-4 or ASO-I3-75 than from the mice treated with ASO-NTC (Fig. 2.7g,h), suggesting that either global or neuron-preferential reduction of APOE4 diminishes these DAIN subtypes. Based on DEG analyses, cells in inhibitory neuron subclusters 15 and 22 had significantly upregulated expression of the following genes relative to the other inhibitory neuron clusters: *Kcnip4, Pex5l, Marchf1, Sorcs3, Adarb2, Ptprd, Thsd7b, St6galnac3, Brinp3,* and *Nkain2* (Fig. 2.11b-d, Supplementary Table 2). Interestingly, *Kcnip4, Pex5l,* and *Nkain2* are genes important for neuronal excitability; hyperexcitability and network dysfunction are established hallmarks of AD.[29–31] Comparison of DEGs in DAIN subcluster 15 between PS19/E4 mice treated with either ASO-E-4 or ASO-I3-75 and the mice treated with ASO-NTC revealed some similar top downregulated genes, but very few shared top upregulated genes (Fig. 2.11e,f). In a similar DEG comparison for DAIN subcluster 22, PS19/E4 mice treated with either ASO-E-4 or ASO-I3-75 versus mice treated with ASO-NTC had very few shared top downregulated and upregulated genes (Fig. 2.7j,k). Taken together, these data illustrate that both global and neuron-preferential reduction of APOE4 by APOE-targeting

ASOs diminishes DAIN. However, the transcriptomic changes induced by the global APOE4 reduction and the neuron-preferential APOE4 reduction are different in these DAINs, particularly DAIN subcluster 22, likely contributing to their differential effects on rescuing hippocampal neurodegeneration.

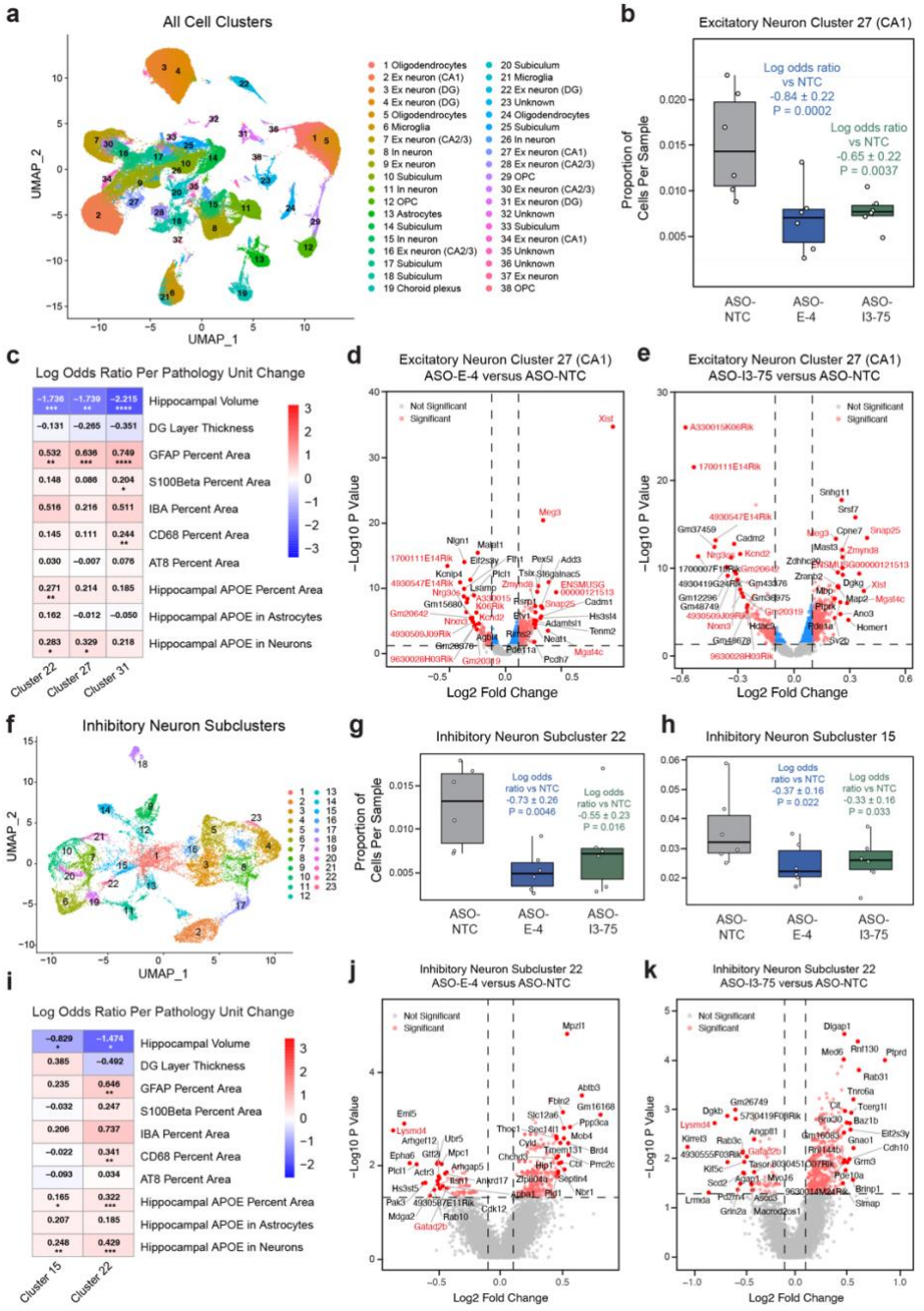


Fig. 2.7 | ASO-E-4 and ASO-I3-75 diminishes disease-associated excitatory and inhibitory neurons (DAEN and DAIN) in the hippocampus of PS19/E4 mice.

a, UMAP plot of all 38 distinct cell clusters in the hippocampi of 9.5-month-old PS19/E4 mice treated with ASO-NTC, ASO-E-4, or ASO-I3-75 for 4 weeks. **b**, Box plot of the proportion of cells from each ASO treatment group in cluster 27. *(figure caption continued on next page)*

(figure caption continued from the previous page) For all box plots, the lower, middle and upper hinges of the box plots correspond to the 25th, 50th and 75th percentiles, respectively. The upper whisker of the box plot extends from the upper hinge to the largest value no further than 1.5 × IQR from the upper hinge. IQR, interquartile range or distance between 25th and 75th percentiles. The lower whisker extends from the lower hinge to the smallest value at most 1.5 × IQR from the lower hinge. Data beyond the end of the whiskers are outlier points. The log odds ratios are the mean ± s.e.m. estimates of log odds ratio for this cluster, which represents the change in the log odds of cells per sample from PS19/E4 mice treated with ASO-E-4 or ASO-I3-75 belonging to the selected cell cluster compared to the log odds of cells per sample from PS19/E4 mice treated with ASO-NTC ASO. **c**, Heat map plot of the log odds ratio per unit change in each pathological parameter for cell clusters 22, 27, and 31. The log odds ratio represents the mean estimate of the change in the log odds of cells per sample from a given treatment group, corresponding to a unit change in a given histopathological parameter. Negative associations are shown in blue and positive associations are shown in red. Unadjusted P values are from fits to a GLMM_histopathology. **d,e,** Volcano plot of the DEGs in excitatory neuron cluster 27 between PS19/E4 mice treated with ASO-E-4 and those treated with ASO-NTC (**d**) and between PS19/E4 mice treated with ASO-I3-75 and those treated with ASO-NTC (**e**). Up- or down-regulated genes shared between **d** and **e** are indicated in red font. **f**, UMAP plot of 23 inhibitory neuron subclusters after subclustering hippocampal cell clusters 8, 11, 15, and 26. **g**,**h**, Box plot of the proportion of cells from each ASO treatment group in inhibitory neuron subcluster 22 (**g**) and inhibitory neuron subcluster 15 (**h**). **i**, Heatmap plot of the log odds ratio per unit change in each pathological parameter for inhibitory neuron subclusters 15 and 22. Negative associations are shown in blue and positive associations are shown in red. Unadjusted P values are from fits to a GLMM_ histopathology. **j,k**, Volcano plot of the DEGs in inhibitory neuron cluster 22 between PS19/E4 mice treated with ASO-E-4 and those treated with ASO-NTC (**j**) and between PS19/E4 mice treated with ASO-I3-75 and those treated with ASO-NTC (**k**). Up- or down-regulated genes shared between **j** and **k** are indicated in red font.

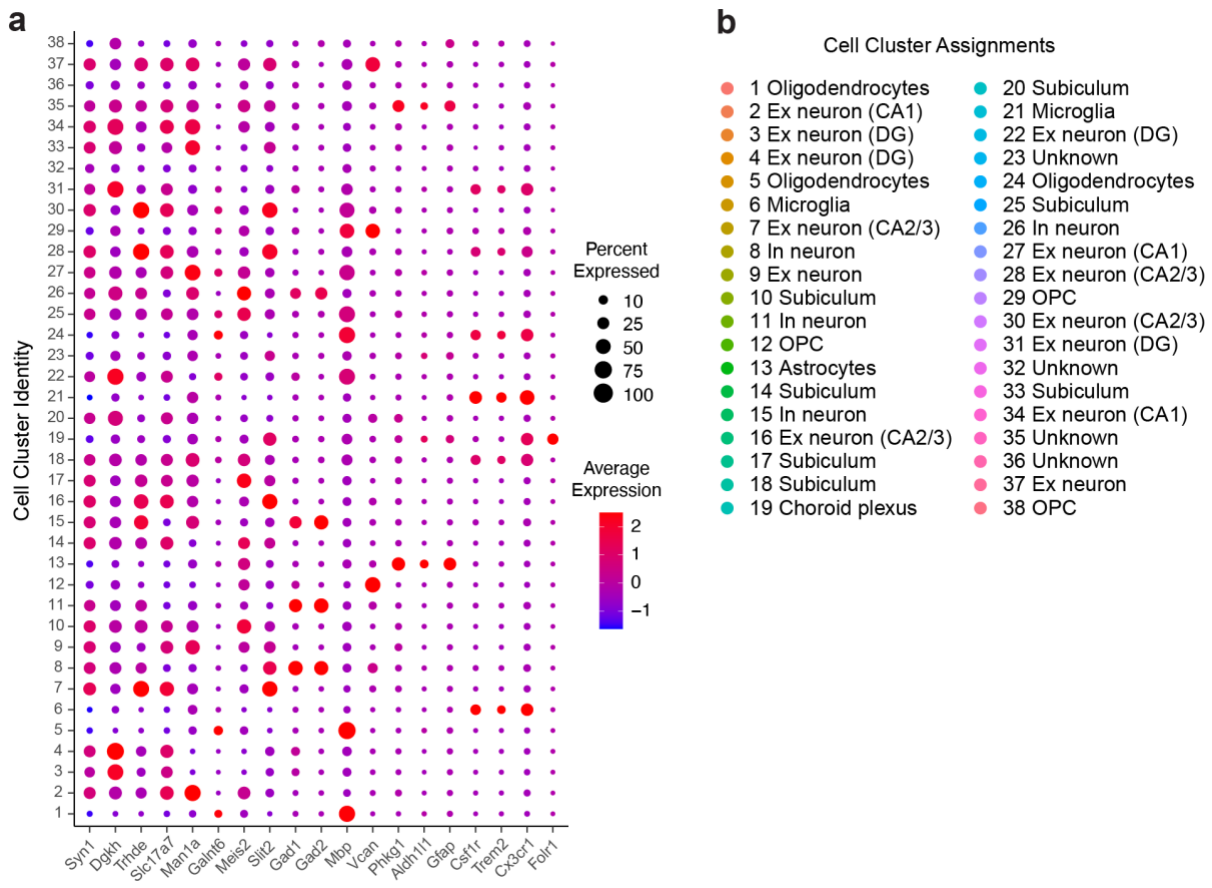


Fig. 2.8 | snRNA-seq identification of cell clusters.
a, Dot-plot depicting normalized average expression of selected cell identity marker genes for all 38 unique hippocampal cell clusters from 9.5-month-old PS19/E4 mice treated with ASO-NTC, ASO-E-4, or ASO-I3-75 for 4 weeks. The size of the dots is proportional to the percentage of cells expressing a given gene. Average expression is on a colored scale (lower expression, blue; higher expression, red). **b**, Assigned identity of 38 distinct cell types. Ex neuron, excitatory neuron; In neuron, inhibitory neuron; DG, dentate gyrus; OPC, oligodendrocyte precursor cell.

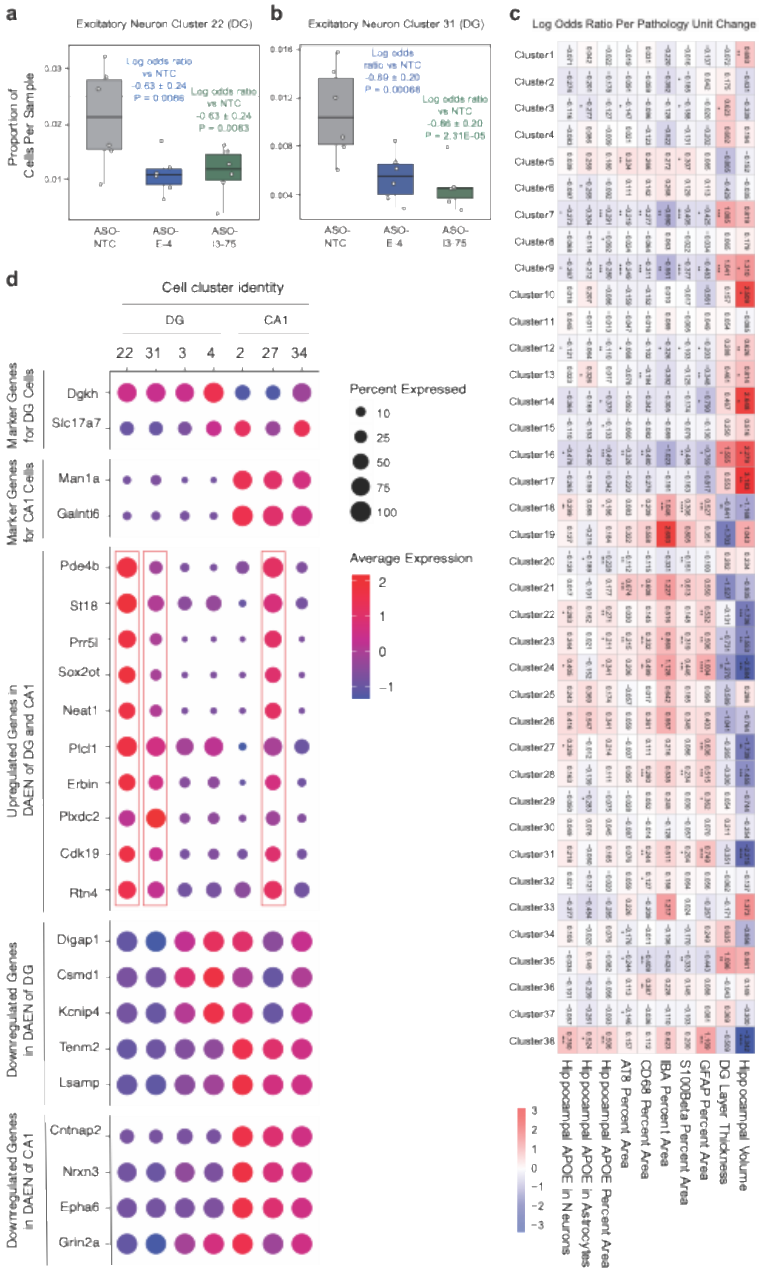


Fig. 2.9 | ASO-E-4 and ASO-I3-75 diminishes disease-associated excitatory neurons (DAEN) in the hippocampus of ASO-treated PS19/E4 mice.

a-b, Box plot of the proportion of cells from each ASO treatment group in excitatory neuron cluster 22 (**a**) and excitatory neuron cluster 31 (**b**). For details see legend in Fig. 2.7b. **c**, Heat map plot of the log odds ratio per unit change in each pathological parameter for all 38 cell clusters. Negative associations are shown in blue and positive associations are shown in red. Unadjusted P values are from fits to a GLMM_ histopathology. *(figure caption continued on next page)*

(figure caption continued from the previous page) **d**, Dot-plot of normalized average expression of marker genes and genes of interest for selected excitatory neuron clusters. The size of the dots is proportional to the percentage of cells expressing a given gene. Average expression is on a colored scale (lower expression, blue; higher expression, red).

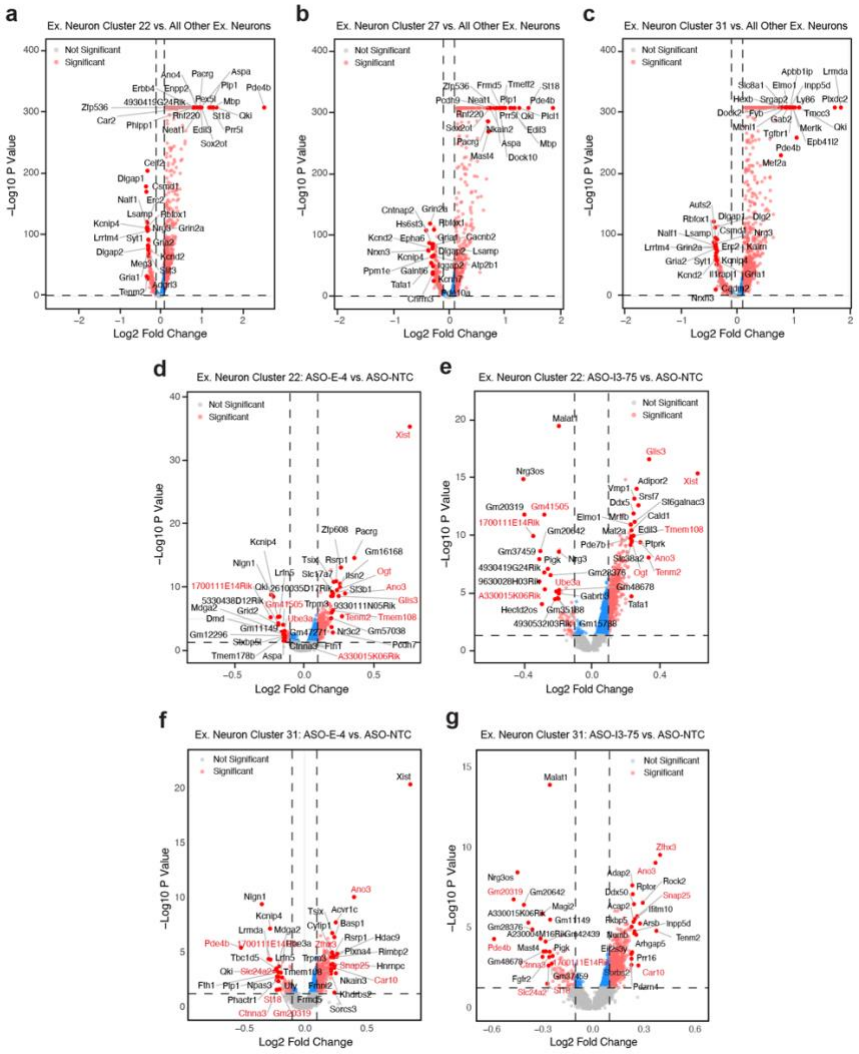


Fig. 2.10 | Differentially expressed genes (DEGs) in disease-associated excitatory neurons (DAEN) in the hippocampus of ASO-treated PS19/E4 mice.

a-c, Volcano plot of the DEGs between excitatory neuron cluster 22 and all other excitatory neurons (**a**), between excitatory neuron cluster 27 and all other excitatory neurons (**b**), and between excitatory neuron cluster 31 and all other excitatory neurons (**c**). **d,e**, Volcano plot of the DEGs in excitatory neuron subcluster 22 between PS19/E4 mice treated with ASO-E-4 and those treated with ASO-NTC (**d**) and between PS19/E4 mice treated with ASO-I3-75 and those treated with ASO-NTC (**e**). *(figure caption continued on next page)*

(figure caption continued from the previous page) Up- or down-regulated genes shared between **d** and **e** are indicated in red font. **f,g**, Volcano plot of the DEGs in excitatory neuron cluster 31 between PS19/E4 mice treated with ASO-E-4 and those treated with ASO-NTC (**f**) and between PS19/E4 mice treated with ASO-I3-75 and those treated with ASO-NTC (**g**). Up- or down-regulated genes shared between **f** and **g** are indicated in red font. For all volcano plots, dashed lines represent $\log_2$ fold change threshold of 0.1 and p value threshold of 0.05. The unadjusted p values and $\log_2$ fold change values used were generated from the gene-set enrichment analysis using the two-sided Wilcoxon rank-sum test as implemented in the FindMarkers function of the Seurat package.

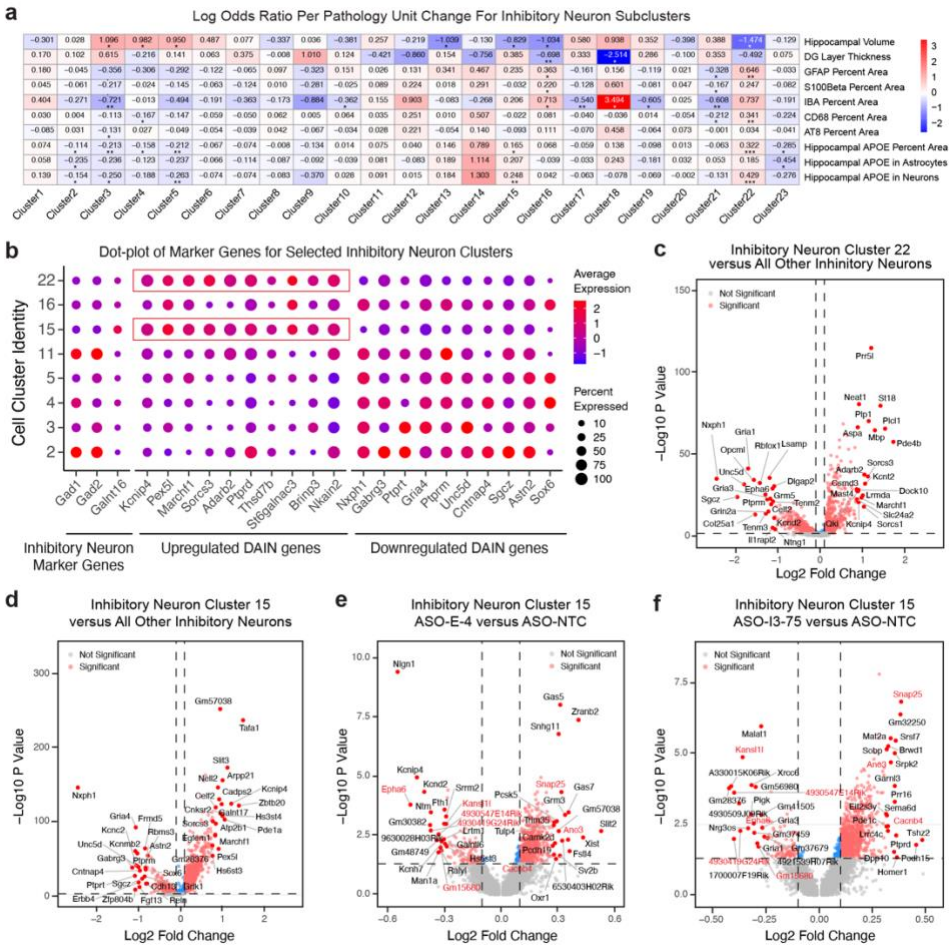


Fig. 2.11 | Characteristics of disease-associated inhibitory neurons (DAIN) in the hippocampus of ASO-treated PS19/E4 mice.

a, Heat map plot of the log odds ratio per unit change in each pathological parameter for inhibitory neuron subclusters. Negative associations are shown in blue and positive associations are shown in red. Unadjusted P values are from fits to a GLMM_ histopathology. *(figure caption continued on next page)*

(figure caption continued from the previous page) **b,** Dot-plot of normalized average expression of marker genes and genes of interest for selected inhibitory neurons. The size of the dots is proportional to the percentage of cells expressing a given gene. Average expression is on a colored scale (lower expression, blue; higher expression, red). **c,d**, Volcano plot of the DEGs between inhibitory neuron subcluster 22 and all other inhibitory neurons (**c**) and between inhibitory neuron subcluster 15 and all other inhibitory neuron (**d**). **e,f**, Volcano plot of the DEGs in inhibitory neuron subcluster 15 between PS19/E4 mice treated with ASO-E-4 and those treated with ASO-NTC **(e)** and between PS19/E4 mice treated with ASO-I3-75 and those treated with ASO-NTC (**f**). Up- or down-regulated genes shared between **e** and **f** are indicated in red font. For all volcano plots, dashed lines represent log2 fold change threshold of 0.1 and p value threshold of 0.05. The unadjusted p values and log2 fold change values used were generated from the gene-set enrichment analysis using the two-sided Wilcoxon rank-sum test as implemented in the FindMarkers function of the Seurat package.

ASO-I3-75 is more effective than ASO-E-4 at reducing disease-associated astrocytes in the hippocampus of PS19/E4 mice

We next wanted to better understand the effects of the two APOE-targeting ASOs on astrocytes. To do so, we further subclustered the astrocytes of the snRNA-seq dataset (cluster 13 in Fig. 2.7a) and identified 15 astrocyte subpopulations (Fig. 2.12a, Supplementary Table 3). LOR estimates from a GLMM_histopathology revealed that the proportion of cells in astrocyte subclusters 4 and 9 exhibited a significant negative association with hippocampal volume and a significant positive association with GFAP coverage area (Fig. 2.12d, Fig. 2.13a, Supplementary Table 3). Subcluster 4 also had a significant negative association with DG neuronal layer thickness and a significant positive association with S100β and CD68 coverage area; and subcluster 9 exhibited a positive association with IBA1 and hippocampal neuronal APOE coverage area (Fig. 2.12d, Fig. 2.13a, Supplementary Table 3). Altogether, these associations suggest that astrocyte subclusters 4 and 9 represent disease-associated astrocyte (DAA) subtypes.

LOR estimates from a GLMM_AM revealed that astrocyte subcluster 4 had significantly lower odds of having cells from PS19/E4 mice treated with ASO-I3-75 than from the mice treated with ASO-NTC (Fig. 2.12b), suggesting that neuron-preferential reduction of APOE4 is particularly effective at diminishing this DAA subtype. Interestingly, astrocyte subcluster 9 had significantly lower odds of having cells from PS19/E4 mice treated with either ASO-E-4 or ASO-I3-75 than from the mice treated with ASO-NTC (Fig. 2.12c), suggesting that either global or neuron-preferential reduction of APOE4 is effective at diminishing this particular DAA subtype.

DEG analyses revealed that cells in DAA subclusters 4 and 9 had significantly upregulated expression of the following genes relative to the other astrocyte clusters: *Grm5, Ncam2, Enox1, Chl1, Lrp1b, Cadm2, Nav2, Rfx3, Stxbp6,* and *Cadps* (Fig. 2.13b, Fig. 2.14a,b, Supplementary Table 3). Comparison of DEGs in DAA subcluster 4 between PS19/E4 mice treated with ASO-E-4 or ASO-I3-75 and the mice treated with ASO-NTC revealed some similar top downregulated genes, but very few shared top upregulated genes (Fig. 2.12e,f). This suggests that the upregulation of genes induced by the global APOE4 reduction and the neuron-preferential APOE reduction are different in DAA subcluster 4, likely contributing to their differential effects on rescuing hippocampal neurodegeneration. Interestingly, DEG comparison in subcluster 9 between PS19/E4 mice treated with ASO-E-4 or ASO-I3-75 and the mice treated with ASO-NTC yielded many similar top upregulated and downregulated genes (Fig. 2.14e,f). This suggests that ASO-E-4 and ASO-I3-75 induce similar transcriptomic changes in DAA subcluster 9, supporting the conclusion that the DEGs induced by global APOE4 reduction in this subtype of DAA in PS19/E4 mice are primarily driven by neuronal APOE4 reduction. Taken together, all these data illustrate that both global and

neuron-preferential reduction of APOE4 diminishes subtypes of DAA in PS19/E4 mice. However, neuron-preferential reduction of APOE4 seems to be more effective at reducing multiple subtypes of DAA, probably contributing to its more effective rescue of hippocampal neurodegeneration in this tauopathy mouse model.

ASO-I3-75, but not ASO-E-4, reduces disease-associated microglia and increases disease-protective microglia in the hippocampus of PS19/E4 mice

Lastly, to better understand the effects of the two APOE-targeting ASOs on microglia, we further subclustered microglia (cluster 6 and 21 in Fig. 2.7a), identifying 13 microglia subpopulations (Fig. 2.12g, Supplementary Table 4). LOR estimates from a GLMM_histopathology revealed that the proportion of cells in microglia subcluster 3 exhibited a significant negative association with hippocampal volume and a significant positive association with GFAP coverage area, S100β coverage area, and CD68 coverage area (Fig. 2.12j, Fig. 2.13c, Supplementary Table 4), suggesting that microglia subcluster 3 represents a disease-associated microglia (DAM) subtype.

LOR estimates from a GLMM_AM revealed that microglia subcluster 3 had significantly lower odds of having cells from PS19/E4 mice treated with ASO-I3-75 than from the mice treated with ASO-NTC (Fig. 2.12h), suggesting that neuron-preferential, but not global, reduction of APOE4 diminishes this subtype of DAM. DEG analyses revealed that cells in microglia subcluster 3 had significantly upregulated expression of the following genes relative to the other microglia clusters: *Apobec1, Gpnmb, Lyst, Fnip2, Igf1, Myo5a, Atp6v0d2, Pid1, Colec12,* and *Arhgap15* (Fig. 2.13d, Fig. 2.14c, Supplementary Table 4). *Gpnmb* is an important DAM gene and is known to increase

in an age-dependent manner in transgenic AD models.[32] Both *Lyst* and *Atp6v0d2* are important genes for lysosomal function, and lysosomal dysfunction leading to profuse accumulations of neuronal waste is a known pathology in AD.[33] Notably, comparison of DEGs in DAM subcluster 3 between PS19/E4 mice treated with either ASO-E-4 or ASO-I3-75 and the mice treated with ASO-NTC yielded several similar top downregulated genes and very few similar top upregulated genes (Fig. 2.12k,l). This suggests that the upregulation of genes induced by the global APOE4 reduction and the neuron-preferential APOE reduction are different in DAM subcluster 3, likely contributing to their differential effects on rescuing hippocampal neurodegeneration. Overall, neuron-preferential reduction of APOE4 seems to be more effective at reducing DAM in PS19/E4 mice compared to global reduction of APOE4.

Interestingly, LOR estimates from a GLMM_histopathology also revealed that the proportion of cells in microglia subcluster 1 exhibited a significant positive association with hippocampal volume and a significant negative association with GFAP coverage area and CD68 coverage area (Fig. 2.12j, Fig. 2.13c, Supplementary Table 4), suggesting that microglia subcluster 1 represents a disease protective microglia (DPM) subtype.

LOR estimates from a GLMM_AM revealed that DPM subcluster 1 had strong trending higher odds ($p = 0.053$) of having cells from PS19/E4 mice treated with ASO-I3-75 than from the mice treated with ASO-NTC (Fig. 2.12i). Based on DEG analyses, cells in microglia subcluster 1 had significantly upregulated expression of the following genes relative to the other microglia clusters: *Malat1, Ttr, Tmsb4x, Arhgap45, Gpr34, Dynll1, Tanc2, Siglech, St3gal5,* and *Rhobtb1* (Fig. 2.13d, Fig. 2.14d,

Supplementary Table 4). Interestingly, DPM subcluster 1 had significant downregulated expression of the *Apobec1*, *Myo5a*, *Fnip2*, *Lyst* and *Arhgap15* – genes that were upregulated in DAM subcluster 3—further supporting the conclusion that it is a DPM subtype (Fig. 2.13d, Fig. 2.14c,d). Furthermore, *Tanc2*, which is upregulated in DPM subcluster 1, is downregulated in DAM subcluster 3 (Fig. 2.13d, Fig. 2.14c,d). Comparing DEGs in DPM subcluster 1 between PS19/E4 mice treated with either ASO-E-4 or ASO-I3-75 and the mice treated with ASO-NTC yielded similar top upregulated and top downregulated DEGs (Fig. 2.14g,h, Supplementary Table 4). This suggests that ASO-E-4 and ASO-I3-75 induce similar transcriptomic changes in this DPM subtype, supporting the conclusion that the DEGs induced by global APOE4 reduction in this DPM subtype in PS19/E4 mice are primarily driven by neuronal APOE4 reduction. However, neuron-preferential reduction of APOE4 appears to be more effective than global reduction of APOE4 at increasing this DPM subtype. Taken together, these data illustrate that neuron-preferential reduction of APOE4 is more effective than global reduction of APOE4 at decreasing DAM and increasing DPM in PS19/E4 mice.

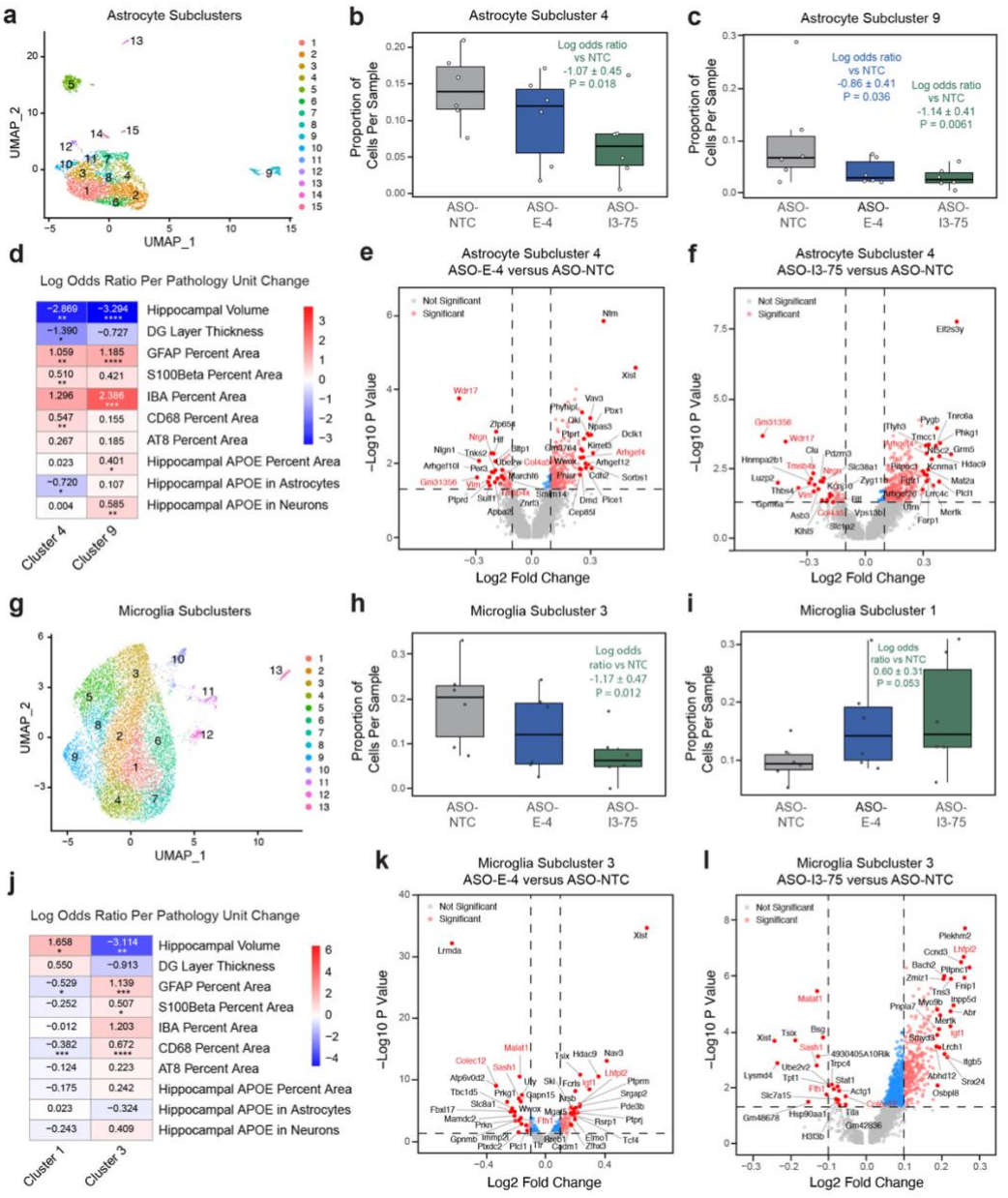


Fig. 2.12 | ASO-I3-75 is more effective than ASO-E-4 at reducing disease-associated astrocytes (DAA), reducing disease-associated microglia (DAM), and increasing disease-protective microglia (DPM) in the hippocampus of PS19/E4 mice.

a, UMAP plot of 15 astrocyte subclusters after subclustering hippocampal cell cluster 13. **b,c**, Box plot of the proportion of cells from each ASO treatment group in astrocyte subcluster 4 (**b**) and astrocyte subcluster 9 (**c**). For details see legend in Fig. 2.7b. **d**, Heatmap plot of the log odds ratio per unit change in each pathological parameter for astrocyte subclusters 4 and 9. Negative associations are shown in blue and positive associations are shown in red. Unadjusted P values are from fits to a GLMM_ histopathology. *(figure caption continued on next page)*

(figure caption continued from the previous page) **e,f**, Volcano plot of the DEGs in astrocyte subcluster 4 between PS19/E4 mice treated with ASO-E-4 and those treated with ASO-NTC (**e**) and between PS19/E4 mice treated with ASO-I3-75 and those treated with ASO-NTC (**f**). Up- or down-regulated genes shared between **e** and **f** are indicated in red font. **g**, UMAP plot of 13 microglia subclusters after subclustering hippocampal cell clusters 6 and 21. **h,i**, Box plot of the proportion of cells from each ASO treatment group in microglia subclusters 3 (**h**) and 1 (**i**). For details see legend in Fig. 2.7b. **j**, Heatmap plot of the log odds ratio per unit change in each pathological parameter for microglia subclusters 1 and 3. Negative associations are shown in blue and positive associations are shown in red. Unadjusted P values are from fits to a GLMM_ histopathology. **k,l**, Volcano plot of the DEGs in microglia subcluster 3 between PS19/E4 mice treated with ASO-E-4 and those treated with ASO-NTC (**k**) and between PS19/E4 mice treated with ASO-I3-75 and those treated with ASO-NTC (**l)**. Up- or down-regulated genes shared between **k** and **l** are indicated in red font.

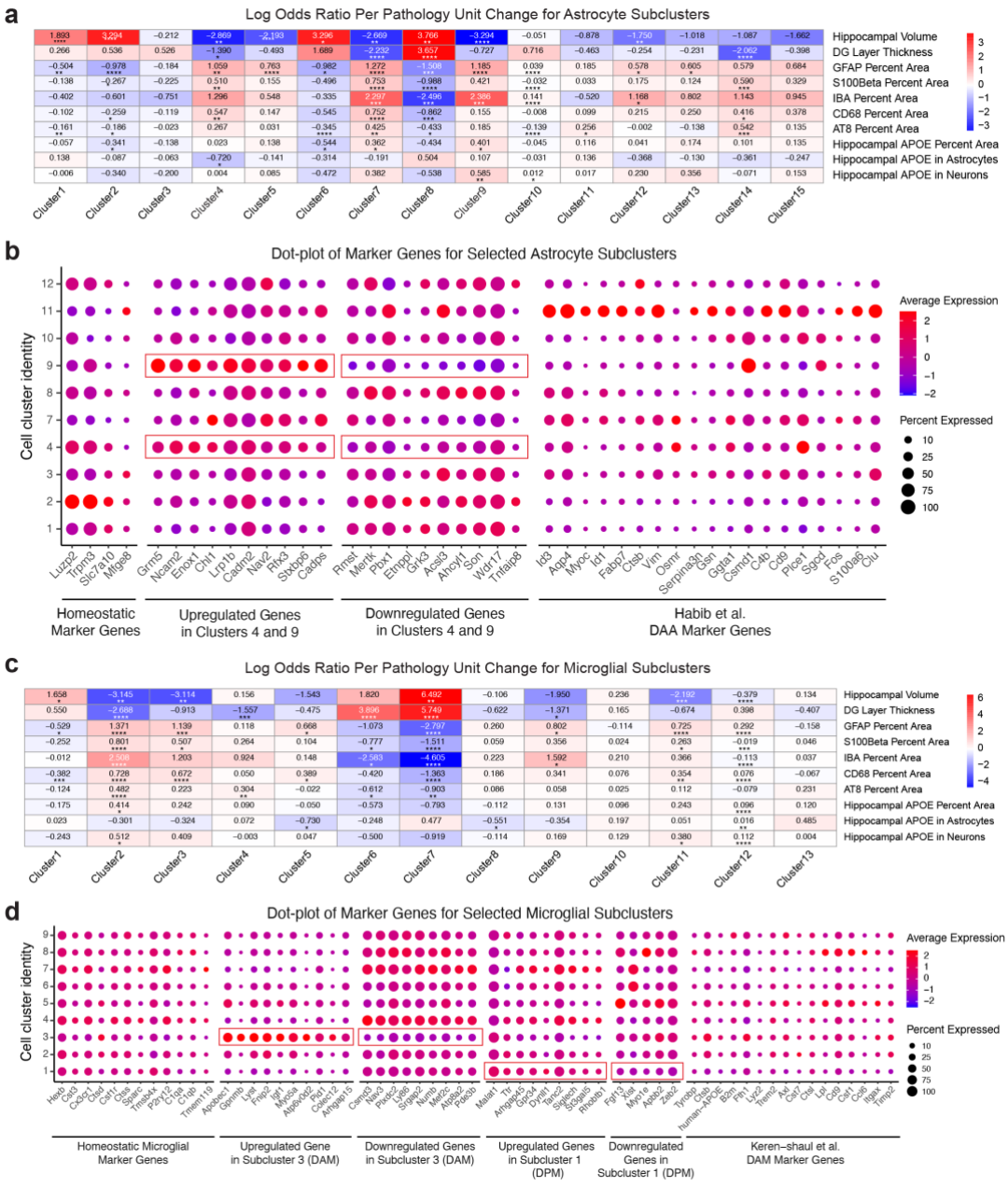


Fig. 2.13 | Characteristics of disease-associated astrocytes (DAA), disease-associated microglia (DAM), and disease-protective microglia (DPM) in the hippocampus of ASO-treated PS19/E4 mice.

a, Heat map plot of the log odds ratio per unit change in each pathological parameter for all astrocyte subclusters. Negative associations are shown in blue and positive associations are shown in red. Unadjusted P values are from fits to a GLMM_ histopathology. **b,** Dot-plot of normalized average expression of marker genes and genes of interest for selected astrocyte subclusters. *(figure caption continued on next page)*

(figure caption continued from the previous page) The size of the dots is proportional to the percentage of cells expressing a given gene. Average expression is on a colored scale (lower expression, blue; higher expression, red). **c**, Heat map plot of the log odds ratio per unit change in each pathological parameter for all microglia subclusters. Negative associations are shown in blue and positive associations are shown in red. Unadjusted P values are from fits to a GLMM_ histopathology. **d**, Dot-plot of normalized average expression of marker genes and genes of interest for selected microglia subclusters. The size of the dots is proportional to the percentage of cells expressing a given gene. Average expression is on a colored scale (lower expression, blue; higher expression, red).

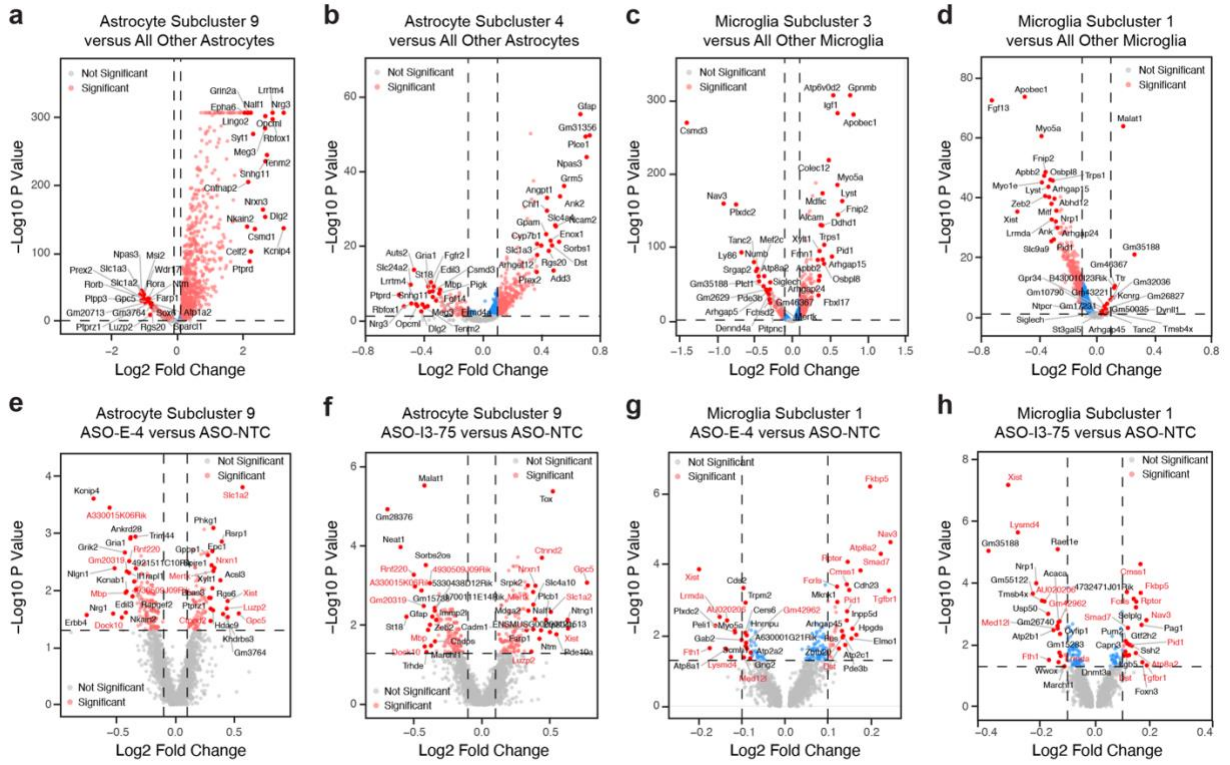


Fig. 2.14 | Differentially expressed genes (DEGs) in disease-associated astrocytes (DAA), disease-associated microglia (DAM), and disease-protective microglia (DPM) in the hippocampus of ASO-treated PS19/E4 mice.

a,b, Volcano plot of the DEGs between astrocyte subcluster 9 and all astrocytes (**a**) and between astrocyte subcluster 4 and all other astrocytes (**b**). **c,d,** Volcano plot of the DEGs between microglia subcluster 3 and all other microglia (**c**) and between microglia subcluster 1 and all other microglia (**d**). **e,f**, Volcano plot of the DEGs in astrocyte subcluster 9 between PS19/E4 mice treated with ASO-E-4 and those treated with ASO-NTC **(e)** and between PS19/E4 mice treated with ASO-I3-75 and those treated with ASO-NTC (**f**). Up- or down-regulated genes shared between **e** and **f** are indicated in red font. *(figure caption continued on next page)*

(figure caption continued from the previous page) **g,h**, Volcano plot of the DEGs in microglia subcluster 1 between PS19/E4 mice treated with ASO-E-4 and those treated with ASO-NTC **(g)** and between PS19/E4 mice treated with ASO-I3-75 and those treated with ASO-NTC (**h**). Up- or down-regulated genes shared between **g** and **h** are indicated in red font. For all volcano plots, dashed lines represent log2 fold change threshold of 0.1 and p value threshold of 0.05. The unadjusted p values and log2 fold change values used were generated from the gene-set enrichment analysis using the two-sided Wilcoxon rank-sum test as implemented in the FindMarkers function of the Seurat package.

Discussion

In this study, we investigated the therapeutic benefit of decreasing APOE4 expression globally or preferentially in neurons in the brain of an AD mouse model via the use of ASOs. We designed an ASO targeting APOE produced by all cell types in the brain (ASO-E-4) and an ASO preferentially targeting APOE produced by neurons (ASO-I3-75). First, we validated the efficacy of these ASOs *in vitro* using various cell culture systems and determined that ASO-I3-75 does preferentially reduce neuronal APOE by targeting a neuron-specific APOE-I3 transcript. Then, we demonstrate that treating PS19/E4 mice with ASO-I3-75 significantly rescues hippocampal neurodegeneration, alters p-tau contribution to neurodegeneration, decreases astrogliosis, alters microgliosis contribution to neurodegeneration, diminishes disease-associated excitatory and inhibitory neurons, reduces disease-associated astrocytes and microglia, and increases disease-protective microglia. While treating PS19/E4 mice with the global brain APOE-targeting ASO, ASO-E-4, recapitulates some of the abovementioned beneficial effects, such as decreasing astrogliosis and diminishing disease-associated neurons, it does not recapitulate all of them. Overall, these findings illustrate that preferentially reducing neuronal APOE4 is more beneficial than globally reducing APOE4 in the brain for protecting against key AD-related pathologies.

In vitro studies using mouse neuroblastoma cells stably transfected with human APOE3 genomic DNA and mouse primary neurons expressing human APOE4 from a mini-APOE4 gene (containing all exons and intron-3) demonstrated that treatment with either ASO-E-4 or ASO-I3-75 effectively reduces neuronal APOE expression. This is likely because the exon-4-targeting ASO-E-4 targets both mature APOE transcripts without intron-3 and neuron-specific APOE-I3 transcripts, whereas the intron-3-targeting ASO-I3-75 only targets the neuron-specific APOE-I3 transcripts, but not mature APOE transcripts. Similarly, *in vivo* studies with PS19/E4 mice show that both ASOs effectively reduce APOE4 expression in neurons. Therefore, the decreased astrogliosis and diminished disease-associated excitatory neurons that we observed following treatment with the global brain APOE-targeting ASO, ASO-E-4, could likely be achieved, at least in part, by decreasing neuronal APOE4 expression.

PS19/E4 mice treated with the neuronal-APOE-preferential ASO, ASO-I3-75, exhibited a significantly larger hippocampal volume compared to PS19/E4 mice treated with ASO-NTC, suggesting that preferentially reducing neuronal APOE4 effectively rescues hippocampal neurodegeneration. Strikingly, a significant negative correlation was observed between neuronal APOE4 levels and hippocampal volume in mice treated with ASO-I3-75, but not in mice treated with ASO-E-4 or ASO-NTC. This suggests that in a context where we can successfully decrease neuronal APOE4 expression levels, the extent of APOE4 reduction in neurons is a good predictor for the efficacy of hippocampal volume rescue.

When correlating hippocampal volume to gliosis measurements, such as S100β percent coverage area, IBA1 percent coverage area, and CD68 percent coverage area, a significant or trending negative correlation was observed in mice treated with ASO-NTC or ASO-E-4, suggesting that, in these mice, the severity of gliosis is a good predictor for hippocampal volume loss. Interestingly, for all three gliosis measurements in mice treated with ASO-I3-75, there was no longer a significant negative correlation with hippocampal volume, suggesting that in mice with neuronal APOE4 being preferentially reduced, higher levels of gliosis are no longer a good predictor for hippocampal volume loss. One possible explanation is that ASO-I3-75 treatment increases disease-protective microglial or astrocytic subpopulations, contributing to the increase in hippocampal volume. An example of such a disease-protective microglial subtype is the DPM subcluster 1.

A limitation of our current study is that we were unable to directly compare neuronal-APOE ASO reduction with an astrocyte-specific or microglia-specific APOE ASO reduction approach, largely due to the lack of technology enabling glial-specific ASO delivery. However, reducing glial APOE could confer protection against some AD-related pathologies. Studies have found that removal of APOE4 from astrocytes in a tauopathy mouse model reduces the extent of tau pathology, neurodegeneration, and gliosis.[27] To get a better understanding of this, further therapeutic studies should investigate cell-type specific APOE4 reduction in astrocytes or microglia starting at a similar age and in a similar PS19/E4 mouse model to see if reduction of APOE4 in only these cell types rescues AD pathologies. Since traditional ASO designs are not feasible to specifically target astrocytes or microglial APOE4, unique approaches are needed to reach this goal in the future.

It is also worth noting that PS19/E4 mice treated with ASO-I3-75 exhibited a noticeable decrease, despite not reaching statistical significance, in astrocytic APOE as well. This could be due to an effect of the ASO-I3-75 binding to some pre-mRNAs in astrocytes that contain intron-3 and thus, decreasing their conversion into mature APOE mRNA. Alternatively, given that previous studies found intron-3 containing APOE transcripts are not abundant in non-neuronal cell types,[20] this reduction could instead be due to secondary effects of the ASO-I3-75 efficiently decreasing neuronal APOE4. Decreased neuronal APOE4 could result in a decrease in astrocyte response (astrogliosis) to neuronal damage, and thus a decrease in astrocytic APOE4 because the numbers of astrocytes have decreased or their APOE4 expression levels have been reduced.

We reported previously that selective neuronal APOE4 removal in PS19/E4 mice from birth led to a wide range of beneficial effects, including reductions in the accumulation and spread of p-tau, neurodegeneration, myelin deficits, neuronal network hyperexcitability, microgliosis, astrogliosis, and disease-associated cell subpopulations.[11] In the present study, we expand on this body of work and demonstrate that preferentially reducing neuronal APOE4 by ASO-I3-75 treatment in 8.5-month-old PS19/E4 mice, after pathologies have initiated, also protects against and recues APOE4-driven AD pathologies.

Furthermore, studies have found that global depletion of APOE4 may have deleterious side effects,[34-38] suggesting that it would be more beneficial to achieve specific reduction of APOE4 in a certain cell type most vulnerable to APOE4 detrimental effects, such as neurons, while leaving the physiological functions of APOE4 largely intact in other types of cells. Our current study

provides a proof-of-concept case showing that preferentially reducing neuronal APOE4 with ASO-I3-75 treatment can eliminate most of the pathogenic effects of APOE4 while largely leaving APOE4 intact in other cells for its physiological functions. Clearly, further preclinical studies need to be done to better understand the underlying mechanisms and to identify optimal treatment dose and duration for potential clinical trial tests in AD patients with APOE4 in the future.

Methods

Mice

Human LoxP-floxed APOE4 knock-in (fE4) mice[39] and tau-P301S fE4 (PS19-fE4) mice[11,25] were generated as previously described. All mice were on a pure C57BL/6 genetic background and were housed in a pathogen-free barrier facility on a 12-h light cycle at 19–23°C and 30–70% humidity. Animals were identified by ear punch and genotyped by TransnetYX automated genotyping PCR services using tail clippings. For all studies, both male and female mice were used. All animal experiments were conducted in accordance with the guidelines and regulation of the National Institutes of Health, the University of California and the Gladstone Institutes under the protocols AN176773 and AN195565. All protocols and procedures followed the guidelines of the Laboratory Animal Resource Center at the University of California, San Francisco (UCSF) and the ethical approval of the UCSF institutional animal care and use committee.

Mice were sedated with avertin and transcardially perfused with sterile saline. The right hemi-brains were drop-fixed for 48 h in 4% paraformaldehyde (Electron Miscropscopy Science, Cat. #15710-S), washed for 24 h in 1X PBS (Thermo Scientific, Cat. #J75889K2) and cryoprotected in 30% sucrose (Millipore Sigma, Cat. #S7903) for 48 h at 4°C. The fixed right hemispheres were cut into 30-µm thick coronal sections on a freeze sliding microtome (Leica, Cat. #SM2010R) and stored in cryoprotectant solution at −20°C (30% ethylene glycol, Fisher Chemical, Cat. #E178-4; 30% glycerol, Millipore Sigma, Cat. #G9012-1GA; and 40% 1x PBS). Left hemispheres were snap-frozen on dry ice and stored at −80°C.

Antisense oligonucleotides (ASOs)

The ASOs used were synthesized by Integrated DNA Technologies (IDT). They were designed to have a central core of phosphorothioate-modified DNA flanked by 2'-O-methoxyethyl (2'-MOE) modified RNA bases. Specific modifications include: 5 nucleotides on the 5' and 3' termini containing 2'-MOE modifications, 10 unmodified central oligodeoxynucleotides, and a phosphorothioate backbone. These modifications were incorporated to enhance nuclease resistance, lower cell toxicity, increase binding affinity to the desired target, and promote cellular uptake. For *in vitro* and *ex vivo* studies, ASOs were solubilized in 10 mM Tris, 0.1 mM EDTA (TE) buffer (Thermo Scientific Chemicals, Cat. #J75793.AP). For *in vivo* studies, ASOs were HPLC-purified, underwent sodium-salt exchange, and were solubilized in 0.9% sterile saline (Hospira, Cat. #0409-4888-02). ASO-targeting regions were as follows:

ASO Name	**Targeting Region in the APOE Gene**
$APOE^{ASO\text{-}4}$	Exon-4
$APOE^{ASO\text{-}75}$	Intron-3
Non-targeting negative control (NTC)	Non-Targeting Control
$APOE^{ASO\text{-}133}$	Exon-3
$APOE^{ASO\text{-}174}$	Exon-3
$APOE^{ASO\text{-}269}$	Exon-4
$APOE^{ASO\text{-}842}$	Exon-4
$APOE^{ASO\text{-}485}$	Intron-3
$APOE^{ASO\text{-}201}$	Intron-3
$APOE^{ASO\text{-}431}$	Intron-3
$APOE^{ASO\text{-}415}$	Intron-3

Stereotaxic surgery and surgical placement of ICV pumps in mice

Mice were anesthetized with isoflurane and maintained on 1.8-2.0% isoflurane (Dechra, Cat. #200-129) for the surgery. After anesthesia, the mice were secured in a stereotaxic frame with a nose cone (Kopf instruments Model 940). The hair on the head was removed and a subcutaneous injection of anesthetic (Lidocaine; Vedco) was injected above the skull where the cut in the scalp was going to be made. After cutting open the scalp with sterilized scissors, cranial sutures were visualized using 3% hydrogen peroxide. Next, a unilateral stereotaxic site was drilled with a 0.5-mm microburr (Fine Science Tools, Cat. #19007-05) to target the right lateral ventricle with the following coordinates based on bregma: −0.25 mm posterior, 1 mm lateral (right), and −2.0 mm ventral. A 28-day Alzet osmotic pump (Model 2004, Cat. #0000298) with ASO was then implanted in a subcutaneous pocket formed on the back of the mice with the catheter placed in the drill site. Following surgery, mice were sutured with nylon monofilament non-absorbable 6-0 sutures (Surgical Specialties Look, Cat. #911B) and administered analgesics buprenorphine (Henry Schein, Cat. #55175) and ketofen (Henry Schein, Cat. #005487). Mice were monitored on a heating pad until ambulatory, provided diet gel, and housed individually with extra enrichment provided.

Quantitative real-time polymerase chain reaction

RNA analyses were performed using quantitative real-time polymerase chain reaction (qRT-PCR). Total RNA was extracted from cells using a Qiagen RNeasy Micro Kit (Qiagen, Cat. #74004). RNA was reverse-transcribed and cDNA generated using the SuperScript IV First-Strand Synthesis System (Invitrogen, Cat. # 18091050). The qRT-PCRs were run and analyzed using the QuantStudio 5 Real-Time PCR System (Applied Biosystems, Cat. # A28140). Total human APOE and APOE-I3

mRNA expression levels were normalized to mouse glyceraldehyde-3-phosphate dehydrogenase (GAPDH) mRNA levels analyzed using the DDCt method for relative expression analysis. Primers were synthesized by ElimBio and the sequences were as follows:

Primer Name	Sequence
Human APOE	5'-CCCAGGTCACCCAGGAACT-3' (forward) 5'-TCCGATTTGTAGGCCTTCAACT-3' (reverse)
Human APOE-I3	5'-CCCAGGTCACCCAGGAACT-3' (forward) 5'-TCCGATTTGTAGGCCTTCAACT-3' (reverse)
Mouse GAPDH	5'-GTCTCCTGCGACTTCAGC-3' (forward) 5'-TCATTGTCATACCAGGAAATGAGC-3' (reverse)

Cell cultures and ASO treatment

Mouse neuroblastoma Neuro-2a cells stably transfected with human apoE3 genomic DNA that were established as previously described[22] were used for the initial screen of ASOs. Neuro-2a cells were maintained at 37°C in a humidified 5% CO2 incubator in DMEM, high glucose (Gibco, Cat. #11965092) supplemented with 10% FBS (Gibco, Cat. #A56697-01), 1X nonessential amino acids (NEAA) (Gibco, Cat. #11140050), and 0.5% penicillin/streptomycin (Gibco, Cat. #15140122). For ASO treatments, Neuro-2a were transfected using Lipofectamine 2000 Transfection Reagent (Invitrogen, Cat. #11668019). The day before transfection with ASOs, cells were lifted using 0.05% Trypsin-EDTA (Gibco, Cat. #25300054), counted, and plated at a concentration of 1.5 x 10^5 cells per well in a 24-well plate using media without antibiotics. For transfection, an Opti-MEM Reduced Serum Media (Gibco, Cat. #31985070) combined with ASO mixture and an Opti-MEM Reduced Serum Media combined with Lipofectamine 2000 mixture were made and incubated at room temperature (RT) for 5 min. The Opti-MEM + ASO mixture was made using various ASOs

and various concentrations depending on experiment. The diluted ASO mixture and the diluted Lipofectamine 2000 mixture were next mixed together gently by pipetting up and down and incubated at RT for 25 min. After feeding the Neuro-2a cells with fresh media without antibiotics, the transfection mix was added dropwise into the well and gently rocked back and forth. After ASO treatment, the cells were collected for either qRT-PCR or western blot analysis. For qRT-PCR, cells were lysed directly in the well using Buffer RLT provided in the Qiagen RNeasy Kit supplemented with 2M dithiothreitol (DTT) (Bioworld, Cat. #20840007) at a concentration of 20 uL per mL of RLT. After collection, the samples were snap frozen on dry ice and stored −80 °C. For western blot analysis, cells were lysed in the well using a high-detergent buffer: 50 mM Tris, 150 mM NaCl, 2% NP-40 (Millipore Sigma, Cat. #492016), 1% sodium deoxycholate and 4% sodium dodecyl sulfate and supplemented with complete protease inhibitor cocktail pellet (Roche, Cat. 11697498001), phosphatase inhibitor cocktail 2 (Millipore Sigma, Cat. #P5726), phosphatase inhibitory cocktail 3 (Millipore Sigma, Cat. #P0044) and Benzonase Nuclease (Millipore Sigma, Cat. #E1014-25KU). After collection, the samples were centrifuged at maximum speed for 5 min and the supernatant was collected and stored at −80°C.

Human astrocytoma cells, SW-1088, were maintained at 37°C in a humidified 0% CO2 incubator in Leibovitz's L-15 Medium (Gibco, Cat. #11415064) supplemented with 10% FBS and 1% penicillin/streptomycin. ASOs were introduced to cells via gymnotic delivery. The day before treatment with ASOs, cells were lifted using 0.05% Trypsin-EDTA and plated at a concentration of 1.5 x 10^5 cells per well in a 24-well plate. ASOs were diluted from 100 µM stock concentration to

3 µM with 500 uL of media per well. After 48 h, SW-1088 cells were collected for qRT-PCR via the same method as described above for Neuro-2a cells.

Primary neuron culture and ASO treatment

Primary neuron culture was prepared from post-natal day 0 (P0) pups as previously described.[12] Briefly, after removing the head from the pup, the brain was dissected out and placed into a dish with ice-cold dissociation media (DM) containing kynurenic acid (KY), called DM/KY media. More specifically, DM/KY is made up of 90% DM and 10% KY stock. DM: 81.8 mM Na_2SO_4 (Millipore Sigma, Cat. #S5640), 30 mM K_2SO_4 (Millipore Sigma, Cat. #P8541), 5.8 mM $MgCl_2$ (Millipore Sigma, Cat. #M1028), 0.25 mM $CaCl_2$ (Millipore Sigma, Cat. #C5670), 1 mM HEPES (Millipore Sigma, Cat. #H0887), 20 mM Glucose (Millipore Sigma, Cat. #G8769), 0.001% Phenol Red (Millipore Sigma, Cat. #P-0290), 0.16 mM NaOH (Ricca Chemical Cat. #7470-32). KY: 10 mM kynurenic acid (Millipore Sigma, Cat. #K3375), 0.0025% Phenol Red, 5 mM HEPES, 100 mM $MgCl_2$, NaOH to titrate pH to 7.4. With the dissected brain, the meninges were removed and the cortex was isolated using a dissection microscope. Next, the tissue was minced using a sterilized razor blade and digested using a Papain (Worthington, Cat. #LS003124) solution. The Papain solution was made by diluting Papain in DM/KY such that there were 5.5 units per mL of DM/KY. After digestion at RT for 13 min, with gentle tube inversions every couple of minutes, the Papain solution was removed, and a Trypsin inhibitor solution was added. The Trypsin inhibitor solution was made by diluting 1 g of Trypsin inhibitor (Millipore Sigma, Cat. #T9253) with 100 mL of DM/KY and titrating the pH to 7.4 with NaOH. After two washes with the Trypsin inhibitor solution for 5 min, the tissue pellet was washed twice with an Opti-MEM/Glucose solution for 5 min. During

the second wash with the Opti-MEM/Glucose solution, the tissue pellet was gently triturated using a 5 mL pipette into a single cell suspension. The Opti-MEM/Glucose solution was made by adding Glucose to Opti-MEM (Thermo) to be a total concentration of 20 mM. The cells were then spun down at 200G for 5 min, resuspended in B27/Neurobasal growth media, counted, and plated at a concentration of 6.0 x 10^5 cells per well in a 24-well plate. The B27/Neurobasal growth media consisted of Neurobasal medium (Gibco, Cat. #21103-049), 1X B27 (Gibco, Cat. #17504-044), 1% Glutamax (Gibco, Cat. #35050061), and 1% penicillin/streptomycin (Gibco, Cat. #15140122). Prior to plating cells on the 24-well plates, the wells were coated with PLL (Millipore Sigma, Cat. #P4707) and washed three times with DPBS (Thermo Scientific Chemicals, Cat. #J67653AP). ASOs were introduced to primary neurons via gymnotic delivery. The primary neuron cultures were treated with 10 µM of ASO on Day 3 for 1 week and collected on Day 10 for qRT-PCR via the same method as described above for Neuro-2a cells.

Primary astrocyte culture and ASO treatment

Mouse primary mixed glia culture was prepared from neonatal mice at P2-3 from PS19/E4 mice as previously described.[40] Briefly, the cortices were separated from the meninges and minced with a sterile razor blade. The tissue was digested with 2.5% trypsin (Gibco, Cat. # 15090046) + DNase (Millipore Sigma, Cat. #D4513) for 25 minutes at 37°C. After incubation, the trypsin was neutralized with 30% FBS (Gibco, Cat. #A56697-01) in DMEM, high glucose, GlutaMAX Supplement, pyruvate (Gibco, Cat. #10569010) and triturated until cells formed a uniform suspension. The cells were spun at 300G for 10 min and pellet was resuspended in 10% FBS in DMEM. For each brain from a single pup, cells were plated onto PDL (Millipore Sigma, Cat.

#P7280) coated T25 flasks supplemented with 50ng/mL GM-CSF (Millipore Sigma, Cat. # G0282). On Day 4, the fresh media was added onto the cells. On Day 10-12, the flasks containing mixed glial were placed onto an incubated shaker at 37°C for 1 h at 180RPM to shake off the microglia. After the microglia were shaken off, the remaining astrocytes in the T25 flasks were fed with fresh media and kept at 37°C until they were lifted and replated onto 24-well plates. To replate astrocytes, the media was removed and 3 mL of 2.5% trypsin was added to the flask. Next the cells were incubated at 37°C for 5 min until the cells lifted up from the surface of the flask. Then, using a 5 mL pipette, the cells were pipetted up and down a few times to break down the sheet of cells before being incubated at 37°C for another 5 min. After this, the cells were triturated using a 5 mL pipette until the cells were a uniform, cloudy solution. An equal volume of growth media was then added to the cells to quench the trypsin before the cell solution was passed through a 40 mm filter (Corning, Cat. #431750). The cells were then spun at 300G for 5 min, the cell pellet resuspended in media, and plated at a concentration of 3.0×10^5 cells per well in a 24-well plate. Prior to plating primary astrocytes on 24-well plates, the wells were coated with PLL (Millipore Sigma, Cat. #P4707) and washed three times with DPBS (Thermo Scientific Chemicals, Cat. #J67653AP). ASOs were introduced to primary astrocytes via gymnotic delivery. The primary astrocytic cultures were treated with 20 or 40 µM of ASO on Day 14 for 1 week and collected on Day 21 for qRT-PCR via the same method as described above for Neuro-2a cells.

Immunohistochemistry

For immunofluorescence staining, 30 µm-thick brain sections were washed three times with PBS-T (PBS + 0.1% Tween-20; Millipore Sigma, Cat. #P2287) and incubated in boiling 1M Tris-HCl buffer

(pH 8, Corning, Cat. #46-031-CM) for 5 min. Next, sections were washed three times with PBS-T followed by blocking with 10% normal donkey serum (NDS; Jackson ImmunoResearch, Cat. #017000121) made in PBS-Tx (PBS + 0.5% TritonX; Millipore Sigma, Cat. #T8787) for 1 hr. Sections were then incubated in Mouse on Mouse (MOM; Vector Laboratories, Cat. #MKB-2213-1) blocking buffer (one drop MOM per 4ml of PBS) to block endogenous mouse staining. Then, the sections were incubated overnight at 4°C with primary antibodies. The following primary antibodies were used for studies: anti-APOE (rb) 1:500 (Cell Signaling Technology, Cat. #13366); anti-NeuN 1:500 (Millipore Sigma, Cat. #ABN90); anti-GFAP 1:750 (Millipore Sigma, Cat. #MAB3402); anti-S100B 1:200 (Abcam, Cat. #ab52642); anti-IBA1 (gt) 1:500 (Abcam, Cat. #ab5076); and anti-CD68 1:200 (Bio-Rad, Cat. #MCA1957). All primary antibodies were diluted in 3% NDS made in PBS. The next day, sections were washed three times with PBS-T and incubated in the dark for 1 hour at room temperature with secondary antibodies. The following secondary antibodies were used: donkey anti-rabbit 488 1:1000 (Invitrogen, Cat. #A-21206); donkey anti-guinea pig 647 1:1000 (Jackson Immuno, Cat. #706-605-148); donkey anti-mouse 594 1:1000 (Invitrogen, Cat. #A-21203); donkey anti-rabbit 647 1:1000 (Invitrogen, Cat. #A231573); donkey anti-goat 594 1:1000 (Invitrogen, Cat. #A11058); donkey anti-rat 594 (Invitrogen, Cat. #A21209). All secondary antibodies were diluted in 3% NDS made in PBS. During the incubation with secondary antibodies, for some stains, DAPI (1:20,000; Thermo Scientific, Cat. #62248) was added. After incubation with secondary antibodies, the sections were then washed three times with PBS-T before getting mounted onto microscope slides (Fisher Scientific, Cat. #22-037-246). Slides were coverslipped with ProLong Gold mounting medium (Invitrogen, Cat. #P36930),

allowed to dry, and followed by imaging on a FV3000 confocal laser scanning microscope (Olympus).

For diaminobenzidine (DAB) staining, 30um-thick brain sections were washed three times with PBS-T, incubated in boiling citrate buffer (10mM sodium citrate; Fisher Bioreagents, Cat. # BP327-1) for 5 min, washed two times with PBS-T, incubated in endogenous peroxidase block (3% H2O2; Millipore Sigma, Cat. #H1009-500mL, and 10% methanol; Fisher Scientific, Cat. #A412SK-4, in PBS) for 15 min, washed two more times with PBS-T, washed one time with PBS-Tx (PBS + 0.2% TritonX; Millipore Sigma, Cat. #T8787), and blocked with 10% NDS made in PBS-Tx for 1 hr. Sections were then incubated in avidin and biotin blocks (3 drops of each; Vector Laboratories, Cat. #SP-2001) for 15 min and MOM Blocking buffer (one drop MOM per 4 ml of PBS-T) for 1 hr. Sections were incubated overnight at 4°C with an anti-AT8 primary antibody 1:100 (Invitrogen, Cat. #MN1020) diluted in 3% NDS made in PBS-T. The following day, sections were washed three times with PBS-T and incubated for 1 hr at room temperature with biotinylated donkey anti-mouse secondary (1:2000; Jackon ImmunoResearch, Cat. #715-065-150) diluted in 3% NDS in PBS-T. Next, the sections were rinsed two times with PBS-T, once with PBS, and incubated with ABC buffer (2 drops A and B per 5ml PBS; Vector Laboratories, Cat. #PK-6100) for 1 hr. The ABC buffer was made and allowed to incubate 15-30 min before use. Next, the sections were rinsed twice with PBS and once with water before a 1 min and 30 sec incubation in DAB buffer (2 drops buffer stock solution, 4 drops DAB, and 2 drops H_2O_2 in 5ml milliQ water; Vector Laboratories, Cat. #SK-4100). Sections were then immediately washed three times with milliQ water and then washed with PBS and mounted onto microscope slides. Slides were allowed to dry overnight and then submerged in

two washes of xylene (Fisher Scientific, Cat. #HC7001GAL). Slides were coverslipped with DPX mounting medium (Millipore Sigma, Cat. #06522) and imaged with an Aperio VERSA slide scanning microscope (Leica).

Immunohistochemical quantification analysis

For all image quantifications, researchers were blinded to samples and automated imaging analysis via Fiji was used to exclude bias from quantifications. For analyses where immunostaining as a percentage of hippocampal area covered was conducted, two brain sections for each mouse was stained and imaged according to the immunohistochemistry section above. Next, four fields of view from the two brain sections (two fields of view from the DG and two fields of view from the CA1) were taken and used to calculate an average percent area coverage for each mouse.

For percent APOE area coverage in astrocytes and neuron quantifications, brain sections were stained according to the immunohistochemistry section above with anti-GFAP or anti-NeuN to highlight astrocytes or neurons, respectively. Next a selection was created based on the stain and restored onto the APOE channel of the same brain section. Then APOE percent area in either astrocytes or neurons was measured.

For DG granule cell layer thickness measurements, two brain sections were stained according to the protocol above with anti-NeuN to highlight the cell layers. The thickness was measured manually in Fiji as follows: a line was drawn perpendicular to the NeuN cell layer at four locations in both sections, and an average was taken for each mouse.

Western blot analysis

Biochemically extracted mouse neuroblastoma cell lysates were loaded onto 12% NuPAGE Bis-Tris polyacrylamide gel (Invitrogen, Cat. #NP0343) and separated by gel electrophoresis at 160 V using MOPS running buffer (Invitrogen, Cat. #NP0001). The separated proteins were transferred onto nitrocellulose membranes (Bio-Rad, Cat. #1620215) at 18 V for 60 min (Trans-Blot Turbo Transfer System, Bio-Rad). Membranes were washed for 3 × 5 min in PBS-T (PBS + 0.1% Tween-20; Millipore Sigma, Cat. #P2287) and then incubated in Intercept blocking buffer (LI-COR, Cat. #927-70001) for 1 h at room temperature to block nonspecific binding sites. After blocking, membranes were washed for 3 × 5 min in PBS-T and incubated with primary antibody overnight at 4 °C (APOE at 1:5000 dilution (Cell Signaling Technology, Cat. #13366) and beta actin at 1:2500 dilution (Abcam, Cat. #ab8226)). Membranes were washed for 3 × 5 min in PBS-T and incubated in fluorescently labeled secondary antibody: donkey anti-mouse 488 (1:2000; Invitrogen, Cat. #A21202) and donkey anti-rabbit 800RD (1:20000; LI-COR, Cat. #926-32213) for 1 h in the dark at room temperature. Resulting bands were detected with the ChemiDoc MP system (Bio-Rad), and the fluorescent intensity of each band was measured with Image Lab (Bio-Rad). The fluorescence intensity of the bands was quantified as a ratio of APOE:beta actin signal normalized to cells treated with ASO-NTC.

Hippocampal volumetric analysis

Every tenth coronal brain section spanning the hippocampus was mounted on a microscope slide (Fisher Scientific, Cat. #22-037-246) for each mouse (seven sections per mouse, 30 µm thick, 300 µm apart) and dried for 1 hr at room temperature. Then, the brain sections were treated for 10

min with a 1% Sudan Black solution, washed with 70% ethanol for 2 min, washed with PBS-T for 2 min three times until the debris was washed away, and coverslipped with ProLong Gold mounting medium (Invitrogen, Cat. #P36930). To prepare the 1% Sudan Black solution, Sudan Black powder (Millipore Sigma, Cat. #S-2380) was combined with 70% ethanol (KOPTEC, Cat. #V1016) and mixed using a magnetic stirrer. The solution was then centrifuged at 1,100g for 10 min and the collected supernatant was filtered using a 0.2-µm filter syringe (Thermo Scientific, Cat. #723-2520). The stained, mounted brain sections were imaged on the Keyence microscope at x10 magnification. To quantify the volumes of the hippocampus and posterior lateral ventricle, we traced the areas of interest in ImageJ and used the formula: volume = distance between sections (30µm per section x 10 sections in between stained sample sections = 0.3mm) x sum of areas of all stained sections. We took a sum of seven brain sections per mouse, roughly between coordinates AP = −1.5 and AP = −3.3.

Single-nuclei preparation for 10x loading

Single-nuclei preparation was conducted as previously described.[11,25] In brief, hippocampi previously dissected and stored at -80°C were combined with 1 ml of ice-cold homogenization buffer (HB) (250 mM sucrose, 25 mM KCl, 5 mM MgCl2, 20 mM tricine-KOH pH 7.8, 1 mM dithiothreitol, 0.5 mM spermidine, 0.15 mM spermine, 0.3% NP40) supplemented with 0.2 U/µl RNasin Plus RNAse inhibitor (Promega, Cat. #N2615) and protease inhibitor (Roche, Cat. 11836170001). Samples were dounced with ‘A’ loose pestle and ‘B’ tight pestle for 10 strokes each. Homogenate was filtered with a 70 µm Flowmi strainer (Bel-Art, Cat. #H13680-0070) and spun at 350 g for 5 min at 4°C. Supernatant was discarded and the pelleted nuclei were

resuspended in 400 µL 1X HB. Next, 400 µl of 50% Iodixanol solution was added to the nuclei to create a 25% mixture, and then slowly layered with 600 µl of 30% Iodixanol solution underneath. Mixture was then layered again with 600 µl of 40% Iodixanol solution under the 30% mixture. The nuclei were spun at 3000 g for 20 min at 4°C before 200 µl of the nuclei band at the 30%–40%interface was combined with 800 µl of 2.5% BSA (Millipore Sigma; Cat. #A9576) in PBS supplemented with RNase inhibitor. Samples were spun for 10 min at 500 g and 4°C. The nuclei were resuspended with 2.5% BSA in PBS supplemented with RNase inhibitor to reach at least 500 nuclei per µl. Nuclei were then filtered with a 40 µm Flowmi stainer (Millipore Sigma; Cat. #BAH136800040) and counted. Roughly 14,000 nuclei per sample were loaded onto a 10x Genomics Next GEM chip G. The snRNAseq libraries were prepared using the Chromium Next GEM Single Cell 3' Library and Gel Bead kit v.3.1 (10x Genomics, Cat. #1000121) according to the manufacturer's instructions. Libraries were sequenced on an Illumina NovaSeq X Plus sequencer at the UCSF CAT Core.

Pre-processing and clustering of mouse snRNA-seq samples

The snRNA-seq dataset included a total of 18 samples with 6 mice from each of the 3 treatment groups: PS19-E4 mice treated with ASO 4, PS19-E4 mice treated with ASO 75, and PS19-E4 mice treated with NTC ASO. The 6 PS19-E4 mice treated with ASO 4 had 4 male and 2 female mice; the 6 PS19-E4 mice treated with ASO 75 had 3 male and 3 female mice; and the 6 PS19-E4 mice treated with NTC ASO had 3 male and 3 female mice. The demultiplexed FASTQ files for these samples were aligned to a custom mouse reference genome using the 10x Genomics Cell Ranger Count pipeline[41] (version 9.0.1), following the Cell Ranger documentation. To accommodate the

Homo sapiens MAPT (NCBI reference sequence NM_001123066.4) and the H. sapiens APOE (NCBI reference sequence NM_001123066.4) genes, the custom mouse reference genome was made using the reference mouse genome sequence (GRCm38) from Ensembl (release 98) and the mouse gene annotation file from GENCODE (release M23). The H. sapiens MAPT sequence and H. sapiens APOE sequence were appended as separate chromosomes to the end of the mouse reference genome sequence and the corresponding gene annotations were appended to the filtered mouse reference gene annotation GTF file. The include-introns flag was set to TRUE to capture reads mapping to intronic regions.

The filtered count matrices generated by the Cell Ranger count pipeline for the 18 samples were processed using the R package Seurat[42] (version 4.4.0) for single-nucleus analysis. Each sample was pre-processed as a Seurat object, then all 18 samples were merged into a single Seurat object. Low-quality nuclei were removed using the following criteria: fewer than 500 total UMI counts, fewer than 200 features, or a mitochondrial gene ratio higher than 0.25%. Sparse gene features expressed in fewer than 10 cells were also excluded. After quality control, normalization and variance stabilization were performed using SCTransform[43] (version 0.4.2) method for initial parameter estimation. Graph-based clustering was conducted using the Seurat functions, FindNeighbors and FindClusters. Cells were embedded in a k-nearest neighbor (KNN) graph on the first 50 principal components (PCs) using Euclidean distance in the PCA space, and edge weights between two cells were refined using Jaccard similarity. Clustering via the Louvain algorithm (FindClusters) with 15 PCs and a resolution of 0.7 produced 38 distinct biologically relevant clusters, which were subsequently used for further analyses.

Cell type assignment

Cell type identities were annotated following a method we previously described.[44–46] Briefly, Seurat's AddModuleScore() function was applied to the object using features from lists of known brain marker genes (up to 8 per cell type).[45,47] Further subdivisions of hippocampus cell types, such as CA1 and CA3 pyramidal cells, were identified using hippocampus-specific marker genes curated from Hipposeq (https://hipposeq.janelia.org). A module score of each cell type was computed for each individual cell, and each cell was assigned the cell type that produced the highest module score among all tested cell types. Cells with their top two scores within 10% of each other were classified as potential hybrids and excluded from downstream analyses. Cells with negative scores for all cell types computed were classified as negative and excluded from downstream analyses. The cell type assignments per cluster was evaluated by inspecting homogeneity, distribution, and spatial separation of clusters in UMAP space and the expression of major cell type marker genes across clusters. Clusters containing comparable proportions of two or more cell types were deemed unknown or mixed.

Gene set enrichment analysis

DE genes between clusters of interest or between two genotype groups were identified using the FindMarkers Seurat function on the RNA assay data. This algorithm uses the Wilcoxon rank-sum test to identify DE genes between two populations. DE genes were limited to genes detected in at least 10% of the cells in either population and with at least 0.1 $\log_2$ fold change. Volcano plots with $\log_2$ fold change and p value from the DE gene lists were generated using the ggplot2 R

package[48] (version 3.5.2). The p values are based on a hypergeometric test and are adjusted for multiple testing using the Benjamini–Hochberg method.[49]

Association between clusters and genotype

A GLMM_AM was implemented in the lme4 (version 1.1-37) R package[50] and used to estimate the associations between cluster membership and the mouse model. These models were run separately for each cluster of cells. The GLM model was performed with the family argument set to the binomial probability distribution and with the 'nAGQ' parameter set to 10, corresponding to the number of points per axis for evaluating the adaptive Gauss–Hermite approximation for the log-likelihood estimation. Cluster membership of cells by sample was modeled as a response variable by a two-dimensional vector representing the number of cells from the given sample belonging to and not belonging to the cluster under consideration. The corresponding mouse ID from which the cell was derived was the random effect variable, and the animal model for this mouse ID was included as the fixed variable. The reference treatment was set to PS19-E4 mice treated with NTC ASO. The resulting p values for the estimated LOR across the three animal models (with respect to the PS19-E4 mice treated with NTC ASO) and clusters were adjusted for multiple testing using the Benjamini–Hochberg method.[49]

Association between proportion of cell types and histopathological parameters

A GLMM_histopathology was implemented in the lme4 (version 1.1-37) R package[50] and used to identify cell types whose proportions are significantly associated with changes in histopathology across the samples. These models were performed separately for each combination of all clusters

and each histological parameter. The GLM model was performed with the family argument set to the binomial probability distribution family and with the 'nAGQ' parameter set to 1 corresponding to a Laplace approximation for the log-likelihood estimation. Cluster membership of cells by sample was modeled as a response variable by a two-dimensional vector representing the number of cells from the given sample belonging to and not belonging to the cluster under consideration. The corresponding mouse model from which the cell was derived was included as a random effect, and, further, the mouse ID within the given mouse model was modeled as a random effect as well. Note, this represents the hierarchical nature of these data for the GLMM, and the mouse models are first assumed to be sampled from a 'universe' of mouse models; this is then followed by sampling mice within each mouse model. The modeling choice of including the mouse model as a random effect as opposed to a fixed effect is meant to increase the degrees of freedom (or maximize the statistical power) to detect the association of interest, particularly in light of the relatively small number of replicates (3–4) per animal model. The histological parameter under consideration was modeled as a fixed effect in this model. We visualized the LOR estimates (derived from the GLMM fits) in a heat map using pheatmap package 1.0.13 after adjusting the p values distribution across histopathological parameters across cell types with Benjamini–Hochberg multiple testing correction.[49]

Subclustering of inhibitory neuronal, astrocytic, and microglial snRNA-seq data

The hippocampal cell clusters 8, 11, 15, and 26 were annotated as inhibitory neurons, cell cluster 13 was annotated as the astrocyte cells, and hippocampal cell clusters 6 and 21 were annotated as the microglial cells. Each of these cell types were further subclustered. Normalization and

variance stabilization was performed using sctransform[51] with the 'glmGamPoi' (Bioconductor package v.1.14.3) method[52] for initial parameter estimation. Graph-based clustering was performed using the Seurat v.4.4.0 functions FindNeighbors and FindClusters. First, the cells were embedded in a k-nearest neighbor graph based on the Euclidean distance in the principal-component analysis space. The edge weights between two cells were further modified using Jaccard similarity. Next, clustering was performed using the Louvain algorithm implementation in the FindClusters Seurat function. Clustering was performed for all combinations of 10, 15, 20, 25 and 30 PCs with 0.4, 0.5, 0.6, 0.7, 0.8 and 0.9 resolutions. Subclustering with 15 PCs and 0.9 resolution resulted in 23 distinct biologically relevant subclusters for inhibitory neurons. Subclustering with 15 PCs and 0.9 resolution resulted in 15 distinct biologically relevant subclusters for astrocytes. Subclustering with 15 PCs and 0.9 resolution resulted in 13 distinct biologically relevant microglia subclusters.

General Statistics and Reproducibility

Sample sizes for mouse studies were chosen on the basis of estimates to provide statistical power of ≥80% and alpha of 0.05 based on preliminary data. The differences between ASO treatment groups were evaluated by ordinary one-way ANOVA with Tukey's multiple comparisons test, where the mean of each column was compared to the mean of every other column, or Welch's ANOVA followed by Dunnett's T3 multiple comparison test, where the mean of each column was compared to the mean of the control column. All data are shown as mean ± s.d. or ± s.e.m. Data distribution was assumed to be normal, though this was not formally tested. For correlations between two data sets, simple linear regression was used. $p < 0.05$ was considered to be

significant, and all significant p values were included in figures or noted in figure legends. Statistical significance analysis and plots were completed with GraphPad Prism 10 for Mac (GraphPad Software). No randomization method was used for the assignment of mice to study groups, and no animals or data points were excluded from these studies.

For mouse snRNA-seq studies, sample sizes were determined by a power analysis based on effect sizes from our previous studies and literature.[11,25] Mice selected for snRNA-seq consisted of both males and females that together represented average pathologies for all parameters quantified. Nuclei were isolated from six mice per genotype to ensure n ≥ 3 mice per group. Pathology data were correlated with snRNA-seq data. Investigators were not blinded during analysis of the snRNA-seq datasets, as sample metadata were needed to conduct any comparisons. Studies were all performed using one cohort of mice.

References

Chapter 1

1. Huang, Y. & Mucke, L. Alzheimer mechanisms and therapeutic strategies. *Cell* **148**, 1204–1222 (2012).
2. Long, J. M. & Holtzman, D. M. Alzheimer disease: an update on pathobiology and treatment strategies. *Cell* **179**, 312–339 (2019).
3. Sperling, R. A. *et al.* Toward defining the preclinical stages of Alzheimer's disease: recommendations from the National Institute on Aging-Alzheimer's Association workgroups on diagnostic guidelines for Alzheimer's disease. *Alzheimers Dement. J. Alzheimers Assoc.* **7**, 280–292 (2011).
4. Albert, M. S. *et al.* The diagnosis of mild cognitive impairment due to Alzheimer's disease: recommendations from the National Institute on Aging-Alzheimer's Association workgroups on diagnostic guidelines for Alzheimer's disease. *Alzheimers Dement.* **7**, 270–279 (2011).
5. Vermunt, L. *et al.* Duration of preclinical, prodromal, and dementia stages of Alzheimer's disease in relation to age, sex, and APOE genotype. *Alzheimers Dement.* **15**, 888–898 (2019).
6. Gustavsson, A. *et al.* Global estimates on the number of persons across the Alzheimer's disease continuum. *Alzheimers Dement.* **19**, 658–670 (2023).
7. Sherrington, R. *et al.* Cloning of a gene bearing missense mutations in early-onset familial Alzheimer's disease. *Nature* **375**, 754–760 (1995).
8. Goate, A. *et al.* Segregation of a missense mutation in the amyloid precursor protein gene with familial Alzheimer's disease. *Nature* **349**, 704–706 (1991).
9. Corder, E. H. *et al.* Protective effect of apolipoprotein E type 2 allele for late onset Alzheimer disease. *Nat. Genet.* **7**, 180–184 (1994).

10. Corder, E. H. *et al.* Gene dose of apolipoprotein E type 4 allele and the risk of Alzheimer's disease in late onset families. *Science* **261**, 921–923 (1993).
11. Mahley, R. W. & Rall, S. C. Apolipoprotein E: far more than a lipid transport protein. *Annu. Rev. Genomics Hum. Genet.* **1**, 507–537 (2000).
12. Weisgraber, K. H. Apolipoprotein E: structure-function relationships. *Adv. Protein Chem.* **45**, 249–302 (1994).
13. Huang, Y. & Mahley, R. W. Apolipoprotein E: structure and function in lipid metabolism, neurobiology, and Alzheimer's diseases. *Neurobiol. Dis.* **72 Pt A**, 3–12 (2014).
14. Farrer, L. A. *et al.* Effects of age, sex, and ethnicity on the association between apolipoprotein E genotype and Alzheimer disease. A meta-analysis. APOE and Alzheimer Disease Meta Analysis Consortium. *JAMA* **278**, 1349–1356 (1997).
15. Genin, E. *et al.* APOE and Alzheimer disease: a major gene with semi-dominant inheritance. *Mol. Psychiatry* **16**, 903–907 (2011).
16. Wang, Y.-Y. *et al.* The Proportion of APOE4 carriers among non-demented individuals: a pooled analysis of 389,000 community-dwellers. *J. Alzheimers Dis. JAD* **81**, 1331–1339 (2021).
17. Ward, A. *et al.* Prevalence of apolipoprotein E4 genotype and homozygotes (APOE e4/4) among patients diagnosed with Alzheimer's disease: a systematic review and meta-analysis. *Neuroepidemiology* **38**, 1–17 (2012).
18. Zhong, N. & Weisgraber, K. H. Understanding the association of apolipoprotein E4 with Alzheimer disease: clues from its structure. *J. Biol. Chem.* **284**, 6027–6031 (2009).
19. Liu, C.-C., Kanekiyo, T., Xu, H. & Bu, G. Apolipoprotein E and Alzheimer disease: risk, mechanisms and therapy. *Nat. Rev. Neurol.* **9**, 106–118 (2013).
20. Koutsodendris, N., Nelson, M. R., Rao, A. & Huang, Y. Apolipoprotein E and Alzheimer's Disease: Findings, Hypotheses, and Potential Mechanisms. *Annu. Rev. Pathol. Mech. Dis.* **17**, 73–99 (2022).

21. Martens, Y. A. *et al.* ApoE Cascade Hypothesis in the pathogenesis of Alzheimer's disease and related dementias. *Neuron* **110**, 1304–1317 (2022).

22. Huang, Y. *et al.* Apolipoprotein E fragments present in Alzheimer's disease brains induce neurofibrillary tangle-like intracellular inclusions in neurons. *Proc. Natl. Acad. Sci.* **98**, 8838–8843 (2001).

23. Shi, Y. *et al.* ApoE4 markedly exacerbates tau-mediated neurodegeneration in a mouse model of tauopathy. *Nature* **549**, 523–527 (2017).

24. Koutsodendris, N. *et al.* Neuronal APOE4 removal protects against tau-mediated gliosis, neurodegeneration and myelin deficits. *Nat. Aging* **3**, 275–296 (2023).

25. Serrano-Pozo, A., Das, S. & Hyman, B. T. APOE and Alzheimer's disease: advances in genetics, pathophysiology, and therapeutic approaches. *Lancet Neurol.* **20**, 68–80 (2021).

26. Iannucci, J., Sen, A. & Grammas, P. Isoform-specific effects of apolipoprotein E on markers of inflammation and toxicity in brain glia and neuronal cells in vitro. *Curr. Issues Mol. Biol.* **43**, 215–225 (2021).

27. Haney, M. S. *et al.* APOE4/4 is linked to damaging lipid droplets in Alzheimer's microglia. *bioRxiv*. 2023.07.21.549930. https://doi.org/10.1101/2023.07.21.549930 (2023).

28. Nelson, M. R. *et al.* The APOE-R136S mutation protects against APOE4-driven Tau pathology, neurodegeneration and neuroinflammation. *Nat. Neurosci*. https://doi.org/10.1038/s41593-023-01480-8 (2023).

29. Marschallinger, J. *et al.* Lipid-droplet-accumulating microglia represent a dysfunctional and proinflammatory state in the aging brain. *Nat. Neurosci.* **23**, 194–208 (2020).

30. Parhizkar, S. & Holtzman, D. M. APOE mediated neuroinflammation and neurodegeneration in Alzheimer's disease. *Semin. Immunol.* **59**, 101594 (2022).

31. Blanchard, J. W. *et al.* APOE4 impairs myelination via cholesterol dysregulation in oligodendrocytes. *Nature* **611**, 769–779 (2022).

32. Cheng, G. W.-Y. *et al.* Apolipoprotein E ε4 mediates myelin breakdown by targeting oligodendrocytes in sporadic Alzheimer disease. *J. Neuropathol. Exp. Neurol.* **81**, 717–730 (2022).

33. Shi, Y. *et al.* Overexpressing low-density lipoprotein receptor reduces tau-associated neurodegeneration in relation to apoE-linked mechanisms. *Neuron* **109**, 2413-2426.e7 (2021).

34. Barisano, G. *et al.* A 'multi-omics' analysis of blood-brain barrier and synaptic dysfunction in APOE4 mice. *J. Exp. Med.* **219**, e20221137 (2022).

35. Montagne, A. *et al.* APOE4 leads to blood-brain barrier dysfunction predicting cognitive decline. *Nature* **581**, 71–76 (2020).

36. Montagne, A. *et al.* APOE4 accelerates advanced-stage vascular and neurodegenerative disorder in old Alzheimer's mice via cyclophilin A independently of amyloid-β. *Nat. Aging* **1**, 506–520 (2021).

37. Raulin, A.-C. *et al.* ApoE in Alzheimer's disease: pathophysiology and therapeutic strategies. *Mol. Neurodegener.* **17**, 72 (2022).

38. Yamazaki, Y., Zhao, N., Caulfield, T. R., Liu, C.-C. & Bu, G. Apolipoprotein E and Alzheimer disease: pathobiology and targeting strategies. *Nat. Rev. Neurol.* **15**, 501–518 (2019).

39. Xu, Q. *et al.* Profile and regulation of apolipoprotein E (ApoE) expression in the CNS in mice with targeting of green fluorescent protein gene to the ApoE locus. *J. Neurosci.* **26**, 4985–4994 (2006).

40. Pitas, R. E., Boyles, J. K., Lee, S. H., Foss, D. & Mahley, R. W. Astrocytes synthesize apolipoprotein E and metabolize apolipoprotein E-containing lipoproteins. *Biochim. Biophys. Acta BBA - Lipids Lipid Metab.* **917**, 148–161 (1987).

41. Boyles, J. K., Pitas, R. E., Wilson, E., Mahley, R. W. & Taylor, J. M. Apolipoprotein E associated with astrocytic glia of the central nervous system and with nonmyelinating glia of the peripheral nervous system. *J. Clin. Invest.* **76**, 1501–1513 (1985).

42. Knoferle, J. *et al.* Apolipoprotein E4 produced in GABAergic interneurons causes learning and memory deficits in mice. *J. Neurosci.* **34**, 14069–14078 (2014).
43. Wang, C. *et al.* Selective removal of astrocytic APOE4 strongly protects against tau-mediated neurodegeneration and decreases synaptic phagocytosis by microglia. *Neuron* **109**, 1657-1674.e7 (2021).
44. Xiong, M. *et al.* Astrocytic APOE4 removal confers cerebrovascular protection despite increased cerebral amyloid angiopathy. *Mol. Neurodegener.* **18**, 17 (2023).
45. Xia, Y. *et al.* C/EBPβ is a key transcription factor for APOE and preferentially mediates ApoE4 expression in Alzheimer's disease. *Mol. Psychiatry* **26**, 6002–6022 (2021).
46. Wynne, M. E. *et al.* APOE expression and secretion are modulated by mitochondrial dysfunction. *eLife* **12**, e85779 (2023).
47. Lanfranco, M. F., Sepulveda, J., Kopetsky, G. & Rebeck, G. W. Expression and secretion of apoE isoforms in astrocytes and microglia during inflammation. *Glia* **69**, 1478–1493 (2021).
48. Harris, F. M. *et al.* Astroglial regulation of apolipoprotein E expression in neuronal cells: implications for Alzheimer's disease. *J. Biol. Chem.* **279**, 3862–3868 (2004).
49. Cashikar, A. G. *et al.* Regulation of astrocyte lipid metabolism and ApoE secretion by the microglial oxysterol, 25-hydroxycholesterol. *J. Lipid Res.* **64**, 100350 (2023).
50. Mhatre-Winters, I., Eid, A., Han, Y., Tieu, K. & Richardson, J. R. Sex and APOE genotype alter the basal and induced inflammatory states of primary astrocytes from humanized targeted replacement mice. *ASN NEURO* **15**, 17590914221144549 (2023).
51. de Leeuw, S. M. *et al.* APOE2, E3, and E4 differentially modulate cellular homeostasis, cholesterol metabolism, and inflammatory response in isogenic iPSC-derived astrocytes. *Stem Cell Rep.* **17**, 110–126 (2022).
52. Chung, W.-S. *et al.* Novel allele-dependent role for APOE in controlling the rate of synapse pruning by astrocytes. *Proc. Natl. Acad. Sci. U. S. A.* **113**, 10186–10191 (2016).

53. Fernandez, C. G., Hamby, M. E., McReynolds, M. L. & Ray, W. J. The role of APOE4 in disrupting the homeostatic functions of astrocytes and microglia in aging and Alzheimer's disease. *Front. Aging Neurosci.* **11**, 14 (2019).

54. Lin, Y.-T. *et al.* APOE4 causes widespread molecular and cellular alterations associated with Alzheimer's disease phenotypes in human iPSC-derived brain cell types. *Neuron* **98**, 1141-1154.e7 (2018).

55. Staurenghi, E. *et al.* ApoE3 vs. ApoE4 astrocytes: a detailed analysis provides new insights into differences in cholesterol homeostasis. *Antioxidants* **11**, 2168 (2022).

56. Zhao, J. *et al.* APOE ε4/ε4 diminishes neurotrophic function of human iPSC-derived astrocytes. *Hum. Mol. Genet.* **26**, 2690–2700 (2017).

57. Nishitsuji, K., Hosono, T., Nakamura, T., Bu, G. & Michikawa, M. Apolipoprotein E regulates the integrity of tight junctions in an isoform-dependent manner in an in vitro blood-brain barrier model. *J. Biol. Chem.* **286**, 17536–17542 (2011).

58. Bell, R. D. *et al.* Apolipoprotein E controls cerebrovascular integrity via cyclophilin A. *Nature* **485**, 512–516 (2012).

59. Arnaud, L. *et al.* APOE4 drives inflammation in human astrocytes via TAGLN3 repression and NF-κB activation. *Cell Rep.* **40**, 111200 (2022).

60. Tcw, J. *et al.* Cholesterol and matrisome pathways dysregulated in astrocytes and microglia. *Cell* **185**, 2213-2233.e25 (2022).

61. Windham, I. A. *et al.* APOE traffics to astrocyte lipid droplets and modulates triglyceride saturation and droplet size. *bioRxiv*. 2023.04.28.538740. https://doi.org/10.1101/2023.04.28.538740 (2023).

62. Chen, Z.-P. *et al.* Lipid-accumulated reactive astrocytes promote disease progression in epilepsy. *Nat. Neurosci.* **26**, 542–554 (2023).

63. Fang, W. *et al.* APOE4 genotype exacerbates the depression-like behavior of mice during aging through ATP decline. *Transl. Psychiatry* **11**, 507 (2021).

64. Farmer, B. C. *et al.* APOE4 lowers energy expenditure in females and impairs glucose oxidation by increasing flux through aerobic glycolysis. *Mol. Neurodegener.* **16**, 62 (2021).

65. Williams, H. C. *et al.* APOE alters glucose flux through central carbon pathways in astrocytes. *Neurobiol. Dis.* **136**, 104742 (2020).

66. Lee, H. *et al.* ApoE4-dependent lysosomal cholesterol accumulation impairs mitochondrial homeostasis and oxidative phosphorylation in human astrocytes. *Cell Rep.* **42**, 113183 (2023).

67. Li, X. *et al.* Astrocytic ApoE reprograms neuronal cholesterol metabolism and histone-acetylation-mediated memory. *Neuron* **109**, 957-970.e8 (2021).

68. Huang, S., Zhang, Z., Cao, J., Yu, Y. & Pei, G. Chimeric cerebral organoids reveal the essentials of neuronal and astrocytic APOE4 for Alzheimer's tau pathology. *Signal Transduct. Target. Ther.* **7**, 1–10 (2022).

69. Chen, Y., Durakoglugil, M. S., Xian, X. & Herz, J. ApoE4 reduces glutamate receptor function and synaptic plasticity by selectively impairing ApoE receptor recycling. *Proc. Natl. Acad. Sci. U. S. A.* **107**, 12011–12016 (2010).

70. Jackson, R. J. *et al.* APOE4 derived from astrocytes leads to blood–brain barrier impairment. *Brain* **145**, 3582–3593 (2021).

71. Simonovitch, S. *et al.* Impaired autophagy in APOE4 astrocytes. *J. Alzheimers Dis.* **51**, 915–927 (2016).

72. Fagan, A. M. *et al.* Human and murine ApoE markedly alters A beta metabolism before and after plaque formation in a mouse model of Alzheimer's disease. *Neurobiol. Dis.* **9**, 305–318 (2002).

73. Holtzman, D. M. *et al.* Apolipoprotein E isoform-dependent amyloid deposition and neuritic degeneration in a mouse model of Alzheimer's disease. *Proc. Natl. Acad. Sci. U. S. A.* **97**, 2892–2897 (2000).

74. Mahan, T. E. *et al.* Selective reduction of astrocyte apoE3 and apoE4 strongly reduces Aβ accumulation and plaque-related pathology in a mouse model of amyloidosis. *Mol. Neurodegener.* **17**, 13 (2022).

75. Brecht, W. J. *et al.* Neuron-specific apolipoprotein E4 proteolysis is associated with increased tau phosphorylation in brains of transgenic mice. *J. Neurosci.* **24**, 2527–2534 (2004).

76. Tesseur, I. *et al.* Expression of human apolipoprotein E4 in neurons causes hyperphosphorylation of protein tau in the brains of transgenic mice. *Am. J. Pathol.* **156**, 951–964 (2000).

77. Saroja, S. R., Gorbachev, K., TCW, J., Goate, A. M. & Pereira, A. C. Astrocyte-secreted glypican-4 drives APOE4-dependent tau hyperphosphorylation. *Proc. Natl. Acad. Sci. U. S. A.* **119**, e2108870119 (2022).

78. Habib, N. *et al.* Disease-associated astrocytes in Alzheimer's disease and aging. *Nat. Neurosci.* **23**, 701–706 (2020).

79. Mathys, H. *et al.* Single-cell transcriptomic analysis of Alzheimer's disease. *Nature* **570**, 332–337 (2019).

80. Wang, C., Sun, B., Zhou, Y., Grubb, A. & Gan, L. Cathepsin B degrades amyloid-β in mice expressing wild-type human amyloid precursor protein. *J. Biol. Chem.* **287**, 39834–39841 (2012).

81. Mucke, L. *et al.* Astroglial expression of human α1-antichymotrypsin enhances Alzheimer-like pathology in amyloid protein precursor transgenic Mice. *Am. J. Pathol.* **157**, 2003–2010 (2000).

82. Dupont-Wallois, L. *et al.* ApoE synthesis in human neuroblastoma cells. *Neurobiol. Dis.* **4**, 356–364 (1997).

83. Soulié, C. *et al.* Synthesis of apolipoprotein E (ApoE) mRNA by human neuronal-type SK N SH-SY 5Y cells and its regulation by nerve growth factor and ApoE. *Neurosci. Lett.* **265**, 147–150 (1999).

84. DeKroon, R. M. & Armati, P. J. The endosomal trafficking of apolipoprotein E3 and E4 in cultured human brain neurons and astrocytes. *Neurobiol. Dis.* **8**, 78–89 (2001).

85. Wang, C. *et al.* Gain of toxic apolipoprotein E4 effects in human iPSC-derived neurons is ameliorated by a small-molecule structure corrector. *Nat. Med.* **24**, 647–657 (2018).

86. Lee, H. *et al.* Cell-type-specific regulation of APOE and CLU levels in human neurons by the Alzheimer's disease risk gene SORL1. *Cell Rep.* **42**, 112994 (2023).

87. Einstein, G. *et al.* Intraneuronal ApoE in human visual cortical areas reflects the staging of Alzheimer disease pathology. *J. Neuropathol. Exp. Neurol.* **57**, 1190–1201 (1998).

88. Xu, P.-T. *et al.* Specific regional transcription of apolipoprotein E in human brain neurons. *Am. J. Pathol.* **154**, 601–611 (1999).

89. Xu, P.-T. *et al.* Regionally specific neuronal expression of human APOE gene in transgenic mice. *Neurosci. Lett.* **246**, 65–68 (1998).

90. Zalocusky, K. A. *et al.* Neuronal ApoE upregulates MHC-I expression to drive selective neurodegeneration in Alzheimer's disease. *Nat. Neurosci.* **24**, 786–798 (2021).

91. Xu, Q. *et al.* Intron-3 retention/splicing controls neuronal expression of apolipoprotein E in the CNS. *J. Neurosci.* **28**, 1452–1459 (2008).

92. Mahley, R. W. & Huang, Y. Apolipoprotein E: from atherosclerosis to Alzheimer's disease and beyond. *Curr. Opin. Lipidol.* **10**, 207–217 (1999).

93. Weisgraber, K. H. & Mahley, R. W. Human apolipoprotein E: the Alzheimer's disease connection. *FASEB J.* **10**, 1485–1494 (1996).

94. Li, G. *et al.* GABAergic interneuron dysfunction impairs hippocampal neurogenesis in adult apolipoprotein E4 knockin mice. *Cell Stem Cell* **5**, 634–645 (2009).

95. Mahley, R. W. & Huang, Y. Apolipoprotein e sets the stage: response to injury triggers neuropathology. *Neuron* **76**, 871–885 (2012).

96. Chen, Z. *et al.* Human-lineage-specific genomic elements are associated with neurodegenerative disease and APOE transcript usage. *Nat. Commun.* **12**, 2076 (2021).

97. Watts, J. A. *et al.* A common transcriptional mechanism involving R-loop and RNA abasic site regulates an enhancer RNA of APOE. *Nucleic Acids Res.* **50**, 12497–12514 (2022).

98. Wang, Z.-H. *et al.* Neuronal ApoE4 stimulates C/EBPβ activation, promoting Alzheimer's disease pathology in a mouse model. *Prog. Neurobiol.* **209**, 102212 (2022).

99. Buttini, M. *et al.* Expression of human apolipoprotein E3 or E4 in the brains of Apoe-/- mice: isoform-specific effects on neurodegeneration. *J. Neurosci.* **19**, 4867–4880 (1999).

100. Raber, J. *et al.* Apolipoprotein E and cognitive performance. *Nature* **404**, 352–354 (2000).

101. Raber, J. *et al.* Isoform-specific effects of human apolipoprotein E on brain function revealed in ApoE knockout mice: increased susceptibility of females. *Proc. Natl. Acad. Sci. U. S. A.* **95**, 10914–10919 (1998).

102. Cakir, Z. *et al.* Quantitative Proteomic Analysis Reveals apoE4-Dependent Phosphorylation of the Actin-Regulating Protein VASP. *Mol. Cell. Proteomics* **22**, 100541 (2023).

103. Jang, S.-S. *et al.* Neuronal apoE4 induces early hyperexcitability in select populations of hippocampal neurons by altering Nell2 expression. *bioRxiv*. 2023.08.28.555153. https://doi.org/10.1101/2023.08.28.555153 (2023).

104. Nuriel, T. *et al.* Neuronal hyperactivity due to loss of inhibitory tone in APOE4 mice lacking Alzheimer's disease-like pathology. *Nat. Commun.* **8**, 1464 (2017).

105. Gillespie, A. K. *et al.* Apolipoprotein E4 causes age-dependent disruption of slow gamma oscillations during hippocampal sharp-wave ripples. *Neuron* **90**, 740–751 (2016).

106. Jones, E. A., Gillespie, A. K., Yoon, S. Y., Frank, L. M. & Huang, Y. Early hippocampal sharp-wave ripple deficits predict later learning and memory impairments in an Alzheimer's disease mouse model. *Cell Rep.* **29**, 2123-2133.e4 (2019).

107. Andrews-Zwilling, Y. *et al.* Apolipoprotein E4 causes age- and Tau-dependent impairment of GABAergic interneurons, leading to learning and memory deficits in mice. *J. Neurosci.* **30**, 13707–13717 (2010).

108. Leung, L. *et al.* Apolipoprotein E4 causes age- and sex-dependent impairments of hilar GABAergic interneurons and learning and memory deficits in mice. *PloS One* **7**, e53569 (2012).

109. Yin, J. *et al.* Effect of ApoE isoforms on mitochondria in Alzheimer disease. *Neurology* **94**, e2404–e2411 (2020).

110. Mahley, R. W., Weisgraber, K. H. & Huang, Y. Apolipoprotein E4: a causative factor and therapeutic target in neuropathology, including Alzheimer's disease. *Proc. Natl. Acad. Sci. U. S. A.* **103**, 5644–5651 (2006).

111. Mahley, R. W. Apolipoprotein E4 targets mitochondria and the mitochondria-associated membrane complex in neuropathology, including Alzheimer's disease. *Curr. Opin. Neurobiol.* **79**, 102684 (2023).

112. Chen, H.-K. *et al.* Apolipoprotein E4 domain interaction mediates detrimental effects on mitochondria and is a potential therapeutic target for Alzheimer disease. *J. Biol. Chem.* **286**, 5215–5221 (2011).

113. Orr, A. L. *et al.* Neuronal apolipoprotein E4 expression results in proteome-wide alterations and compromises bioenergetic capacity by disrupting mitochondrial function. *J. Alzheimers Dis.* **68**, 991–1011 (2019).

114. Buttini, M. *et al.* Cellular source of apolipoprotein E4 determines neuronal susceptibility to excitotoxic injury in transgenic mice. *Am. J. Pathol.* **177**, 563–569 (2010).

115. Cataldo, A. M. *et al.* Endocytic pathway abnormalities precede amyloid beta deposition in sporadic Alzheimer's disease and Down syndrome: differential effects of APOE genotype and presenilin mutations. *Am. J. Pathol.* **157**, 277–286 (2000).

116. Ji, Z.-S. *et al.* Apolipoprotein E4 potentiates amyloid beta peptide-induced lysosomal leakage and apoptosis in neuronal cells. *J. Biol. Chem.* **277**, 21821–21828 (2002).

117. Wadhwani, A. R., Affaneh, A., Van Gulden, S. & Kessler, J. A. Neuronal apolipoprotein E4 increases cell death and phosphorylated Tau release in Alzheimer disease. *Ann. Neurol.* **85**, 726–739 (2019).

118. Yamauchi, Y. *et al.* Role of the N- and C-terminal domains in binding of apolipoprotein E isoforms to heparan sulfate and dermatan sulfate: a surface plasmon resonance study. *Biochemistry* **47**, 6702–6710 (2008).

119. Rauch, J. N. *et al.* Tau internalization is regulated by 6-O sulfation on heparan sulfate proteoglycans (HSPGs). *Sci. Rep.* **8**, 6382 (2018).

120. Stopschinski, B. E. *et al.* Specific glycosaminoglycan chain length and sulfation patterns are required for cell uptake of tau versus α-synuclein and β-amyloid aggregates. *J. Biol. Chem.* **293**, 10826–10840 (2018).

121. Holmes, B. B. & Diamond, M. I. Prion-like properties of Tau protein: the importance of extracellular Tau as a therapeutic target. *J. Biol. Chem.* **289**, 19855–19861 (2014).

122. Arboleda-Velasquez, J. F. *et al.* Resistance to autosomal dominant Alzheimer's disease in an APOE3 Christchurch homozygote: a case report. *Nat. Med.* **25**, 1680–1683 (2019).

123. Sepulveda-Falla, D. *et al.* Distinct tau neuropathology and cellular profiles of an APOE3 Christchurch homozygote protected against autosomal dominant Alzheimer's dementia. *Acta Neuropathol. (Berl.)* **144**, 589–601 (2022).

124. Shi, Y. *et al.* Microglia drive APOE-dependent neurodegeneration in a tauopathy mouse model. *J. Exp. Med.* **216**, 2546–2561 (2019).

125. Antara Rao. Microglia depletion reduces human neuronal APOE4-driven pathologies in a chimeric Alzheimer's disease model. *bioRxiv*. 2023.11.10.566510. https://doi.org/10.1101/2023.11.10.566510 (2023).

126. Harris, F. M. *et al.* Carboxyl-terminal-truncated apolipoprotein E4 causes Alzheimer's disease-like neurodegeneration and behavioral deficits in transgenic mice. *Proc. Natl. Acad. Sci.* **100**, 10966–10971 (2003).

127. Bien-Ly, N. *et al.* C-terminal-truncated apolipoprotein (apo) E4 inefficiently clears amyloid-beta (Abeta) and acts in concert with Abeta to elicit neuronal and behavioral deficits in mice. *Proc. Natl. Acad. Sci. U. S. A.* **108**, 4236–4241 (2011).

128. Rohn, T. T. Proteolytic cleavage of apolipoprotein E4 as the keystone for the heightened risk associated with Alzheimer's disease. *Int. J. Mol. Sci.* **14**, 14908–14922 (2013).

129. Koutsodendris, N. *et al.* APOE4-promoted gliosis and degeneration in tauopathy are ameliorated by pharmacological inhibition of HMGB1 release. *Cell Rep.* **42**, 113252 (2023).

130. Tanaka, H. *et al.* YAP-dependent necrosis occurs in early stages of Alzheimer's disease and regulates mouse model pathology. *Nat. Commun.* **11**, 507 (2020).

131. Foo, H. *et al.* Interaction between APOE-ε4 and HMGB1 is associated with widespread cortical thinning in mild cognitive impairment. *J. Neurol. Neurosurg. Psychiatry* **89**, 225–226 (2018).

132. Wan, Z. *et al.* TLR4-HMGB1 signaling pathway affects the inflammatory reaction of autoimmune myositis by regulating MHC-I. *Int. Immunopharmacol.* **41**, 74–81 (2016).

133. Grundtman, C. *et al.* Effects of HMGB1 on in vitro responses of isolated muscle fibers and functional aspects in skeletal muscles of idiopathic inflammatory myopathies. *FASEB J.* **24**, 570–578 (2010).

134. Brase, L. *et al.* Single-nucleus RNA-sequencing of autosomal dominant Alzheimer disease and risk variant carriers. *Nat. Commun.* **14**, 2314 (2023).

135. Mathys, H. *et al.* Single-cell atlas reveals correlates of high cognitive function, dementia, and resilience to Alzheimer's disease pathology. *Cell* **186**, 4365-4385.e27 (2023).

136. Horvath, A. A. *et al.* Subclinical epileptiform activity accelerates the progression of Alzheimer's disease: A long-term EEG study. *Clin. Neurophysiol.* **132**, 1982–1989 (2021).

137. Vossel, K. A. *et al.* Incidence and impact of subclinical epileptiform activity in Alzheimer's disease. *Ann. Neurol.* **80**, 858–870 (2016).

138. Olah, M. *et al.* A transcriptomic atlas of aged human microglia. *Nat. Commun.* **9**, 539 (2018).

139. Rangaraju, S. *et al.* Quantitative proteomics of acutely-isolated mouse microglia identifies novel immune Alzheimer's disease-related proteins. *Mol. Neurodegener.* **13**, 34 (2018).

140. Keren-Shaul, H. *et al.* A unique microglia type associated with restricting development of Alzheimer's disease. *Cell* **169**, 1276-1290.e17 (2017).

141. Lee, S. *et al.* APOE modulates microglial immunometabolism in response to age, amyloid pathology, and inflammatory challenge. *Cell Rep.* **42**, 112196 (2023).

142. Grubman, A. *et al.* A single-cell atlas of entorhinal cortex from individuals with Alzheimer's disease reveals cell-type-specific gene expression regulation. *Nat. Neurosci.* **22**, 2087–2097 (2019).

143. Krasemann, S. *et al.* The TREM2-APOE pathway drives the transcriptional phenotype of dysfunctional microglia in neurodegenerative diseases. *Immunity* **47**, 566-581.e9 (2017).

144. Mancuso, R. *et al.* CSF1R inhibitor JNJ-40346527 attenuates microglial proliferation and neurodegeneration in P301S mice. *Brain* **142**, 3243–3264 (2019).

145. Voloboueva, L. A., Emery, J. F., Sun, X. & Giffard, R. G. Inflammatory response of microglial BV-2 cells includes a glycolytic shift and is modulated by mitochondrial glucose-regulated protein 75/mortalin. *FEBS Lett.* **587**, 756–762 (2013).

146. Huynh, T.-P. V. *et al.* Lack of hepatic apoE does not influence early Aβ deposition: observations from a new APOE knock-in model. *Mol. Neurodegener.* **14**, 37 (2019).

147. Victor, M. B. *et al.* Lipid accumulation induced by APOE4 impairs microglial surveillance of neuronal-network activity. *Cell Stem Cell* **29**, 1197-1212.e8 (2022).

148. Sienski, G. *et al. APOE4* disrupts intracellular lipid homeostasis in human iPSC-derived glia. *Sci. Transl. Med.* **13**, eaaz4564 (2021).

149. Liu, C.-C. *et al.* Cell-autonomous effects of APOE4 in restricting microglial response in brain homeostasis and Alzheimer's disease. *Nat. Immunol.* **24**, 1854–1866 (2023).

150. Wang, N. *et al.* Opposing effects of apoE2 and apoE4 on microglial activation and lipid metabolism in response to demyelination. *Mol. Neurodegener.* **17**, 75 (2022).

151. Fote, G. M. *et al.* Isoform-dependent lysosomal degradation and internalization of apolipoprotein E requires autophagy proteins. *J. Cell Sci.* **135**, jcs258687 (2022).

152. Machlovi, S. I. *et al.* APOE4 confers transcriptomic and functional alterations to primary mouse microglia. *Neurobiol. Dis.* **164**, 105615 (2022).

153. Overmyer, M. *et al.* Reactive microglia in aging and dementia: an immunohistochemical study of postmortem human brain tissue. *Acta Neuropathol. (Berl.)* **97**, 383–392 (1999).

154. Egensperger, R., Kösel, S., Eitzen, U. & Graeber, M. B. Microglial activation in Alzheimer disease: association with APOE genotype. *Brain Pathol.* **8**, 439–447 (2006).

155. Vitek, M. P., Brown, C. M. & Colton, C. A. APOE genotype-specific differences in the innate immune response. *Neurobiol. Aging* **30**, 1350–1360 (2009).

156. Muth, C., Hartmann, A., Sepulveda-Falla, D., Glatzel, M. & Krasemann, S. Phagocytosis of apoptotic cells is specifically upregulated in ApoE4 expressing microglia in vitro. *Front. Cell. Neurosci.* **13**, 181 (2019).

157. Yang, Y. *et al.* APOE3, but not APOE4, bone marrow transplantation mitigates behavioral and pathological changes in a mouse model of Alzheimer disease. *Am. J. Pathol.* **183**, 905–917 (2013).

158. Yin, Z. *et al.* APOE4 impairs the microglial response in Alzheimer's disease by inducing TGFβ-mediated checkpoints. *Nat. Immunol.* **11**, 1839-1853 (2023)

159. Najm, R. *et al.* In vivo chimeric Alzheimer's disease modeling of apolipoprotein E4 toxicity in human neurons. *Cell Rep.* **32**, 107962 (2020).

160. Lau, S.-F. *et al.* The VCAM1–ApoE pathway directs microglial chemotaxis and alleviates Alzheimer's disease pathology. *Nat. Aging* **10**, 1219-1236 (2023)

161. Gratuze, M. *et al.* TREM2-independent microgliosis promotes tau-mediated neurodegeneration in the presence of ApoE4. *Neuron* **111**, 202-219.e7 (2023).
162. Asai, H. *et al.* Depletion of microglia and inhibition of exosome synthesis halt tau propagation. *Nat. Neurosci.* **18**, 1584–1593 (2015).
163. Clayton, K. *et al.* Plaque associated microglia hyper-secrete extracellular vesicles and accelerate tau propagation in a humanized APP mouse model. *Mol. Neurodegener.* **16**, 18 (2021).
164. Hopp, S. C. *et al.* The role of microglia in processing and spreading of bioactive tau seeds in Alzheimer's disease. *J. Neuroinflammation* **15**, 269 (2018).
165. Ferrari-Souza, J. P. *et al. APOE* ε4 associates with microglial activation independently of Aβ plaques and tau tangles. *Sci. Adv.* **9**, eade1474 (2023).
166. Chen, X. *et al.* Microglia-mediated T cell infiltration drives neurodegeneration in tauopathy. *Nature* **615**, 668–677 (2023).
167. Serrano-Pozo, A. *et al.* Effect of APOE alleles on the glial transcriptome in normal aging and Alzheimer's disease. *Nat. Aging* **1**, 919–931 (2021).
168. Frigerio, C. S. *et al.* The major risk factors for Alzheimer's disease: age, sex, and genes modulate the microglia response to Aβ plaques. *Cell Rep.* **27**, 1293-1306.e6 (2019).
169. Gerrits, E. *et al.* Distinct amyloid-β and tau-associated microglia profiles in Alzheimer's disease. *Acta Neuropathol. (Berl.)* **141**, 681–696 (2021).
170. Serrano-Pozo, A., Gómez-Isla, T., Growdon, J. H., Frosch, M. P. & Hyman, B. T. A phenotypic change but not proliferation underlies glial responses in Alzheimer disease. *Am. J. Pathol.* **182**, 2332–2344 (2013).
171. Perlmutter, L. S., Scott, S. A., Barrón, E. & Chui, H. C. MHC class II-positive microglia in human brain: association with Alzheimer lesions. *J. Neurosci. Res.* **33**, 549–558 (1992).
172. Chen, M., Xie, M., Peng, C. & Long, S. The absorption of apolipoprotein E by damaged neurons facilitates neuronal repair. *Cell Biol. Int.* **43**, 623–633 (2019).

173. Mok, K. K.-S. *et al.* Apolipoprotein E ε4 disrupts oligodendrocyte differentiation by interfering with astrocyte-derived lipid transport. *J. Neurochem.* **165**, 55–75 (2023).

174. Safina, D. *et al.* Low-density lipoprotein receptor-related protein 1 is a novel modulator of radial glia stem cell proliferation, survival, and differentiation. *Glia* **64**, 1363–1380 (2016).

175. Kenigsbuch, M. *et al.* A shared disease-associated oligodendrocyte signature among multiple CNS pathologies. *Nat. Neurosci.* **25**, 876–886 (2022).

176. Casey, C. S. *et al.* Apolipoprotein E inhibits cerebrovascular pericyte mobility through a RhoA protein-mediated pathway. *J. Biol. Chem.* **290**, 14208–14217 (2015).

177. Wilhelmus, M. M. M. *et al.* Apolipoprotein E genotype regulates amyloid-β cytotoxicity. *J. Neurosci.* **25**, 3621–3627 (2005).

178. Blanchard, J. W. *et al.* Reconstruction of the human blood–brain barrier in vitro reveals a pathogenic mechanism of APOE4 in pericytes. *Nat. Med.* **26**, 952–963 (2020).

179. Majack, R. A. *et al.* Expression of apolipoprotein E by cultured vascular smooth muscle cells is controlled by growth state. *J. Cell Biol.* **107**, 1207–1213 (1988).

180. Rieker, C. *et al.* Apolipoprotein E4 expression causes gain of toxic function in isogenic human induced pluripotent stem cell-derived endothelial cells. *Arterioscler. Thromb. Vasc. Biol.* **39**, e195–e207 (2019).

181. Bruinsma, I. B. *et al.* Apolipoprotein E protects cultured pericytes and astrocytes from D-Aβ1–40-mediated cell death. *Brain Res.* **1315**, 169–180 (2010).

182. Yang, A. C. *et al.* A human brain vascular atlas reveals diverse mediators of Alzheimer's risk. *Nature* **603**, 885–892 (2022).

183. Yamazaki, Y. *et al.* ApoE in brain pericytes regulates endothelial function in an isoform-dependent manner by modulating basement membrane components. *Arterioscler. Thromb. Vasc. Biol.* **40**, 128–144 (2020).

184. Halliday, M. R. *et al.* Accelerated pericyte degeneration and blood–brain barrier breakdown in apolipoprotein E4 carriers with Alzheimer's disease. *J. Cereb. Blood Flow Metab.* **36**, 216–227 (2016).

185. Yamazaki, Y. *et al.* Vascular apoE4 impairs behavior by modulating glio-vascular function. *Neuron* **109**, 438-447.e6 (2021).

186. Sun, N. *et al.* Single-nucleus multiregion transcriptomic analysis of brain vasculature in Alzheimer's disease. *Nat. Neurosci.* **26**, 970–982 (2023).

187. Honig, L. S. *et al.* ARIA in patients treated with lecanemab (BAN2401) in a phase 2 study in early Alzheimer's disease. *Alzheimers Dement. Transl. Res. Clin. Interv.* **9**, e12377 (2023).

188. Salloway, S. *et al.* Amyloid-Related Imaging Abnormalities in 2 Phase 3 Studies Evaluating Aducanumab in Patients With Early Alzheimer Disease. *JAMA Neurol.* **79**, 13–21 (2022).

189. Pankiewicz, J. E. *et al.* APOE Genotype Differentially Modulates Effects of Anti-Aβ, Passive Immunization in APP Transgenic Mice. *Mol. Neurodegener.* **12**, 12 (2017).

190. Bien-Ly, N., Gillespie, A. K., Walker, D., Yoon, S. Y. & Huang, Y. Reducing human apolipoprotein E levels attenuates age-dependent Aβ accumulation in mutant human amyloid precursor protein transgenic mice. *J. Neurosci.* **32**, 4803–4811 (2012).

191. Kim, J. *et al.* Haploinsufficiency of human APOE reduces amyloid deposition in a mouse model of amyloid-β amyloidosis. *J. Neurosci.* **31**, 18007–18012 (2011).

192. Chemparathy, A. *et al.* APOE loss-of-function variants: Compatible with longevity and associated with resistance to Alzheimer's Disease pathology. *MedRxiv* 2023.07.20.23292771. doi:10.1101/2023.07.20.23292771 (2023).

193. Mak, A. C. Y. *et al.* Effects of the absence of apolipoprotein e on lipoproteins, neurocognitive function, and retinal function. *JAMA Neurol.* **71**, 1228–1236 (2014).

194. Rajabli, F. *et al.* Ancestral origin of ApoE ε4 Alzheimer disease risk in Puerto Rican and African American populations. *PLoS Genet.* **14**, e1007791 (2018).

195. Griswold, A. J. *et al.* Increased APOE ε4 expression is associated with the difference in Alzheimer's disease risk from diverse ancestral backgrounds. *Alzheimers Dement.* **17**, 1179–1188 (2021).

196. Huynh, T.-P. V. *et al.* Age-dependent effects of apoE reduction using antisense oligonucleotides in a model of β-amyloidosis. *Neuron* **96**, 1013-1023.e4 (2017).

197. Kim, J. *et al.* Anti-apoE immunotherapy inhibits amyloid accumulation in a transgenic mouse model of Aβ amyloidosis. *J. Exp. Med.* **209**, 2149–2156 (2012).

198. Litvinchuk, A. *et al.* Apolipoprotein E4 reduction with antisense oligonucleotides decreases neurodegeneration in a tauopathy model. *Ann. Neurol.* **89**, 952–966 (2021).

199. Bulcha, J. T., Wang, Y., Ma, H., Tai, P. W. L. & Gao, G. Viral vector platforms within the gene therapy landscape. *Signal Transduct. Target. Ther.* **6**, 53 (2021).

200. Zhao, Z., Anselmo, A. C. & Mitragotri, S. Viral vector-based gene therapies in the clinic. *Bioeng. Transl. Med.* **7**, e10258 (2021).

201. Brodbeck, J. *et al.* Structure-dependent impairment of intracellular apolipoprotein E4 trafficking and its detrimental effects are rescued by small-molecule structure correctors. *J. Biol. Chem.* **286**, 17217–17226 (2011).

202. Chen, H.-K. *et al.* Small molecule structure correctors abolish detrimental effects of apolipoprotein E4 in cultured neurons. *J. Biol. Chem.* **287**, 5253–5266 (2012).

Chapter 2

1. Corder, E. H. *et al.* Gene dose of apolipoprotein E type 4 allele and the risk of Alzheimer's disease in late onset families. *Science* **261**, 921–923 (1993).

2. Mahley, R. W., Weisgraber, K. H. & Huang, Y. Apolipoprotein E4: A causative factor and therapeutic target in neuropathology, including Alzheimer's disease. *Proc. Natl. Acad. Sci.* **103**, 5644–5651 (2006).
3. Blumenfeld, J., Yip, O., Kim, M. J. & Huang, Y. Cell type-specific roles of APOE4 in Alzheimer disease. *Nat. Rev. Neurosci.* **25**, 91–110 (2024).
4. Farrer, L. A. *et al.* Effects of age, sex, and ethnicity on the association between apolipoprotein E genotype and Alzheimer Disease: a meta-analysis. *JAMA* **278**, 1349–1356 (1997).
5. Reiman, E. M. *et al.* Exceptionally low likelihood of Alzheimer's dementia in APOE2 homozygotes from a 5,000-person neuropathological study. *Nat. Commun.* **11**, 667 (2020).
6. Yamazaki, Y., Zhao, N., Caulfield, T. R., Liu, C.-C. & Bu, G. Apolipoprotein E and Alzheimer disease: pathobiology and targeting strategies. *Nat. Rev. Neurol.* **15**, 501–518 (2019).
7. Koutsodendris, N., Nelson, M. R., Rao, A. & Huang, Y. Apolipoprotein E and Alzheimer's disease: findings, hypotheses, and potential mechanisms. *Annu. Rev. Pathol. Mech. Dis.* **17**, 73–99 (2022).
8. Brecht, W. J. *et al.* Neuron-specific apolipoprotein E4 proteolysis is associated with increased tau phosphorylation in brains of transgenic mice. *J. Neurosci.* **24**, 2527–2534 (2004).
9. Knoferle, J. *et al.* Apolipoprotein E4 produced in GABAergic interneurons causes learning and memory deficits in mice. *J. Neurosci.* **34**, 14069–14078 (2014).
10. Blumenfeld, J. *et al.* Neuronal APOE4 alone is sufficient to drive tau pathology, neurodegeneration, and neuroinflammation in an Alzheimer's disease mouse model. 2025.11.25.690488 Preprint at https://doi.org/10.1101/2025.11.25.690488 (2025).
11. Koutsodendris, N. *et al.* Neuronal APOE4 removal protects against tau-mediated gliosis, neurodegeneration and myelin deficits. *Nat. Aging* **3**, 275–296 (2023).

12. Zalocusky, K. A. *et al.* Neuronal ApoE upregulates MHC-I expression to drive selective neurodegeneration in Alzheimer's disease. *Nat. Neurosci.* **24**, 786–798 (2021).
13. DeVos, S. L. & Miller, T. M. Antisense oligonucleotides: treating neurodegeneration at the level of RNA. *Neurotherapeutics* **10**, 486–497 (2013).
14. Scoles, D. R. & Pulst, S. M. Oligonucleotide therapeutics in neurodegenerative diseases. *RNA Biol.* **15**, 707–714 (2018).
15. Crooke, S. T., Baker, B. F., Crooke, R. M. & Liang, X. Antisense technology: an overview and prospectus. *Nat. Rev. Drug Discov.* **20**, 427–453 (2021).
16. Bennett, C. F., Krainer, A. R. & Cleveland, D. W. Antisense oligonucleotide therapies for neurodegenerative diseases. *Annu. Rev. Neurosci.* **42**, 385–406 (2019).
17. Smith, R. A. *et al.* Antisense oligonucleotide therapy for neurodegenerative disease. **42**, 385–406 (2019).
18. Litvinchuk, A. *et al.* Apolipoprotein E4 reduction with antisense oligonucleotides decreases neurodegeneration in a tauopathy model. *Ann. Neurol.* **89**, 952–966 (2021).
19. Huynh, T.-P. V. *et al.* Age-dependent effects of apoE reduction using antisense oligonucleotides in a model of β-amyloidosis. *Neuron* **96**, 1013-1023.e4 (2017).
20. Xu, Q. *et al.* Intron-3 retention/splicing controls neuronal expression of apolipoprotein E in the CNS. *J. Neurosci.* **28**, 1452–1459 (2008).
21. Chen, Z. *et al.* Human-lineage-specific genomic elements are associated with neurodegenerative disease and APOE transcript usage. *Nat. Commun.* **12**, 2076 (2021).
22. Harris, F. M. *et al.* Astroglial regulation of apolipoprotein E expression in neuronal cells: implications for Alzheimer's disease. *J. Biol. Chem.* **279**, 3862–3868 (2004).
23. Raber, J. *et al.* Isoform-specific effects of human apolipoprotein E on brain function revealed in ApoE knockout mice: Increased susceptibility of females. *Proc. Natl. Acad. Sci.* **95**, 10914–10919 (1998).

24. Buttini, M. *et al.* Expression of human apolipoprotein E3 or E4 in the brains of Apoe−/− mice: isoform-specific effects on neurodegeneration. *J. Neurosci.* **19**, 4867–4880 (1999).
25. Nelson, M. R. *et al.* The APOE-R136S mutation protects against APOE4-driven Tau pathology, neurodegeneration and neuroinflammation. *Nat. Neurosci.* **26**, 2104–2121 (2023).
26. Koutsodendris, N. *et al.* APOE4-promoted gliosis and degeneration in tauopathy are ameliorated by pharmacological inhibition of HMGB1 release. *Cell Rep.* **42**, (2023).
27. Wang, C. *et al.* Selective removal of astrocytic *APOE4* strongly protects against tau-mediated neurodegeneration and decreases synaptic phagocytosis by microglia. *Neuron* **109**, 1657-1674.e7 (2021).
28. Armstrong, P. *et al.* Protective effect of PDE4B subtype-specific inhibition in an App knock-in mouse model for Alzheimer's disease. *Neuropsychopharmacology* **49**, 1559–1568 (2024).
29. Palop, J. J. *et al.* Aberrant excitatory neuronal activity and compensatory remodeling of inhibitory hippocampal circuits in mouse models of Alzheimer's disease. *Neuron* **55**, 697–711 (2007).
30. Ranasinghe, K. G. *et al.* Distinct manifestations of excitatory-inhibitory imbalance associated with amyloid-β and tau in patients with Alzheimer's disease. *Nat. Commun.* **16**, 7957 (2025).
31. Zilberter, M. *et al.* Dietary energy substrates reverse early neuronal hyperactivity in a mouse model of Alzheimer's disease. *J. Neurochem.* **125**, 157–171 (2013).
32. Hüttenrauch, M. *et al.* Glycoprotein NMB: a novel Alzheimer's disease associated marker expressed in a subset of activated microglia. *Acta Neuropathol. Commun.* **6**, 108 (2018).
33. Im, E. *et al.* Lysosomal dysfunction in Down syndrome and Alzheimer mouse models is caused by v-ATPase inhibition by Tyr682-phosphorylated APP βCTF. *Sci. Adv.* **9**, eadg1925 (2023).
34. Wu, Y. *et al.* Features of lipid metabolism in humanized ApoE knockin rat models. *Int. J. Mol. Sci.* **22**, 8262 (2021).

35. Li, G. *et al.* GABAergic interneuron dysfunction impairs hippocampal neurogenesis in adult apolipoprotein E4 knockin mice. *Cell Stem Cell* **5**, 634–645 (2009).

36. Lane-Donovan, C. *et al.* Genetic restoration of plasma ApoE improves cognition and partially restores synaptic defects in ApoE-deficient mice. *J. Neurosci.* **36**, 10141–10150 (2016).

37. Tensaouti, Y., Yu, T.-S. & Kernie, S. G. Apolipoprotein E regulates the maturation of injury-induced adult-born hippocampal neurons following traumatic brain injury. *PLOS ONE* **15**, e0229240 (2020).

38. Yin, C., Guo, Z., He, Z., Wang, Z. & Sun, X. Apolipoprotein E affects in vitro axonal growth and regeneration via the MAPK signaling pathway. *Cell Transplant.* **28**, 691–703 (2019).

39. Bien-Ly, N., Gillespie, A. K., Walker, D., Yoon, S. Y. & Huang, Y. Reducing human apolipoprotein E levels attenuates age-dependent Aβ accumulation in mutant human amyloid precursor protein transgenic mice. *J. Neurosci.* **32**, 4803–4811 (2012).

40. Ryu, J. K. *et al.* Blood coagulation protein fibrinogen promotes autoimmunity and demyelination via chemokine release and antigen presentation. *Nat. Commun.* **6**, 8164 (2015).

41. Zheng, G. X. Y. *et al.* Massively parallel digital transcriptional profiling of single cells. *Nat. Commun.* **8**, 14049 (2017).

42. Hao, Y. *et al.* Integrated analysis of multimodal single-cell data. *Cell* **184**, 3573-3587.e29 (2021).

43. Hafemeister, C. & Satija, R. Normalization and variance stabilization of single-cell RNA-seq data using regularized negative binomial regression. *Genome Biol.* **20**, 296 (2019).

44. Li, Y. *et al.* Cell-type-directed network-correcting combination therapy for Alzheimer's disease. *Cell* **188**, 5516-5534.e18 (2025).

45. Lein, E. S. *et al.* Genome-wide atlas of gene expression in the adult mouse brain. *Nature* **445**, 168–176 (2007).

46. Belonwu, S. A. *et al.* Bioinformatics analysis of publicly available single-nuclei transcriptomics Alzheimer's disease datasets reveals APOE genotype-specific changes across cell types in two brain regions. *Front. Aging Neurosci.* **14**, (2022).
47. Saunders, A. *et al.* Molecular diversity and specializations among the cells of the adult mouse brain. *Cell* **174**, 1015-1030.e16 (2018).
48. ggplot2: create elegant data visualisations using the grammar of graphics — ggplot2-package. https://ggplot2.tidyverse.org/reference/ggplot2-package.html.
49. Benjamini, Y. & Hochberg, Y. Controlling the false discovery rate: a practical and powerful approach to multiple testing. *J. R. Stat. Soc. Ser. B Methodol.* **57**, 289–300 (1995).
50. Bates, D., Mächler, M., Bolker, B. & Walker, S. Fitting linear mixed-effects models using lme4. *J. Stat. Softw.* **67**, (2015).
51. Hafemeister, C. & Satija, R. Normalization and variance stabilization of single-cell RNA-seq data using regularized negative binomial regression. *Genome Biol.* **20**, 296 (2019).
52. Ahlmann-Eltze, C. & Huber, W. glmGamPoi: fitting Gamma-Poisson generalized linear models on single cell count data. *Bioinformatics* **36**, 5701–5702 (2021).

Publishing Agreement

It is the policy of the University to encourage open access and broad distribution of all theses, dissertations, and manuscripts. The Graduate Division will facilitate the distribution of UCSF theses, dissertations, and manuscripts to the UCSF Library for open access and distribution. UCSF will make such theses, dissertations, and manuscripts accessible to the public and will take reasonable steps to preserve these works in perpetuity.

I hereby grant the non-exclusive, perpetual right to The Regents of the University of California to reproduce, publicly display, distribute, preserve, and publish copies of my thesis, dissertation, or manuscript in any form or media, now existing or later derived, including access online for teaching, research, and public service purposes.

DocuSigned by:
Oscar Yip
6A45D5E0A186412...
Author Signature

12/10/2025
Date